A STUDY OF THE ENERGY LEVELS IN LIGHT NUCLEI

LIBRARY
RECEIVED
1-4-68

by

Richard Davies Gill

A Dissertation submitted in the University of Oxford

for the Degree of Doctor of Philosophy

Exeter College December, 1967.

C O N T E N T S

		Page
ABSTRACT	.....	i
Acknowledgements		
CHAPTER 1. INTRODUCTION	.....	1.1
CHAPTER 2. EXPERIMENTAL ARRANGEMENTS	.....	2.1
2.1 The Beam Line and Associated Equipment	..	2.1
2.2 The Electronics	.....	2.4
CHAPTER 3. ANGULAR CORRELATION THEORY AND ELECTROMAGNETIC MATRIX ELEMENTS	...	3.1
3.1 The Alignment Condition	.....	3.1
3.2 The effect of the finite size of the particle detector	.....	3.5
3.3 Angular Correlation Theory	.....	3.11
3.4 The Angular Correlation Formulae	....	3.18
3.5 The Finite Size of the Gamma Ray Detector	.....	3.22
3.6 Data Reduction and Fitting Procedures	..	3.25

Page

3.7 Calculation of Electromagnetic Transition Matrix Elements 3.31

CHAPTER 4. A METHOD MEASURING THE LIFETIMES OF EXCITED NUCLEAR STATES 4.1

4.1 The Doppler Shift Attenuation Method ... 4.1

4.2 Treatment of the Experimental Data 4.1

4.3 The Calculation of dR/dx values for Heavy Ions 4.20

CHAPTER 5. THE ANGULAR CORRELATION RESULTS .. 5.1

5.1 Some Positive Parity States in ^{15}N : Experimental Conditions 5.1

5.2 The 7.154 and 7.563 MeV Levels and the $5/2^+$, 5.270 MeV Level 5.4

5.3 The 7.300 MeV Level 5.8

5.4 Some ^{15}O Positive Parity States: Experimental Conditions 5.9

5.5 The 6.789 and 6.857 MeV Levels and the $5/2^+$, 5.240 MeV Level 5.11

5.6 The 5.188 and 5.240 MeV Levels 5.14

Page

5.7 The 2^-, 8.88 MeV Level in ^{16}O : Experimental Conditions and Results 5.15

CHAPTER 6. LIFETIME MEASUREMENTS IN MASS 15 .. 6.1

6.1 Experimental Conditions 6.1

6.2 Extraction of the Lifetimes from the Data 6.8

CHAPTER 7. DISCUSSION OF THE RESULTS 7.1

7.1 The 2^- State of ^{16}O 7.1

7.2 Mass 15 Nuclei 7.6

7.3 The $5/2^+$, 5.2 MeV States 7.8

7.4 The M1 Transition Rates 7.12

7.5 The $3/2^+$, 7.30 and 6.79 MeV States 7.13

REFERENCES

A B S T R A C T

The results of some angular correlation experiments on the low lying states of ^{15}N, ^{15}O and ^{16}O are presented. The result of an investigation of the lifetimes of some of the excited states of ^{15}N and ^{15}O are also to be found.

In Chapters 2, 3 and 4 the experimental methods and the underlying theory are discussed. The results are presented in Chapters 5 and 6 and discussed in Chapter 7.

(1) The ^{15}N angular correlation results

The spins of the positive parity states at 5.27, 7.15, 7.56 and 7.30 MeV were confirmed to be $5/2$, $5/2$, $7/2$ and $3/2$ respectively. The multipole mixing ratios of the de-excitation gamma rays from these levels were determined. The results were :

$\delta(5.27 \rightarrow 0) = -0.165 \pm 0.015$; $\frac{E3}{M2}$

$\delta(7.15 \rightarrow 5.27) = -0.04 \pm 0.03$; $\frac{E2}{M1}$

$\delta(7.56 \rightarrow 5.27) = -0.01 \pm 0.03$; $\frac{E2}{M1}$

$\delta(7.30 \rightarrow 0) = -0.07 \pm 0.02$; $\frac{M2}{E1}$

The smaller results only have been quoted.

(11) ^{15}O angular correlation results

The spins of the ^{15}O levels located at 6.79 and 6.86 MeV were confirmed to be $3/2$ and $5/2$ respectively and the multipole mixing ratios of the de-excitation gamma rays were determined with the following result:

$$\delta(5.24 \rightarrow 0) = +0.14^{+0.04}_{-0.03}; \quad \frac{E3}{M2}$$

$$\delta(6.86 \rightarrow 5.24) = -0.04 \pm 0.03; \quad \frac{E2}{M1}$$

$$\delta(6.79 \rightarrow 0) = -0.10 \pm 0.02; \quad \frac{M2}{E1}$$

The smaller results only have been quoted.

(iii) ^{16}O angular correlation results

The multipole mixing ratios for the de-excitation gamma rays from the 2^-, 8.88 MeV state in ^{16}O were investigated. Apart from the decay scheme of the level the following results were obtained.

$$\delta(8.88 \rightarrow 6.14) = 2.9 \pm 0.2; \quad \frac{E2}{M1}$$

$$|\delta(8.88 \rightarrow 7.12)| > 2.5; \quad \frac{E2}{M1}$$

(iv) <u>The mass 15 lifetime results</u>

The lifetimes of some of the excited states of ^{15}N and ^{15}O were investigated using the Doppler shift attenuation method. Lifetime limits were obtained for several of the levels. It was also found that :

$$\tau(^{15}N,\ 7.56\ MeV) = (0.06 \pm 0.02) \times 10^{-12}\ sec.$$

$$\tau(^{15}O,\ 7.28\ MeV) = (0.70 \pm 0.15) \times 10^{-12}\ sec.$$

ACKNOWLEDGEMENTS

I should like to thank the following :

Dr. R.J. Rose for continued advice and criticism in all stages of this work.

Professors D.H. Wilkinson and D.W. Allen for the use of the facilities of the Oxford University Nuclear Physics Laboratory and for their interest in this work.

Drs. J.S. Lopes and C. Häusser for many valuable discussions and their considerable participation in this work.

Dr. B.E.F. Macefield for his helpful advice.

Professor L. Fox for the use of the University Computing facilities.

Mr. D.C. Robertson and Mr. K.A.I. Bell for their assistance in the later experiments.

Mr. R.N. McK.Ryder and his staff of operators for the efficient running of the Oxford Tandem Generator.

Mr. E. Sparrow and the staff of the Harwell Van de Graaff Generator for their co-operation.

Mr. A. Muggleton for supplying the ^{18}O targets and all the particle detectors.

Mrs. Enid Browne for typing the manuscript.

Finally, I should like to apologise to those whose names I have not included but who have made their contribution.

C H A P T E R 1

INTRODUCTION

The angular distributions of gamma rays following nuclear transformations have been studied extensively. The subject was first treated theoretically by Hamilton in 1940 (Ha 40) and the first successful experimental investigations were made by Brady and Deutsch (Br 47). Since that time numerous theoretical treatments of the different correlations have become available: the major advances in the theory have been due to the introduction of (i) group theory (ii) statistical tensor methods and (iii) Racah algebra. Amongst the vast literature pertaining to the subject, mention should be made of the review article of Devons and Goldfarb (De 57) and of the work of Biedenharn and M.E. Rose (Bi 53; Ro 57; Fi 60). In these articles and in the article by Frauenfelder and Steffan (Fr 65) extensive discussions of the theoretical aspects of the subject may be found together with comprehensive bibliographies.

In the angular correlation experiments reported herein the gamma rays were produced in a nuclear reaction of the

sort A(b,c)D and the correlation between the gamma rays from the excited levels of the "D" nucleus and the particle "c" was observed with "c" detected at 180^{o} with respect to the incident beam direction. This arrangement considerably simplifies the analysis of the observed correlations as was first pointed out by Litherland and Ferguson (Li 61).

After over twenty years of continuous development it might be thought that the theory was completed. However, the separate strands of the theory developed independently by different authors led to ambiguities in the angular correlation formula which would have been applicable to the experiments reported later on. In any transition the different possible multipole matrix elements which may contribute to the total transition matrix element can interfere coherently making it possible to observe the relative signs of the matrix elements or equivalently the signs of the multipole mixing ratios. Both the magnitude and signs of these quantities may be compared with those calculated from a knowledge of the structure of the nuclear levels involved in the transition. However, because of the fragmented development of the angular correlation theory it was not usually possible to place any significance upon the signs of the mixing ratios which were extracted from

the experimental data. There were various reasons for this although it is probably not appropriate to discuss them here; suffice it to say that a detailed re-examination of the problem has been undertaken by Rose and Brink (no 67) who derived angular correlation formulae in which the signs of the mixing ratios were well defined in terms of reduced matrix elements. Throughout the following pages this standard phase convention has been adhered to. The parts of Chapter 3 which discuss angular correlation theory lean heavily upon (no 67) and the notation is the same as in that work although there the formulae were also derived using a semi-classical approach in which the appropriate emission matrix elements were related to the absorption matrix elements using time reversal invariance principles.

It is probably in place to say a word about the motivation behind the experimental work.

(i) Mass 15 nuclei are one nucleon removed from a doubly closed ^{16}O shell and should therefore have relatively simple structure.

(ii) The electromagnetic properties provide stringent tests of theoretical models since it is found that these properties are rather sensitive to the detailed

nuclear structure. Comparisons of the properties of mirror levels are often valuable.

(iii) The first ^{15}N angular correlation experiment suggested that the M1 ground state transition from the 7.30 MeV state was highly retarded and could be measured using the Doppler shift attenuation method.

(iv) The measurements made in ^{16}O were of interest since the negative parity states of ^{16}O should have structural similarities with the positive parity states in mass 15 nuclei.

These points are treated in more detail in Chapter 7.

C H A P T E R 2

EXPERIMENTAL ARRANGEMENTS

2.1 The Beam Line and Associated Equipment

The beams provided by the electrostatic generators which were used in these experiments were collimated by a series of eight tantalum discs which had small holes in their centres and which were spaced by a series of lead blocks with 3" outer diameter. The lead was included in the system to reduce the gamma ray background caused by the beam striking the collimator discs. Since the beam arrives at the experimental station focussed, ideally at the target position, it was found that the best transmission occurred (> 95%) if the holes in the tantalum were in graduated sizes from 4 to 2 mm. with the smallest holes furthest from the accelerating machine. The mount for the annular surface barrier counter was bolted directly onto the end of the collimator support. A small glass target chamber was then coupled onto the counter mount. After passing through the target chamber the beam was stopped by a thick piece of uranium about 20 ft. from the target position.

For the lifetime experiments a somewhat different target chamber was used. It was constructed from stainless steel and included a liquid Nitrogen cold trap which surrounded the target position. The heavy ion beam used was stopped in the target backing and the chamber was pumped with a Mercury diffusion pump to ensure a good vacuum.

The gamma detectors were mounted on rotating trolleys and it was important in the angular correlation experiments that the axis of rotation of the trolleys should pass through the centre of the target. The trolleys were mounted on a flat table which was centred with respect to the target position by hanging a plumbline through the centre of the target chamber. Direct measurements of the distance from the target chamber to the front face of the gamma detector were usually made to check the centreing and which guaranteed it to better than 0.5 mm. Further, from the beam spot formed on the target at the time of the experiment the distance from the target centre to the beam spot could be estimated for which a correction could be applied to the measured distributions if necessary. Since the smallest collimator size was 2 mm. it would seem that the worst error in the centreing which might occur would be 2 to 3 mm. whilst more typically $\sim$ 1.5 mm. would be achieved.

For the angular correlation experiments the target to crystal distance was usually about 17.5 cm and so errors in the measured angular distributions of about 1.7% might be expected. In the lifetime experiment the centreing of the Germanium detector was very much less critical.

In any target chamber there will always be a certain amount of absorption and scattering of the gamma rays produced in the reaction. The latter effect was believed to be small since tht total mass near the target was kept small. The former effect was most important when the gamma detector was at forward angles. In the angular correlation experiments the transmission of the gamma rays through the target chamber wall was proportional to $(1 - \exp(\frac{-t\tau}{\sin\theta}))$ since for this purpose the target chamber can be considered to have a plane wall of thickness t, which is this case is 0.1 cm. θ is the angle between the beam direction and the gamma detector and τ is the absorption coefficient. For a 1.5 MeV gamma ray the absorption at 30° would be 2.6% whilst at 90° would be 1.3%. The corresponding figures for a 6 MeV gamma ray are 1.3 and 0.7%. These small corrections were usually applied to the measured points. Experimentally, the absorption could be measured by placing a radioactive source at the target position. This procedure was sometimes adopted as an

additional check upon both the centreing of the detector and the absorption by the target chamber.

Most of the targets were prepared by what are now standard techniques: the required substance was evaporated in a vacuum onto a self-supporting Carbon film about 15 μgm. cm^{-2} thick. Some difficulty was experienced in obtaining $W^{18}O$ targets of high isotopic content (Ma 61,64). The Deuterium targets used in the lifetime experiment were manufactured at the Radiochemical Centre, Amersham. A layer of Titanium was vacuum evaporated onto a clean metal blank. Deuterium was taken up by the Titanium layer by heating it in an atmosphere of the pure gas. The thickness of the target layer was determined by weighing and should have been accurate to at least 5%.

2.2 The Electronics

A schematic diagram of the electronics used in NaI(Tl) correlation experiments is shown in Fig. 2.1. The gamma rays incident upon the NaI(Tl) crystal produced light quanta due to the interaction with the impurity centres in the crystal of the electrons produced by the photoelectric effect, pair production, or by Compton scattering of the original

gamma quantum. The resulting light quanta were viewed by an E.M.I. type 9583 photomultiplier tube. After being fed through a Cathode Follower which acted as an impedance matcher, the signals from the crystal were further amplified and then fed into the single channel analyzers and the multichannel analyzer. The main amplifier was of the double delay line type which had the advantage of offering excellent time resolution at the zero cross-over point, particularly at high count rates. The overall amplitude resolution of the system was about 7% for a 2.61 MeV gamma ray. The crystal was stabilized against gain shifts by incorporating a pulsed light source into the crystal housing which was viewed by the photomultiplier tube. If, after all the amplification stages, the height of the pulser peak altered then the photomultiplier tube voltage supply was altered to bring the peak back to its original position. (The box that did this was a development of one reported by (Bl 64)).

The solid state counters which were used were manufactured from slices of n-type silicon which had a p layer at the surface to which electrical contact was made by a thin layer of gold. If the device is reverse biased then there will be a region near to the gold surface depleted

of charge carriers. When an energetic charged particle crosses this region it will interact with the crystal to produce electron-hole pairs which will be swept from the crystal by the applied electric field. The thickness (x) of the depleted layer varies with the applied voltage (V) according to :

$$x = k\sqrt{\rho V} \qquad (2.2.1)$$

where ρ is the resistivity of the n-type material. The resulting signals from the detector were fed into a charge sensitive preamplifier. The signals were further amplified using a double delay line amplifier and were then fed into one of the single channel analyzers. Coincidences were made between the pulses from the two detectors using a circuit which had a resolving time variable from about 10 to 100 nsec although at the lower end of the range long term timing drifts were a nuisance. Random coincidences were made by inserting a 1 μsec delay into either the particle or gamma channel.

The electronics used for the coincidence part of the lifetime experiment is shown schematically in Fig. 2.2. The

gamma rays of interest were detected with a coincidence condition imposed between the NaI(Tl) and Ge(Li) crystals. The germanium crystal detects incident gamma rays by the production of electron hole pairs by the energetic electrons into which the incident gamma ray is converted. These electron hole pairs are removed from the crystal by the applied bias and the resulting signal is fed into a charge sensitive preamplifier. The advantage of Ge(Li) crystal compared with a NaI(Tl) detector is its superior resolution: about 0.5% compared with 7% (Ri 66). The signal from the preamplifier was split between the input of a double delay line amplifier which ensured good time resolution and the input of an R-C amplifier with time constants of 1 μsec which ensured good amplitude resolution. The use of a PDP7 online computer to store the accumulated data considerably facilitated the analysis since a large number of programs were available which could be used at the time of the experiment (Mu 68).

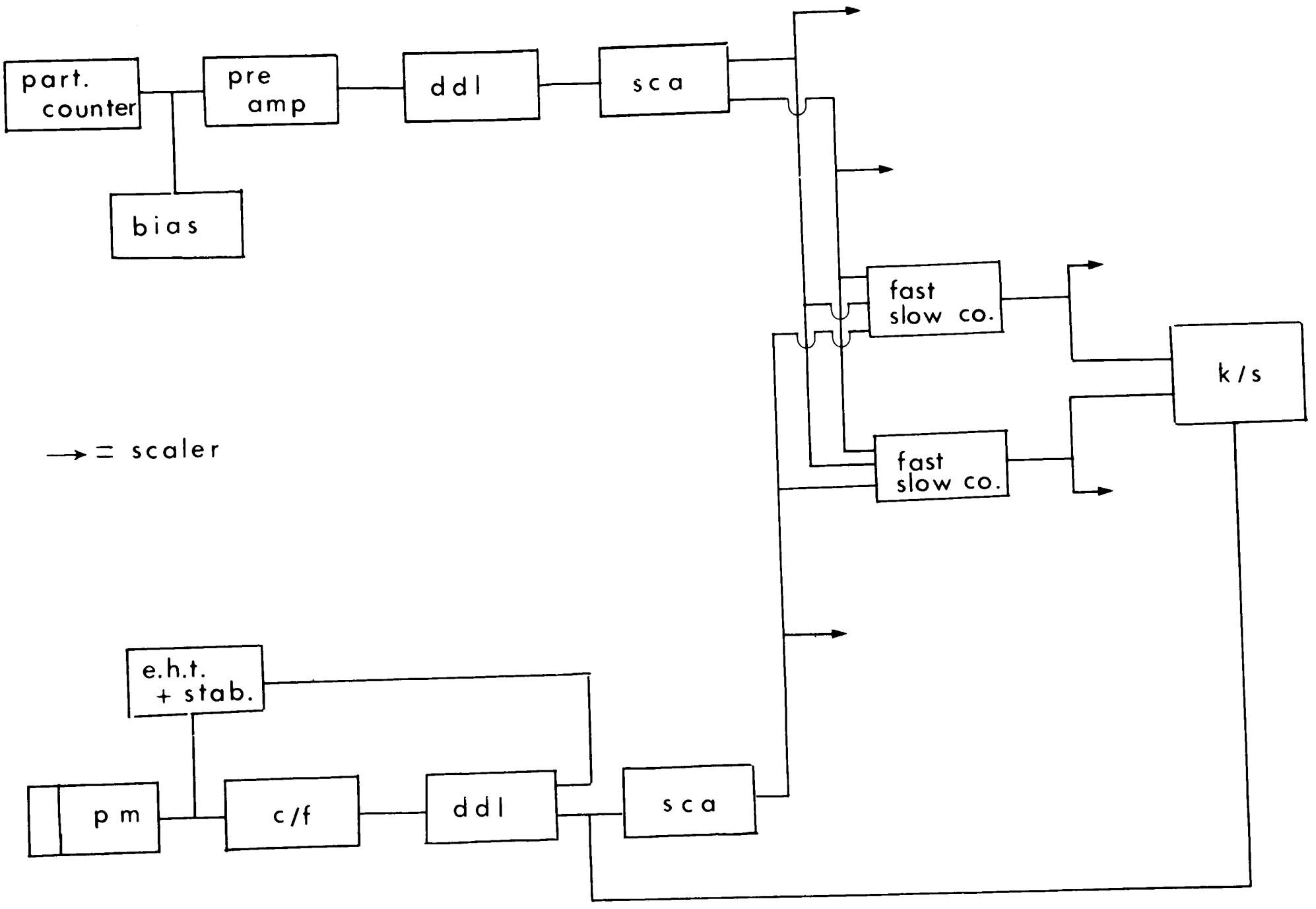

part.
counter
pre
amp
ddl
sca
bias
fast
slow co.
fast
slow co.
k/s
→ = scaler
e.h.t.
+ stab.
p m
c/f
ddl
sca

fig.2.1

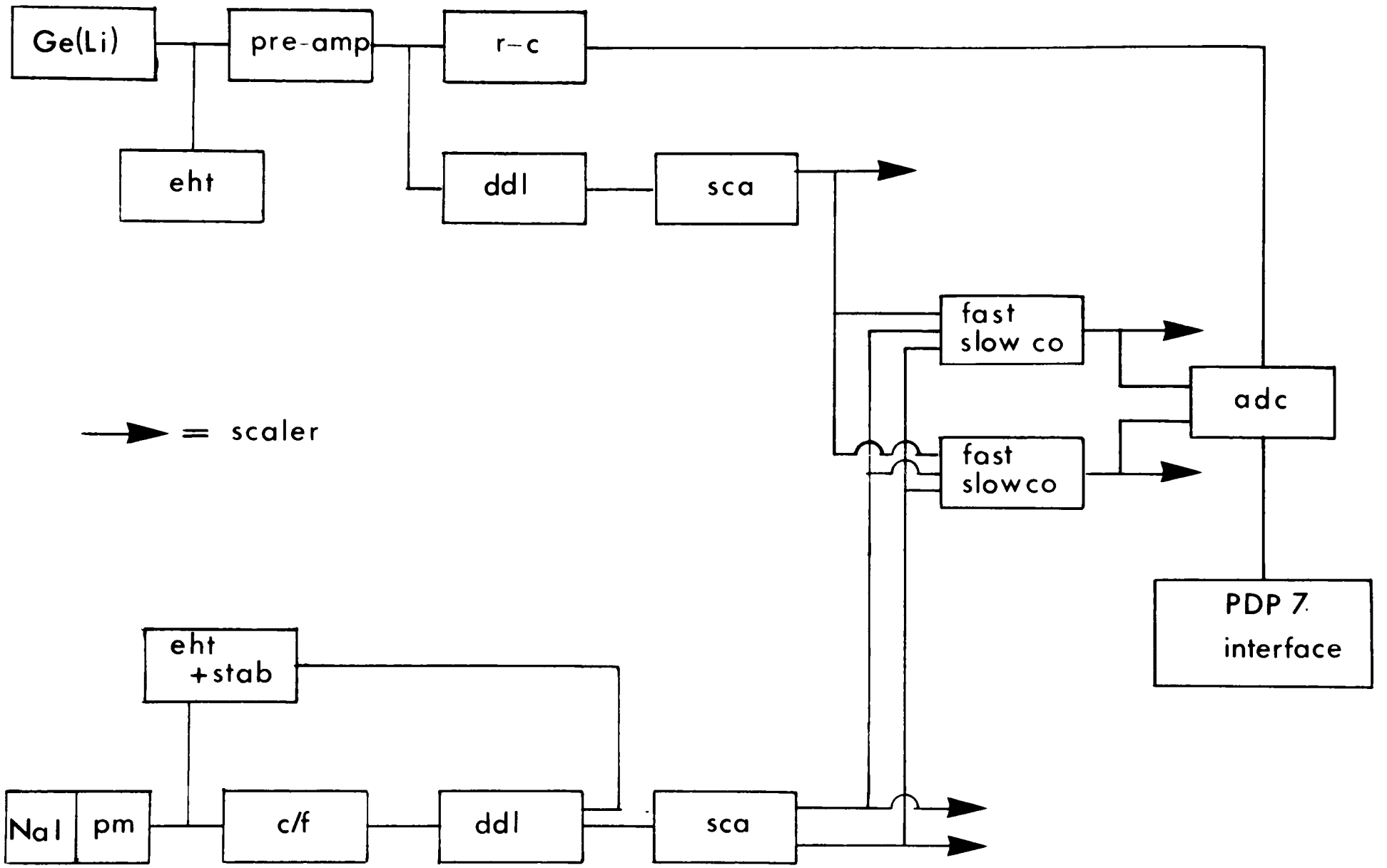

Ge(Li)
pre-amp
r-c
eht
ddl
sca
fast
slow co
adc
fast
slowco
PDP 7
interface
= scaler
eht
+stab
NaI
pm
c/f
ddl
sca

fig. 2.2

C H A P T E R 3

ANGULAR CORRELATION THEORY AND ELECTROMAGNETIC MATRIX ELEMENTS

3.1 The Alignment Condition

In the angular correlation experiments presented in this work, nuclear energy levels were excited in a particle-particle reaction process and the magnetic substates of a particular level were selectively populated by the detection of the outgoing particles from the reaction at nearly 180^{o} with respect to the ingoing beam. The selective population makes it possible to determine level spins and electromagnetic multipole mixing ratios of the de-excitation gamma rays from the particle-gamma angular correlations.

In order to see how the selective population is achieved it is convenient to write down the general scattering amplitudes for a reaction of the sort A(b,c)D. In an uncoupled representation the ingoing channel may be labelled by the set of quantum numbers $(s\ \ell\ \lambda\ \mu\ J\ M\ a)$ where s and ℓ are the spin and orbital angular momenta of the ingoing particles and λ and μ are their projections on a fixed axis. J and M are the spin and magnetic quantum numbers

of the target nucleus and α denotes any further labels which may be required. The corresponding quantities in the outgoing channel will be denoted by primed symbols.

A general expression for the scattering amplitude of the outgoing wave associated with a unit flux incident Coulomb wave may be written (Bu 66; Pr 62) :

$$I^{\alpha'\lambda'M'}_{\alpha\ \lambda\ M}(\underline{k}',\underline{k}) = \frac{2\pi}{ik} \sum_{\substack{\ell\ \lambda \\ \ell'\lambda'}} U_{\alpha'\ell'\mu'\lambda'M';\alpha\ell\mu\lambda M} \times Y_{\ell'\mu'}(\underline{k}')\ Y^{*}_{\ell\mu}(\underline{k}) \qquad (3.1.\ 1)$$

where $\underline{k}$ and $\underline{k}'$ are the propagation vectors of the in- and out-going waves and U is the collision matrix. The angular dependence of the reaction is contained in the spherical harmonics $Y_{\ell\lambda}$ and $\underline{k}$, $\underline{k}'$ are measured in the centre of mass system. When the incident wave is directed along the z axis of the coordinate system the expression above becomes simplified since in this case :

$$Y^{*}_{\ell\lambda}(\underline{k}) = \delta_{\lambda 0} \sqrt{\frac{2\ell+1}{4\pi}} \ . \qquad (3.1.\ 2)$$

Equation (3.1. 1) can be transformed to a representation

in which the spin and orbital angular momenta of the ingoing particles are coupled to (jm) which is then coupled onto the target spin angular momentum to give a total $(J_T\ M_T)$. The following relations are then obeyed:

$$\underline{\ell}+\underline{s} = \underline{j},\quad \underline{j}+\underline{J} = \underline{J}_T,\quad \underline{\ell}'+\underline{s}' = \underline{j}',\quad \underline{j}'+\underline{J}' = \underline{J}'_T,$$

$$\lambda = m,\quad m+M = M_T,\quad \mu'+\lambda' = m',\quad m'+M' = M'_T, \qquad (3.1.\ 3)$$

where $\mu = 0$ because of equation (3.1. 2).

The scattering amplitude of this new representation becomes :

$$I^{a'\lambda'M'}_{a\ \lambda\ M}(\underline{k}') = \frac{\sqrt{\pi}}{ik}\sum\ (2\ell+1)^{\frac{1}{2}}\ (\ell\ s\ 0\lambda/\ jm)(jJmM\ |\ J_TM_T)$$

$$(\ell's'\mu'\lambda'\ /\ j'm')(j'J'm'M'\ /\ J_TM_T)$$

$$U^{J_T}_{a'j'\ell';ajl}\ Y_{\ell'\mu'}(\theta'\phi') \qquad (3.1.\ 4)$$

where the summation is over all quantum numbers which do not appear on the left hand side of the equation. θ' and ϕ' are the angular coordinates of the scattered particle and use has been made of the relations $J_T = J'_T$ and $M_T = M'_T$. The

reaction cross-section for the simplified case in which there is only one ingoing and one outgoing channel is given by :

$$d\sigma^{a'\lambda'M'}_{a\ \lambda\ M} = \left| I^{a'\lambda'M'}_{a\ \lambda\ M} \right|^2 d\Omega_{a'} \qquad (3.1.\ 5)$$

whilst that leading to a particular magnetic substate in the final nucleus may be obtained from this equation by running over the spin orientations of the initial and detected particles. In the case of unpolarised beams and targets :

$$d\sigma^{a'M'}_{a} = \frac{d\Omega_{a'}}{(2s+1)(2\ell+1)} \sum_{\substack{\lambda\lambda' \\ M}} \left| I^{a'\lambda'M'}_{a\ \lambda\ M} \right|^2 \qquad (3.1.\ 6)$$

If the outgoing particles are detected at 180° then the spherical harmonic in equation (3.1. 4) vanishes unless $\mu' = 0$. Inspection of the Clebsch-Gordon coefficients in that equation shows that :

$$M' \leq J + s + s' \qquad (3.1.\ 7)$$

That is, only certain substates of the residual nucleus

will be populated by the particles observed at 180°; a similar argument applies in the 0° case. This equation has also been derived in (Li 61).

For some reactions this inequality can be rather restrictive. In the $^{18}O(p,\alpha)^{15}N$ reaction the target nucleus and the alpha particle have spins of zero whilst the ingoing proton has spin $\frac{1}{2}$ implying that only the $M' = \pm \frac{1}{2}$ substates may be populated by the alpha particles observed at 180°.

Equations (3.1. 4,6) also imply that the populations of the $\pm$ M' magnetic substates will be the same provided that parity is a good quantum number in all reaction channels. This may easily be seen by expanding equation (3.1. 6) using equation (3.1. 4), changing the signs of the magnetic quantum numbers which are summed over and re-arranging the Clebsch-Gordon coefficients. This gives the result :

$$\frac{d\sigma_a^{a'M'}}{d\omega_{a'}} = \frac{d\sigma_a^{a'-M'}}{d\omega_{a'}} \qquad (3.1.\ 8)$$

3.2 The effect of the finite size of the particle detector

The restrictions upon the populations of the magnetic

substates which were stated in the last section are valid for an ideal counter placed at exactly 180° or 0° with respect to the incident beam. In practice, there will be departures from this ideal condition due to the finite size of the particle detector, the effect of which will be to allow the population of substates with higher M' values than those allowed by equation (3.1. 7) and it is important to investigate how large this effect might be.

It can be seen from equations (3.1. 6) and (3.1. 4) that the cross-section for the formation of a particular substate M' is :

$$\frac{d\sigma_{\alpha}^{\alpha' M'}}{d\Omega_{\alpha'}} = \frac{\pi}{k^2(2s+1)(2\ell+1)} \sum \hat{\ell}_1 \hat{\ell} \; (\ell s\, 0\, \lambda | j\, \lambda)(\ell_1 s\, 0\, \lambda | j_1 \lambda)$$

$$\times \; (jJ\, \lambda M \mid J_T M_T)(j_1 J\, \lambda M \mid J_{T_1} M_T)(\ell' s' \mu' \lambda' \mid j' m')$$

$$\times \; (\ell_1' s' \mu' \lambda' \mid j_1' m')(j' J' m' M' \mid J_T M_T)(j_1' J' m' M' \mid J_{T_1} M_T)$$

$$\times \; U^{J_T}_{\alpha' j' \ell'; \alpha j \ell} \; U^{J_{T_1}}_{\alpha' j_1' \ell_1'; \alpha j_1 \ell_1} \; Y_{\ell' \mu'}(\theta' \phi') \; Y_{\ell_1' \mu_1'}(\theta' \phi')$$

(3.2. 1)

where $\hat{\ell} = (2\ell+1)^{\frac{1}{2}}$ and the summation is over all the quantum numbers not appearing on the left hand side. To obtain the measured cross-section leading to a given substate this equation must be integrated over the solid angle subtended by the particle detector. The following integral will be required :

$$I^{\ell'\,\ell'_1}_{\mu'\mu'_1} = \int_{\theta=0}^{2\pi} \int_{\phi=0}^{\varepsilon} Y_{\ell'\mu'}(\theta'\phi')\, Y^{*}_{\ell'_1\mu'_1}(\theta'\phi') \sin\theta'\, d\theta'\, d\phi' \qquad (3.2.\ 2)$$

where ε is the half angle subtended by the particle detector.

Integrating over ϕ gives :

$$I^{\ell'\,\ell'_1}_{\mu'\mu'_1} = \delta_{\mu'\mu'_1}\, \frac{\hat{\ell}'\,\hat{\ell}'_1}{2} \left[\frac{(\ell'-\mu')!\,(\ell'_1-\mu')!}{(\ell'+\mu')!\,(\ell'_1+\mu')!}\right]^{\frac{1}{2}} \int_0^{\varepsilon} P^{\mu'}_{\ell'}(\theta)\, P^{\mu'}_{\ell'_1}(\theta) \sin\theta\, d\theta \qquad (3.2.\ 3)$$

For small values of θ an approximate expression may be used for the associated Legendre functions (Je 66) :

$$P_\ell^\mu(\theta) = \frac{(\ell+\mu)!}{2^\mu\,\mu!\,(\ell-\mu)!}\,(1-\cos^2\theta)^{\mu/2}, \quad \mu \geq 0$$

(3.2. 4)

After carrying out the integration over φ the following expression is obtained for $I^{\ell'\,\ell_1}_{\mu'\mu'_1}$:

$$I^{\ell'\,\ell'_1}_{\mu'\mu'_1} = \delta_{\mu'\mu'_1}\,\varepsilon^{2|\mu|+2}\,\frac{\ell'\,\ell'_1}{(|\mu'|+1)}\left[\frac{(\ell'+|\mu'|)!\,(\ell'_1+|\mu'|)!}{(\ell'-|\mu'|)!\,(\ell'_1-|\mu'|)!}\right]^{\frac{1}{2}}$$

$$\left(|\mu'|!^2 \times 2^{2|\mu'|+2}\right)^{-1} \qquad (3.2.\ 5)$$

The total cross-section for the formation of the substate M' is therefore :

$$\sigma(M') = \varepsilon^2 \sum \varepsilon^{2\times|\mu|}\; C(M'\mu) \qquad (3.2.\ 6)$$

where

$$C(\Lambda'\mu) = \frac{1}{K^2} \sum \frac{\hat{\ell}\ \hat{\ell}_1\ \hat{\ell}'\ \hat{\ell}'_1}{(2s+1)\ (2\ell+1)\ (\ |\mu'|\ +1)\ \mu'!\ \ !\ 2^{-|\mu'|+2}}$$

$$\times \left[\frac{(\ell' + |\mu'|)!\ (\ell'_1 + |\mu'|)!}{(\ell' - |\mu'|)!\ (\ell'_1 - |\mu'|)!}\right]^{\frac{1}{2}} U^{J_P}_{\alpha' J' \ell';\alpha J \ell}\ U^{J_{P_1}}_{\alpha' J' \ell'_1;\alpha J_1 \ell_1}$$

$$(\ell\ s\ \mu\ \lambda\ |\ J\ \lambda)(\ell_1\ s\ \mu\ \lambda\ |\ J_1\ \lambda)(JJ\ \lambda\mu\ |\ J_P\ M_T)(J_1 J\lambda\mu\ |\ J_{P_1}\ M_T)$$

$$(\ell'\ s'\ \mu'\ \lambda'\ |\ J'm')\ (\ell'_1\ s'\ \mu'\ \lambda'\ |\ J'_1\ m')$$

$$(J'J'\ m'M'\ |\ J_P\ M_T)(J'_1 J'\ m'M'\ |\ J_{P_1}\ M_T)$$

(3. 2. 7)

and where the summation is, again, over all quantum numbers not appearing on the left hand side of the equation. If the maximum magnetic quantum number of the final nucleus which may be populated by the particles observed at 180° or 0° is γ then the relative population of the substate $(\gamma+1)$ will be given, to order $\mathcal{E}^2$, by :

$$\omega(\gamma+1) = \frac{\mathcal{E}^2\ C\ (\gamma+1,)}{\sum_{M'\mu} \mathcal{E}^{2|\mu|}\ C(M'\mu)} \qquad (3.2.\ 8)$$

where the bottom line normalises the expression so that :

$$\sum_{m} \omega(m) = 1 \qquad (3.2.9)$$

By inspection of equation (3.2. 7) it can be seen that the dependence of the $C(M'\mu)$ upon M' and μ is contained entirely in the various Clebesch-Gordon coefficients and so an order of magnitude estimate of $\omega(\gamma+1)$ may be made by assuming that all the C coefficients appearing in equation (3.2. 8) are equal. It follows immediately that $\omega(\gamma+1) = \varepsilon^2$. In the experiments described later on, ε was typically about 10° and so it would be expected that the $(\gamma+1)$ substates would have been populated to the extent of about 3 per cent. There will usually be a small correction to this figure due to the fact that the angles measured in the laboratory system will differ slightly from those measured in the centre of mass system.

In cases in which the reaction mechanism is well understood the effect can be calculated in an exact way by calculating the contributing elements of the U^{J_T} matrix. The effect may be investigated experimentally by measuring the gamma angular distributions for differing values of and comparing the resulting distributions.

3.3 Angular Correlation Theory

The probability per unit time for a transition to take place from an initial state $|i\rangle$ to one of a set of final states $|f\rangle$ with a density per unit energy range ρ_f is (Di 58) :

$$\omega_{i \rightarrow f} = \frac{2\pi}{\hbar} \left| \langle f | V | i \rangle \right|^2 \rho_f \qquad (3.3.1)$$

where V is the interaction causing the transition. When the final state includes a plane wave with propagation vector $\underline{k}$ ($k = \frac{2\pi}{\lambda}$) then the density of states will be given by :

$$\rho_f = \frac{L^3 k^2}{\hbar c (2\pi)^3}$$

where L is the dimension of the "box" in which the wave is periodic. If the plane wave in the final state is a photon then the interaction, V, may be obtained from quantum electrodynamics (He 62) and, for cases in which double emission processes are ignored, is given by :

$$V \equiv H_{int} = - \sum_n \frac{e \hbar}{2mc} \left(2 g_{\ell_n} \underline{p}_n \cdot \underline{A}_n + 4 g_{s_n} \underline{\sigma}_n \cdot \underline{H}_n \right) \qquad (3.3.3)$$

where $\underline{H}_n = \underline{\nabla}_n \times \underline{A}_n$, $\underline{p}$ is the momentum operator defined by $\underline{p} = -i\underline{\nabla}$ and $\underline{\sigma}$ is the spin operator with integral eigenvalves. g_{s_n} and g_{ℓ_n} are the gyromagnetic ratios for the spin and orbital angular momenta and the summation is taken over the (n) particles which make up the system. $\underline{A}_n$ is defined by :

$$\underline{A}_n = \left[\frac{2\pi\hbar c}{k L^3}\right]^{\frac{1}{2}} \sum_{\underline{k}\omega} \left(a_{\underline{k}\omega}\, \underline{\varepsilon}_\omega\, e^{i\underline{k}\cdot\underline{r}_n} + a^{+}_{\underline{k}\omega}\, \underline{\varepsilon}^{*}_\omega\, e^{-i\underline{k}\cdot\underline{r}_n}\right) \qquad (3.3.4)$$

where $a_{\underline{k}\omega}$ and $a^{+}_{\underline{k}\omega}$ are the annihilation and creation operators for photons $(\underline{k}\omega)$ with polarisation vectors $\underline{\varepsilon}_\omega$ and $\underline{\varepsilon}^{*}_\omega$ respectively. The probability for the transition $i \rightarrow f$ with the emission of a photon $(\underline{k}\omega)$ may now be calculated from these equations provided that it is remembered that the $a_{\underline{k}\omega}$ and $a^{+}_{\underline{k}\omega}$ operators have eigenvalues 0 or 1 between a state containing no photons and a state containing just one. Only the second part of the $\underline{A}_n$ operator will contribute to the transition probability which will be given by :

$$w_{i \rightarrow f} = \frac{k}{2\pi\hbar} \left| \langle f \mid H_e \mid i \rangle \right|^2$$

where :

$$H_e = - \frac{e\hbar}{2mc} \sum_n \left(2\, g_{l_n}\, \underline{\ell}_n \cdot \underline{\varepsilon}_\omega^*\, e^{-i\, \underline{k}\cdot\underline{r}_n} \right.$$

$$\left. + i\, g_{s_n}\, \underline{\sigma}_n \cdot \left(\underline{\nabla} \times \underline{\varepsilon}_\omega^*\, e^{-i\, \underline{k}\cdot\underline{r}_n} \right) \right)$$

(3.3. 6)

and where the state $\langle f|$ depends only on the coordinates of the particles of the system ($\underline{r}_n$). From inspection of the $\underline{\ell}_n$ operator it is apparent that the operator which will correspond to the absorption of photons will be the hermitian conjugate of that corresponding to emission. It therefore follows that

$$\langle f \mid H_e \mid i \rangle = \langle i \mid H_e^+ \mid f \rangle^* = \langle i \mid H_a \mid f \rangle^*$$

(3.3. 7)

since $H_e = H_a^+$.

Since all observables depend upon the squared modulus of this matrix element all calculations may alternatively be made using the matrix element $\langle i \mid H_a \mid f \rangle$ where :

$$H_a = - \frac{e\hbar}{2mc} \sum_n \left(2\, g_{l_n}\, \underline{\ell}_n \cdot \underline{\varepsilon}_\omega\, e^{i\underline{k}\cdot\underline{r}_n} + \frac{g_{s_n}}{2}\, \underline{\sigma}_n \cdot \left(\underline{\nabla} \times \underline{\varepsilon}_\omega\, e^{i\underline{k}\cdot\underline{r}_n} \right) \right)$$

(3.3. 8)

Before further progress can be made the plane wave $\underline{\varepsilon}_0 e^{i \underline{k}\cdot\underline{r}}$ must be expanded into multipole fields. The details of this process will not be discussed although the result will now be quoted (Mo 67). For a circularly polarised wave $\underline{e}_q e^{i \underline{k}\cdot\underline{r}}$:

$$\underline{e}_q e^{i \underline{k}\cdot\underline{r}} = -\frac{1}{\sqrt{2}} \sum_{L\,M} (q A^{m}_{LM} + A^{e}_{LM}) D^{L}_{Mq}(R) \qquad (3.3.\ 9)$$

where $\underline{e}_q$ is a unit vector, as before, with $q = \pm 1$ and $D^{L}_{Mq}(R)$ is an element of the rotation matrix. (The definition of $D^{L}_{Mq}(R)$ may be found in (Br 62).) The operators A^{m}_{LM} and A^{e}_{LM} are the magnetic and electric parts of the vector field $\underline{A}$ and are defined in the long wave length approximation by :

$$A^{e}_{LM} = \frac{1}{k} \frac{(ik)^{L}}{(2L-1)!!} \left[\frac{L+1}{L}\right]^{\frac{1}{2}} \underline{\nabla} (r^{L} C_{LM})$$

$$A^{m}_{LM} = \frac{1}{(2L-1)!!} \frac{(ik)^{L}}{[L(L+1)]^{\frac{1}{2}}} \underline{\nabla} (r^{L} C_{LM}) \times \underline{r} \qquad (3.3.\ 10)$$

where the C_{LM} coefficients depend only on (θ,ϕ) and are

modified spherical harmonics (Br 62). These expressions can now be inserted into the expression for the absorption operator (equation 3.3. 8) giving :

$$H_a(\underline{k}\,\underline{e}_q) = -\sum_{L\,M} q^M \left[a_L^e \left(Q_{LM} + \omega'_{LM}\right) + a_L^m \left(\Phi_{LM} + M'_{LM}\right)\right] x \; {}^{L}T_{Mq}(\alpha) \qquad (3.3.\ 11)$$

$$a_L^e = \frac{(i\,k)^L}{(2L-1)!!}\left(\frac{L+1}{L}\right)^{\frac{1}{2}}, \quad a_L^m = -\,i\,a_L^e \qquad (3.3.\ 12)$$

where $M = 0$ for electric and 1 for magnetic multipole operators and where the Q's and M's are defined by :

$$Q_{LM} = \frac{2\,\varepsilon_\ell \beta}{k}\,\underline{\nabla}\,(r^L\,C_{LM})\cdot\underline{\nabla}$$

$$\omega'_{LM} = -\,\frac{\varepsilon_s\,\beta}{2}\,\frac{k}{L+1}\,(r^L\,C_{LM})\cdot\underline{\sigma}$$

$$M_{LM} = \frac{2\,\beta\,\varepsilon_\ell}{(L+1)}\,\underline{\nabla}\,(r^L\,C_{LM})\cdot\underline{L}$$

$$M'_{LM} = \frac{\beta\,\varepsilon_s}{2}\,\underline{\nabla}\,(r^L\,C_{LM})\cdot\underline{\sigma} \qquad (3.3.\ 13)$$

where $\underline{L} = \underline{r} \times \underline{p}$ and $\beta = \frac{e\hbar}{2mc}$, the nuclear magneton.

The absorption operator H_a can be put into an even more

compact form using the T^{π}_{LM} operators :

$$T^{0}_{LM} = a^{e}_{L} (R_{LM} + R'_{LM})$$

$$T^{1}_{LM} = a^{m}_{L} (R_{LM} + R'_{LM}) \qquad (3.3.14)$$

Hence :

$$H_{a}(\underline{k}\, \underline{e}_{q}) = - \sum_{\pi\, M\, L} q^{\pi}\; T^{\pi}_{LM}\; D^{L}_{Mq}\,(R) \qquad (3.3.15)$$

The operators T^{π}_{LM} are defined so that they have well defined properties under rotations time reversal and Hermitian conjugation.

It is now convenient to define a probability amplitude, $A^{q}_{M_1M_2}(\underline{k})$, for emission of a photon $(\underline{k}\, \underline{e}_{q})$ following the decay of the state $|J_1M_1\rangle$ to $|J_2M_2\rangle$ where J is the total angular momentum of the state and M its projection onto a fixed axis.

$$A^{q}_{M_1M_2}(\underline{k}) = \sqrt{\frac{k}{2\pi\hbar}}\; \langle i |\, H_a\, | f\rangle \qquad (3.3.16)$$

which is related to the probability $\omega_{i \to f}$ by

$$\omega_{i \to f} = \left| A^{q}_{M_1 M_2}(\underline{k}) \right|^2 \qquad (3.3.17)$$

When the initial state $|J_1 M_1\rangle$ has cylindrical symmetry then the probability of observing a photon with quantum numbers $(\underline{k}\ \varepsilon_q)$ is

$$P(\underline{k}\ \varepsilon_q) = \sum_{M_1 M_2} \omega(M_1) \left| A^{q}_{M_1 M_2}(\underline{k}) \right|^2 \qquad (3.3.18)$$

where the sum runs over M_2 because the final orientation of the state $|J_1\rangle$ is not observed. The summation also runs over q if a polarisation insensitive measurement is made. $\omega(M_1)$ is the relative population of the initial substate M_1 and, for a cylindrically symmetric initial state, is defined by :

$$\sum_{M_1} \omega(M_1) = 1, \quad \omega(M_1) = \omega(-M_1), \quad \omega(M_1) \geq 0 \qquad (3.3.19)$$

Equation (3.3. 18) can be used to calculate the angular correlation following the decay of the aligned state $|J_1\rangle$. The resulting formula are presented in the next section. The probability amplitudes $A^{q}_{M_1 M_2}(\underline{k})$

can also be used to calculate the correlation of a cascade gamma ray from the initial state provided that the intermediate gamma rays are unobserved. If more than one gamma ray is observed then this procedure breaks down since the intermediate states of the cascade can no longer be described in terms of the population parameters $\omega(M)$. The exception to this is provided by the gamma-gamma correlation in which the initial substate is randomly populated. In this case the observation of the first gamma ray defines the axis of cylindrical symmetry allowing the intermediate state to be described by the population parameters. More general correlations require the use of density matrix methods (Di 58; Li 61) and will not be further mentioned.

3.4 The Angular Correlation Formulae

The formula appropriate to the angular correlation experiments presented in the next chapter have been derived in a phase consistent way in (Ro 67) where the definitions of all the quantities are identical to those of the previous section. Formula (3.41) of (Ro 67) relates the measured gamma ray angular distributions to the population parameters

of the initial level, to the multipole mixing ratio of the de-excitation gamma ray and to the initial (J_1) and final (J_2) level spins. The distribution is given by :

$$W(\theta) = \sum_{\substack{L\,L' \\ \pi\,\pi' \\ k\,\text{even}}} \frac{B_k(J_1)\, H_k\,(LL'J_1J_2)\, \delta_L^{\pi}\, \delta_{L'}^{\pi'}\, P_k(\cos\theta)}{\sum_L \left|\delta_L^{\pi}\right|^2} \qquad (3.4.\ 1)$$

where $P_k(\cos\theta)$ is the Legendre polynomial of order k, θ is the angle between the axis of cylindrical symmetry and the gamma ray detector and :

$$B_k(J_1) = \sum_{M_1} \omega(M_1)\, (-)^{J_1-M_1}\, \hat{J}_1 (J_1 J_1 M_1 -M_1 \mid k\ 0)$$

$$B_0(J_1) = 1\ , \quad \sum_{M_1} \omega(M_1) = 1, \quad \omega(M_1) = \omega(-M_1)\ , \qquad (3.4.\ 2)$$

$$H_k(LL'J_1J_2) = (-)^{1+J_1-J_2+L'+L+k}\ \hat{J}_1 \hat{L} \hat{L}'$$

$$(LL'1-1 \mid k\ 0)\ W(J_1J_1LL' \mid k\ J_2) \qquad (3.4.\ 3)$$

and $$\delta_L^{\pi} = \frac{\langle J_1 \parallel T_L^{\pi} \parallel J_2\rangle\ \hat{L}_0}{\langle J_1 \parallel T_{L_0}^{\pi_0} \parallel J_2\rangle\ \hat{L}}\ . \qquad (3.4.\ 4)$$

In this last equation L_o is the lowest order multipolarity possible for the transition $J_1 \rightarrow J_2$ and the reduced matrix elements of the T_{LM}^{π} operators defined in the previous section appear as $\langle J_1 \| T_L^{\pi} \| J_2 \rangle$. δ_L^{π} is known as the multipole mixing ratio when $L \neq L_o$.

A more general formula (equation 3.46 of (Ro 67)) may be derived for cascade gamma rays with the initial state $|J_1\rangle$ aligned and the intermediate gamma rays unobserved. For the case of a general cascade $J_1 \rightarrow J_2 \rightarrow \ldots\ldots \rightarrow J_r \rightarrow J_{r+1}$, the angular distribution of the r^{th} gamma ray would be :

$$W(\theta) = \sum_{k \text{ even}} B_k(J_1) \left[\prod_{i=1}^{i=r-1} U_k(J_i J_{i+1}) \right] F_k(J_r J_{r+1}) P_k(\cos \theta_r) \qquad (3.4.5)$$

where

$$U_k(JJ') = \frac{\sum_{\pi} (\delta_L^{\pi})^2 (-)^k \frac{W(JJ'JJ' \mid Lk)}{W(JJ'JJ' \mid Lo)}}{\sum_{L} (\delta_L^{\pi})^2} \qquad (3.4.6)$$

and

$$F_k(JJ') = \sum_{\substack{LL' \\ \pi\pi'}} \frac{R_k(LL'JJ') \, \delta_L^{\pi} \, \delta_{L'}^{\pi'}}{\sum_{L} (\delta_L^{\pi})^2} \qquad (3.4.7)$$

The ratio of the two Racah coefficients together with the phase factor which both appear in equation (3.4. 6) are denoted by $U_k(L\ JJ')$ and the quantity $(-)^{J_1-M_1}\ \hat{J}_1 \times (J_1 J_1\ M_1-M_1 \mid k\ 0)$ is denoted by the symbol $\rho_k(J_1 M_1)$ and is tabulated in (Ro 67) together with $R_k(LL'\ JJ')$ and $U_k(L\ JJ')$.

The above formulae imply certain triangular restrictions upon the various angular momenta which will limit the complexity of any observed correlation. Some of the more useful restrictions are listed below.

(i) The ρ_k coefficients imply the triangular condition $\Delta(J_1 J_1\ k)$ and so the maximum Legendre coefficient which may be observed is $k_{max} = 2J_1$. If $J_1 = 0$ or $\frac{1}{2}$ then $k_{max} = 0, 1$ and so all distributions are isotropic since k is restricted to even values.

(ii) The U_k coefficients contain the conditions $\Delta(J_i\ J_{i+1}\ L)$, $\Delta(J_i\ J_i\ k)$, $\Delta(J_{i+1}\ J_{i+1}\ k)$. The latter two conditions imply $k_{max} = 2J_i$ or $2J_{i+1}$ whichever is the smaller. Again, the distributions will be isotropic if either J_i or J_{i+1} is 0 or $\frac{1}{2}$.

(iii) The R_k coefficients contain the restrictions :

$\Delta(LL'\ k)$, $\Delta(J_r J_r\ k)$, $\Delta(J_r J_{r+1} L')$, and $\Delta(J_r J_{r+1}\ L)$. The second of these conditions is similar to the one mentioned in (i). The first condition implies that $k_{max} < (L + L')$ where L and L' are the multipolarities contributing to the transition. It should be noted that the different conditions should be taken in conjunction.

3.5 The Finite Size of the Gamma ray Detector

If an angular correlation is measured using a gamma ray detector of finite size then the observed anisotropy will be smaller than would be theoretically expected. This effect may easily be estimated by calculating correction coefficients for the coefficients of the Legendre polynomials given by the theoretical formula (No 53).

In Fig. 3.2 a cylindrical gamma ray detector is shown with radius r, length ℓ and mounted with its axis passing through the (point) source and with its front face a distance h from that source. The absorption of a gamma ray incident on the crystal is proportional to $(1 - e^{-x\tau})$, where τ is the total absorption coefficient per unit path length and x is the possible maximum path length of

the gamma ray in the crystal and is given by :

$$x = \frac{\ell}{\cos \omega} \quad \text{for} \quad \omega \leq \tan^{-1}\left(\frac{r}{h + \ell}\right)$$

and

$$x = \frac{r}{\sin \omega} - \frac{h}{\cos \omega} \quad \text{for} \quad \tan^{-1}\left(\frac{r}{h+\ell}\right) \leq \omega \leq \tan^{-1}\left(\frac{r}{h}\right)$$

(3.5. 1)

If the true correlation is given by the function:

$$W(\omega) = N \sum a_k P_k (\cos \omega) \qquad (3.5. 2)$$

then the measured one will be

$$W'(\omega) = \frac{\int W(\omega') (1 - e^{-x\mu}) \, d\omega'}{\int (1 - e^{-x\mu}) \, d\omega'} \qquad (3.5. 3)$$

where $d\omega'$ is the appropriate solid angle element and N is a normalisation constant. On evaluating equation (3.5. 3) integrals over $d\omega'$ will appear of the form :

$$I_k = \int P_k(\cos \omega') \, (1 - e^{-x\tau}) \, d\omega' \qquad (3.5.\ 4)$$

This integral may be simplified using the relation (Br 62):

$$P_k(\cos \omega') = \sum_q C_{kq}(\epsilon,0) \, C^*_{kq}(\omega,\omega') \qquad (3.5.\ 5)$$

Hence :

$$I_k = \sum_q \int C_{kq}(\epsilon,0) C^*_{kq}(\omega,\omega')(1-e^{-x\tau}) \sin \omega \, d\omega \, d\omega'$$

Integration with respect to ω' yields :

$$I_k = 2\pi \, P_k(\cos \omega) \int P_k(\cos\omega)(1-e^{-x\tau}) \sin \omega \, d\omega \qquad (3.5.\ 6)$$

The measured distribution, $W'(\omega)$, may therefore be written as

$$W'(\omega) = N \sum a_k \, a_k \, P_k \, (\cos \omega) \qquad (3.5.\ 8)$$

where $a_k = I'_k/I_0$ and $I'_k = \dfrac{I_k}{P_k \, (\cos \omega)}$

The experimental distributions will be predicted correctly

by the theoretical formulae if the a_k coefficients are multiplied by the appropriate Q_k coefficients. Tables of Q_k coefficients have been prepared for both Sodium Iodide (Ru 59) and Lithium drifted Germanium (Ha 66) detectors of various sizes.

3.6 Data Reduction and Fitting Procedures

In a typical angular correlation experiment, coincidence spectra are obtained for each level studied at each of several angles. The spectra are usually complex and the decay scheme of the level is obtained by adding a suitable selection of the spectra together. If measurements are taken for equivalent times at various angles θ_j then the appropriate sum for a given channel would be :

$$C_i = \frac{\sum_j c_{ij} \sin \theta_j}{\sum_j \sin \theta_j} \qquad (3.6.1)$$

where C_i and c_{ij} correspond to the contents of the i^{th} channel in the summed and individual spectra after the subtraction of random coincidences. Each spectrum is

weighted by a solid angle factor. Although, in practice, the summing procedure was somewhat approximate, significant errors did not arise from this source in the extraction of the branching ratios (for example, two spectra at 90° would be included for each one at 30° etc.). When the summed spectrum had been obtained in this fashion it was then decomposed into its constituent gamma rays using lineshapes previously accumulated for the Na I (Tl) crystal together with the measurements of (Ja 62). The relative branching ratios were extracted by finding the number of counts in the photopeaks of the gamma rays and correcting for the varying photopeak efficiency with energy (Ja 62). A schematic spectrum decomposed in this way is shown in the upper part of Fig. 3.1. The random coincidences have already been subtracted.

The next step in the treatment of the data is to extract from each individual run the number of events corresponding to a definite gamma ray, allowing for the possible contamination by other gamma rays. The scanning locations and recipe for this procedure are decided from inspection of the summed spectrum. The channel limits are shown in Fig. 3.1. The number of events included in the γ2 summing

window which are due to γ_1 is denoted by $a_{21}\ C_1$ where C_1 is the number of events due to gamma ray number one and is

$$C_1 = S_1 - B_1 \qquad (3.6.2)$$

where B_1 is the appropriate number of random coincidences which is obtained from the random spectrum which is shown in the lower part of Fig. 3.1. S_1 is the total number of counts in the γ_1 window in the experimentally obtained spectrum. The corrected number of counts of $\gamma 2$ is therefore :

$$C_2 = S_2 - B_2 - a_{21}\ C_1 \qquad (3.6.3)$$

and for the i^{th} gamma ray :

$$C_i = S_i - B_i - \sum_{j=1}^{j=i-1} a_{ij}\ C_j \qquad (3.6.4)$$

The error in C_i will be given by

$$E_i^2 = S_i + B_i + \sum_{j=1}^{j=i-1} a_{ij}\ C_j \qquad (3.6.5)$$

which is just the error determined by the statistics (Poisson) of the process. This last equation is not in fact quite correct since the errors in C_j have been neglected. However, if the a's are relatively small compared with one (which they usually are) and if the errors in the C_j's are not very different from $(C_j)^{\frac{1}{2}}$ (which they are usually not), then the estimate of E_i given by equation (3.6. 5) should prove to be rather a reasonable one.

There will usually be errors in the a_{ij} since these reflect the accuracy of the decomposition of the summed spectrum. These errors will vary tremendously from case to case and are not amenable to a general treatment. They have been taken into account where necessary.

In order to find the values of the spins, mixing ratios and, where appropriate, the population parameters which are consistent with the measured angular distributions it is convenient to calculate the value of χ^2 for each set of these values. If measurements Y_i with errors E_i are made at angles θ_i and if the theoretical distribution is $W(\theta) = \sum a_k P_k(\cos \theta)$ then the value of χ^2 is defined by :

$$\chi^2 = \sum_i^2 \frac{\left[Y_i - N \sum \alpha_k a_k P_k(\cos \theta_i) \right]^2}{} \qquad (3.6.6)$$

where N is an arbitrary normalization coefficient and the α_k's are the gamma ray attenuation coefficients defined in Section 3.5. For a given set of spin values the theoretical formula will depend upon mixing ratios and possibly the population parameters. The procedure adopted was to calculate χ^2 for stepped values of the continuous parameters and determine the normalisation constant, N, by imposing the condition

$$\frac{\partial \chi^2}{\partial N} = 0 \qquad (3.6.7)$$

In some cases the population parameter was determined from the further condition

$$\frac{\partial \chi^2}{\partial p} = 0 \qquad (3.6.8)$$

The possible solutions were determined from the minima of the function χ^2 which, for a correct hypothesis (i.e.,

set of spins, mixing ratios and population parameters) has an expectation value equal to the number of degrees of freedom, n, of the system which, in this case, would be the number of measurements (Y_i) minus the number of variables determined by minimisation. If the initial hypothesis is correct then the probability that the value of χ^2/n (which is the value always quoted for "χ^2" herein) should exceed a particular value may be found from various tables and graphs (e.g., We 57, Wa 62) and if the value of χ^2/n calculated from equation (3.6. 6) is less than this value then the solution is acceptable. The choice of the probability level at which solutions begin to become acceptable is, to some extent, arbitrary. Usually the 0.05 probability level (or confidence limit) is regarded as significant whilst the 0.01 level is said to be "most significant". The latter value has been adopted.

The measured distributions were also fitted to Legendre polynomials of even order (Lo 66). It was found convenient to estimate the errors of the mixing ratios from the errors of the Legendre polynomial coefficients. The values of the latter quoted in the text are always uncorrected for the finite size of the gamma ray detector except where explicitly stated.

3.7 Calculation of electromagnetic transition matrix elements

The wavefunctions of a spin ½ particle with orbital angular momentum ℓ, principal quantum number n and total angular quantum numbers (j,m) may be written :

$$|\ell\ n\ j\ m\rangle = \sum_{m_\ell} i^\ell R_{n\ell}(r)\ (\ell\ \tfrac{1}{2}\ m_\ell\ \ -m_\ell\ |\ jm)\ |\tfrac{1}{2}\ m-m_\ell\rangle$$

$$Y_{\ell m_\ell}(\theta,\phi) \qquad (3.7.1)$$

where $R_{n\ell}(r)$ is the radial part of the wavefunction for a spherical harmonic oscillator well (Ma 55) and $Y_{\ell m_\ell}(\theta,\phi)$ is the spherical harmonic (Co 35). The factor i^ℓ is included in the definition to give the wavefunctions the following behaviour under time reversal (Mo 67) :

$$\theta\ |\ell\ n\ j\ m\rangle = (-)^{j-m}\ |\ell\ n\ j\ m\rangle \qquad (3.7.2)$$

where θ is the time reversal operator.

The reduced matrix elements of the $T^{\#}_{LM}$ operators may be calculated using the definitions of Section 3.3 obtaining, for the electric operators :

$$\langle \ell_1 n_1 j_1 \| T_L^e \| \ell_2 n_2 j_2 \rangle = (-)^{\frac{1}{2}(\ell_1 - \ell + L + 2j_1 - 2)} \frac{e\ell\ell^L}{(2L-1)!!} \left[\frac{L+1}{\pi}\right]^{\frac{1}{2}}$$

$$\hat{j}_2 \hat{L} \; (j_1 j_2 \tfrac{1}{2}-\tfrac{1}{2} \,|\, L\,0) \; I(L\,\ell_1\ell_2 n_1 n_2) \qquad (3.7.3)$$

while for the magnetic operators :

$$\langle \ell_1 n_1 j_1 \| T_L^m \| \ell_2 n_2 j_2 \rangle = (-)^{\frac{1}{2}(\ell_1 - \ell + L + 2j_1)} \frac{\beta k^L \hat{j}_2}{2L-1\,!!\,\hat{L}}$$

$$\frac{I(L-1\;\ell_1\ell_2 n_1 n_2)}{\sqrt{2}} \left\{ 2g_\ell \hat{\ell}_1 \hat{\ell} \left[\ell(\ell_2+1)L\right]^{\frac{1}{2}} \right.$$

$$\times (j_1 \ell_1 j_2 \ell_2 \,|\, \tfrac{1}{2}\,L)(\ell_1\ell_2\,0\,1\,|\,L\,1)$$

$$- \frac{g_s\sqrt{L+1}}{2}\left[L-(\ell_1-j_1)(2j_1+1)-(\ell_2-j_2)(2j_2+1)\right]$$

$$\left. (j_1 j_2 \tfrac{1}{2}-\tfrac{1}{2} \,|\, L\,0) \right\} \qquad (3.7.4)$$

where $I(L\,\ell_1\ell_2 n_1 n_2)$ is the radial integral defined by :

$$I(L\ell_1\ell_2 n_1 n_2) = \int R_{n_1\ell_1} R_{n_2\ell_2} r^{L+2}\, dr \qquad (3.7.5)$$

The contribution to the reduced electric matrix element due to $\mathcal{H}'_{LM}$ (see equation 3.3. 13) has been neglected since it is always much smaller than that due to $\mathcal{H}_{LM}$. When the formulae above are used the initial state should always be written on the left hand side of the reduced matrix element if the calculated quantities (i.e., mixing ratios) are to be in accord with the phase consistent angular correlation theory.

The lifetime of a state $|\ell_1 n_1 J_1\rangle$ decaying to the state $|\ell_2 n_2 J_2\rangle$ is given by :

$$\frac{1}{\tau} = \frac{4k}{\hbar} \sum_{L\ \pi} \frac{\left|\langle \ell_1 n_1 J_1 \| T^{\pi}_{L} \| \ell_2 n_2 J_2 \rangle\right|^2}{\hat{L}} \qquad (3.7.\ 6)$$

and the mixing ratio is :

$$\delta = \frac{\langle \ell_1 n_1 J_1 \| T^{\pi}_{L} \| \ell_2 n_2 J_2 \rangle}{\langle \ell_1 n_1 J_1 \| T^{\pi'}_{L'} \| \ell_2 n_2 J_2 \rangle} \frac{\hat{L}'}{\hat{L}} \qquad (3.7.\ 7)$$

Usually only two different order multipole matrix elements will contribute to a given transition and the relation $L = L' + 1$ will hold.

In order to calculate the transition matrix elements between states which may be described as n particle - q hole configurations it is convenient to introduce the second quantised operator formalism (Bi 58; Br 56). A particle state $|\ell\, n\, j\, m\rangle$ may be created from the vacuum state $|o\rangle$ or a closed shell $|C\rangle$ by the application of the operator $a^{+}_{\ell njm}$ assuming that the state $|\ell njm\rangle$ does not belong to $|C\rangle$ in the latter case.

$$\text{i.e.,} \quad |\ell\, n\, j\, m\rangle = a^{+}_{\ell njm}\, |C\rangle$$

$$\text{or} \quad |\ell\, n\, j\, m\rangle = a^{+}_{\ell njm}\, |o\rangle \qquad (3.7.\ 8)$$

A hole state $|\ell njm\rangle$ may be created from the closed shell using the operator $(-)^{j-m}\, a_{\ell nj-m}$

$$\text{i.e.,} \quad |\ell\, n\, j\, m\rangle_{\text{hole}} = (-)^{j-m}\, a_{\ell\, j-m}\, |C\rangle \qquad (3.7.\ 9)$$

The phase $(-)^{j-m}$ is introduced to give the hole states proper behaviour upon rotation of the coordinate system and on application of the time reversal operator. For particles which satisfy Fermi statistics the a and a^{+}

operators have the following commutation rules :

$$a^{+}_{\alpha}\, a_{\beta} + a_{\beta}\, a^{+}_{\alpha} = \delta_{\alpha\beta}$$

$$a^{+}_{\alpha}\, a^{+}_{\beta} + a^{+}_{\beta}\, a^{+}_{\alpha} = 0 \qquad (3.7.10)$$

It is therefore clear that a general many particle wave-function of the form $\prod_i a^{+}_i \,|C\rangle$ will be completely anti-symmetric upon interchange of particles. The operators have the further properties :

$$a_{\alpha}\,|C\rangle = 0 \qquad \langle C|\, a^{+}_{\alpha} = 0$$

$$(a_{\beta}\,|C\rangle)^{\dagger} = \langle C|\, a^{+}_{\beta} \qquad (3.7.11)$$

where the quantum number α refers to a state which is not occupied in the closed shell. If α refers to an occupied state then :

$$a^{+}_{\alpha}\,|C\rangle = 0 \qquad \langle C|\, a_{\alpha} = 0 \qquad (3.7.12)$$

An operator which is a function of the individual

particle coordinates (r_i) of a system of the form :

$$V = \sum_i V(r_i) \qquad (3.7.13)$$

may be expanded in terms of the a and a^+ operators as follows (D1 58) :

$$V = \sum_{\alpha\beta} \langle \alpha | V | \beta \rangle \; a^+_\alpha a_\beta \qquad (3.7.14)$$

In the case of the T^w operators this equation takes the form

$$T^w_{LM} = \sum_{\alpha\beta} \langle j_\alpha m_\alpha | T^w_{LM} | j_\beta m_\beta \rangle \; a^+_{j_\alpha m_\alpha} a_{j_\beta m_\beta}$$

$$= \sum_{\alpha\beta} \langle j_\alpha \| T^w_L \| j_\beta \rangle \; (j_\beta L m_\beta M | j_\alpha m_\alpha) \; a^+_{j_\alpha m_\alpha} a_{j_\beta m_\beta} \qquad (3.7.15)$$

where the Wigner-Eckart theorem has been used and the quantum numbers (ℓ n) have been dropped since this usually

leads to no confusion. The reduced matrix elements appearing in the equation are identical to those defined by equations (3.7. 3,4).

The foregoing treatment applies to a system of similar particles but may be readily extended to a mixed system of, say, protons and neutrons, by the introduction of another set of operators (b^{+}_{α}, b_{β}) for the neutrons which will have the same properties as the a operators and will commute with them.

The T^{*}_{LM} operators in this mixed case may be written :

$$T''_{LM} = \sum_{\alpha\beta} (j_\beta \; m_\beta \; M \;\; | \;\; j_\alpha \; m_\alpha)$$

$$\times \left\{ \langle j_\alpha \,\|\, T^{*}_{L}(p) \,\|\, j_\beta \rangle \;\; a^{+}_{j_\alpha m_\alpha} \, a_{j_\beta m_\beta} \right.$$

$$\left. + \;\; \langle j_\alpha \,\|\, T^{*}_{L}(n) \,\|\, j_\beta \rangle \;\; b^{+}_{j_\alpha m_\alpha} \, b_{j_\beta m_\beta} \right\} \quad (3.7.16)$$

where the p and n labels refer to a proton and a neutron respectively. The matrix elements between complicated particle-hole states can now be calculated.

In the case of one particle-one hole excitations of

a doubly closed shell $|\rangle$ a fully antisymmetric [illegible] wavefunction may be written

$$\left|JM(j_a j_b)\right\rangle = \frac{1}{\sqrt{2}} \sum (j_a j_b\, m_a m_b \mid JM)\,(-)^{j_b - m_b}$$

$$\left[\, a^{+}_{j_a m_a}\, a_{j_b - m_b} + b^{+}_{j_a m_a}\, b_{j_b - m_b} \,\right] |C\rangle \qquad (3.7.17)$$

where the particle is in the state $|j_a m_a\rangle$ and the hole in $|j_b m_b\rangle$. The reduced matrix elements of the T^{M}_{LM} operator between this state and the closed shell, C , may be calculated and are :

$$\left\langle J(j_a j_b) \left\| T^{M}_{L} \right\| C \right\rangle = - \frac{\hat{L}\hat{J}}{\sqrt{2}} \frac{\hat{j}_a}{\hat{L}}$$

$$\left[\left\langle j_a \left\| T^{M}_{L}(p) \right\| j_b \right\rangle + \left\langle j_a \left\| T^{M}_{L}(h) \right\| j_b \right\rangle \right] \qquad (3.7.18)$$

The reduced matrix elements between the two one particle-one hole states $|JM(j_a j_b)\rangle$ and $|J'M'(j_c j_d)\rangle$ are :

$$\langle J(J_a J_b) \| T_L^M \| J'(J_c J_d) \rangle =$$

$$\frac{1}{2} \times \hat{J}' \left[\hat{J}_a (-)^{J_b+J_c-J_b} \delta_{J_b J_d} W(J_a J_c J J' | L J_c) M_L^M (J_a J_c) \right.$$

$$\left. - \hat{J}_d (-)^{J'+J_a-J_d} \delta_{J_a J_c} W(J_b J_d J J' | L J_a) M_L^M (J_d J_b) \right] ,$$

where $M_L^M(J_a J_c) = \langle J_a \| T_L^M(p) \| J_c \rangle + \langle J_a \| T_L^M(n) \| J_c \rangle$

(3.7. 19)

By applying a hole operator to the one-particle-one-hole operator of the previous paragraphs a properly antisymmetric two-hole-one-particle wavefunction may be constructed. The parent one-particle-one-hole configuration has been taken to be $T = 0$ and so the final state will have $T = \frac{1}{2}$ and correspond to a neutron or proton deficiency in the closed shell according to whether the b or the a operator is used. The state produced by applying a proton hole operator to the one-particle-one-hole state above is :

$$|J_f M_f (J_a J_b J_c)\rangle = N \sum_{m_a m_c} (j_c\ J\ m_c\ M\ |\ J_f M_f)(J_a J_b m_a m_b\ |\ J\ M\ )$$

$$(-)^{J_a+J_c-m_a-m_c}\ a_{j_c-m_c}\left\{a^+_{J_a m_a}\ a_{j_b-m_b} + b^+_{J_a m_a}\ b_{j_b-m_b}\right\}\ |c\rangle$$

(3.7. 20)

where N is the normalisation coefficient and is given by :

$$N^2 = 2 - \delta_{j_b j_c}\ (-)^{J_f+j_a}\ \hat{J}\ W(j_c j_a J_f j_c\ |\ JJ) \qquad (3.7.\ 21)$$

J is the angular momentum of the intermediate one-particle-one-hole state which is formed from the vector addition of the particle (j_a) and hole (j_b) angular momenta. The angular momentum of the final state is J_f which is formed by coupling J and the angular momentum (j_c) of the proton hole operator. The wavefunction above will correspond to an excited state of a system of which the ground state will be described by a single hole, the wavefunction of which will be :

$$\left|J_d m_d\right\rangle = (-)^{j_d - m_d} a_{j_d - m_d} \left|0\right\rangle \qquad (3.7.\ 22)$$

This wavefunction is already properly normalised to 1.

The reduced matrix elements of the T_{Lm}^{W} operator between the states given by equations (3.7. 20) and (3.7. 22) are :

$$\left\langle J_f (j_a j_b j_c) \right\| T_L^W \left\| J_d \right\rangle = N \left\{ (-)^{j_a + j_c + j_a + j_f + 1} \delta_{j_b j_d} \hat{J} \hat{j}_a \right.$$

$$\times W(j_b j_a J_f j_c \mid J\ L) \left\langle j_a \right\| T_L^W(p) \left\| j_c \right\rangle$$

$$- \frac{\hat{j}_a}{\hat{L}} \delta_{j_c j_d} \delta_{JL} \left\langle j_a \right\| T_L^W(p) \left\| j_L \right\rangle$$

$$\left. - \frac{\hat{j}_a}{\hat{L}} \delta_{j_c j_b} \delta_{JL} \left\langle j_a \right\| T_L^W(n) \left\| j_b \right\rangle \right\} \qquad (3.7.\ 23)$$

where N is given by equation (3.7. 21) and the initial state $\left|J_f M_f (j_a j_b j_c)\right\rangle$ has been written on the left hand side of the matrix element in the appropriate way.

If the initial and final states were a neutron hole

coupled to a one-particle-one-hole intermediate state and a single neutron hole state then the reduced matrix elements could be identical to those above but with the label p replacing n and vice versa.

The evaluation of the electric reduced matrix elements requires a certain amount of care (So 66). The appropriate operator is

$$T^{e}_{LM} \propto \nabla (r^{L} C_{LM}) \cdot \underline{p}$$

which may be replaced by the equivalent form

$$T^{e}_{LM} \propto [\, H, r^{L} C_{LM} \,]$$

The matrix elements of this operator between the single particle states $(j_i m_i)$ and $(j_f m_f)$ corresponding to the transition j_i to j_f will be proportional to

$$(E_i - E_f) \quad \langle j_i m_i \,|\, r^{L} C_{LM} \,|\, j_f m_f \rangle$$

In cases in which the state i has higher energy than the state f the factor $(E_i - E_f)$ is positive and so the operator

$r^L C_{Lh}$ may be used as it stands to calculate the matrix elements of the $T^{\bullet}_{Lh}$ operator. However, if the reverse were true then an extra negative sign would have to be inserted into the expression for the matrix element as calculated using the $r^L C_{Lh}$ operator in order to compensate for the change of sign of the $(E_i - E_f)$ factor. In the case of the one particle-one hole reduced matrix elements it can be seen that in the part of the matrix element which corresponds to the particle transition $(j_a j_b) \rightarrow (j_c j_b)$ the reduced single particle matrix element has the form $\langle j_a \| T_L^{\bullet} \| j_c \rangle$ whilst for the one hole contribution, $(j_a j_b) \rightarrow (j_a j_d)$, the single particle reduced matrix element $\langle j_d \| T_L^{\bullet} \| j_b \rangle$ appears. In both these cases the single particle energy of the state $\langle a|$ of the matrix element has a higher energy than that of the state $|c\rangle$. Hence the factor $(E_i - E_f)$ is always positive and the formulae may be taken at their face value using the operator $r^L C_{Lh}$ to evaluate all the single particle reduced matrix elements. This is, in fact, generally true for any electric transition matrix element which is calculated using the second quantisation technique.

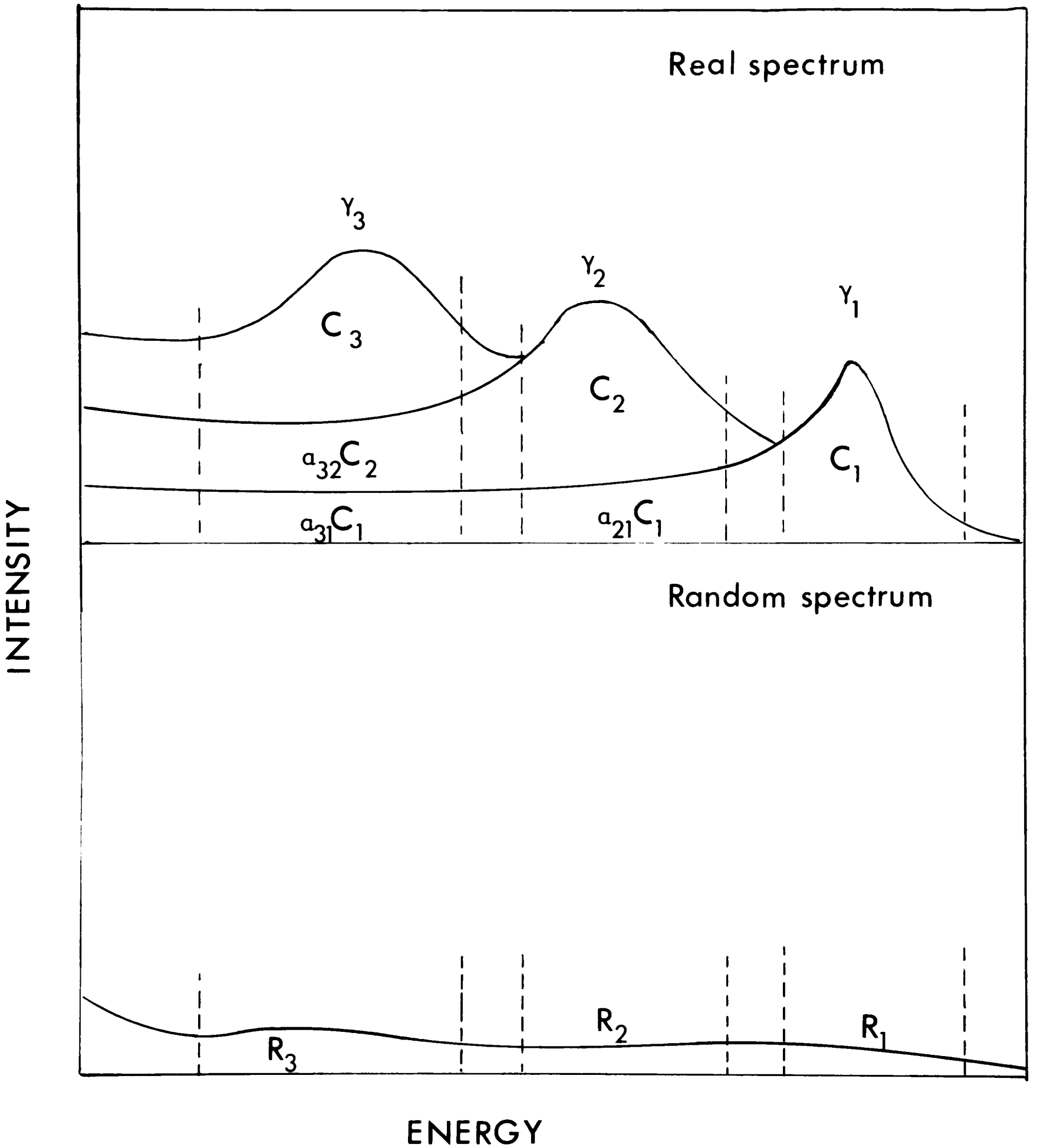

Real spectrum
Y_3
Y_2
Y_1
C_3
C_2
C_1
$a_{32}C_2$
$a_{31}C_1$
$a_{21}C_1$
Random spectrum
R_3
R_2
R_1
INTENSITY
ENERGY

fig. 3.1

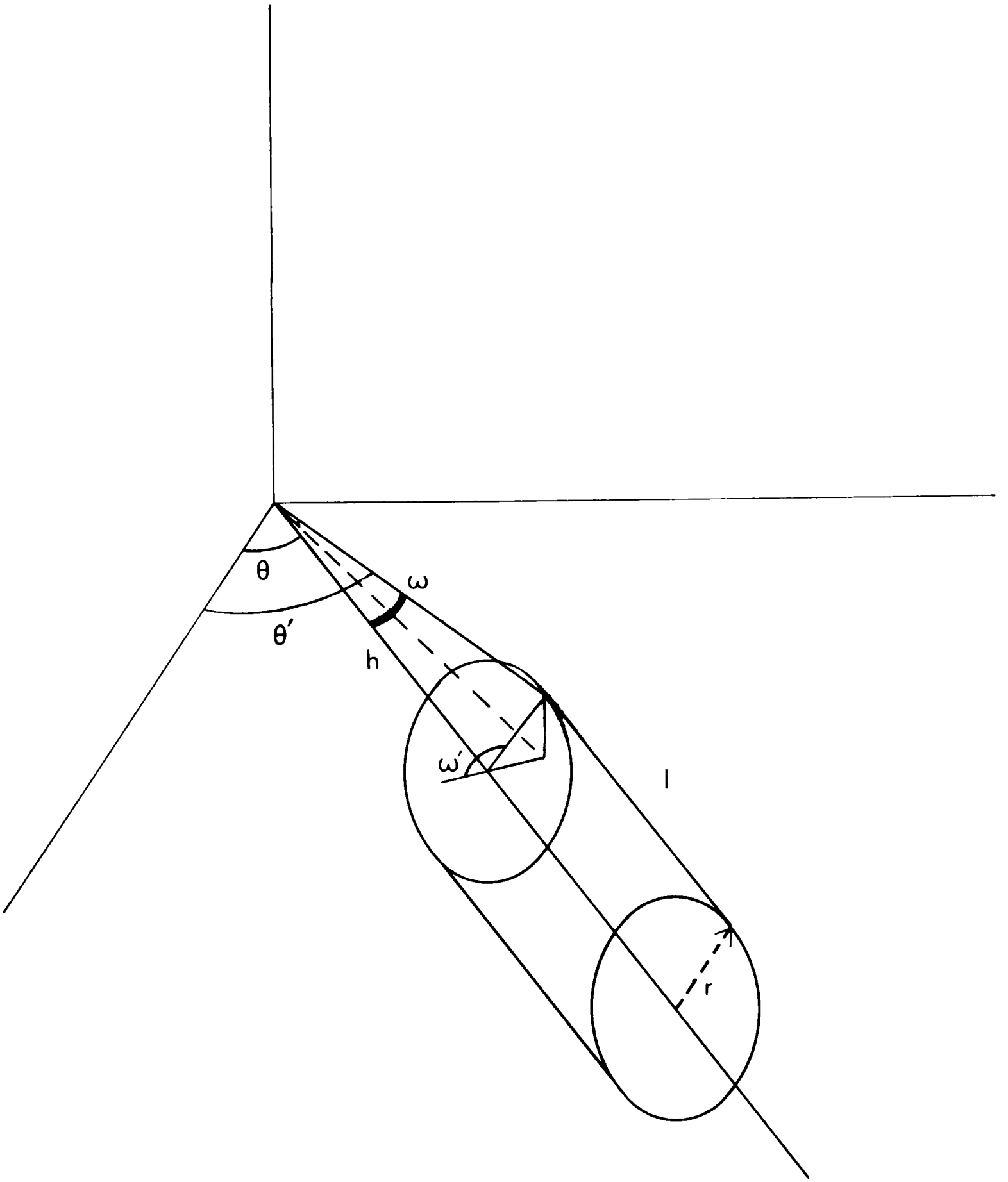


fig.3.2

C H A P T E R 4

A METHOD OF MEASURING THE LIFETIMES OF EXCITED NUCLEAR STATES

4.1 The Doppler Shift Attenuation Method

If a nucleus moving with velocity, v, emits a gamma ray corresponding to a transition energy of E_o then the velocity of the decaying nucleus will impart a Doppler shift to the gamma ray which will therefore have an energy given by (Pa 62) :

$$E = E_o (1 + \beta \cos\theta + \frac{\beta^2}{2} \cos 2\theta), \beta = \frac{v}{c} \qquad (4.1.1)$$

where the angle between v and the gamma direction is θ and is measured in the laboratory coordinate system. The formula is relativistically correct to terms up to order β^2 and c is the velocity of light.

In a nuclear reaction of the sort A(bc)D the final nuclei will recoil with a velocity v_o, say, as a result of the interaction and so an accurate measurement of the energy of de-excitation gamma rays will provide a method of

measuring the velocity of the excited nucleus at the moment of its decay. If the excited nuclei recoil into a solid medium then the excited nuclei may well have been slowed down due to energy loss in the medium before the emission of a gamma ray. In this case the Doppler shift which would be observed would be smaller than that expected from equation (4.1. 1) and the kinematics of the reaction (i.e., the value of v_0) making it possible, in principle, to deduce information about the lifetime of the decaying state. For this sort of method to be applicable the lifetime of the excited state must be comparable with the time taken for the nucleus to lose an appreciable fraction of its initial velocity. For lifetimes which are much shorter than this characteristic time of the medium the energy of the gamma ray will be given by equation (4.1. 1) with $v = v_0$ whilst for lifetimes much longer than the characteristic slowing down time the energy of the gamma rays will be just E_0. In either case it is not possible to extract a value for the lifetime of the excited state. A simple minded calculation will now be presented which should illustrate the main features of the process. The treatment of (Li 63) will be followed closely.

Suppose that the excited nuclei are produced with

initial velocity v_0 and are all travelling in the same direction. Over a quite wide range of velocities the energy loss of the excited nuclei will be proportional to their velocity. There are theoretical reasons to support this idea (Li 63b) although the empirical data suggests (Wi 62; Or 63) that the energy loss is proportional to v^{δ} where δ is in the region 0.8 to 1.0 where δ varies according to the ion being considered. However, for the present, the value $\delta = 1.0$ will be adopted.

$$\text{i.e.,} \qquad \frac{dE}{dx} = -k\,v \qquad (4.1.\ 2)$$

where k is a constant and E and x are the energy and distance travelled of the nuclei. A set of n_0 excited nuclei will decay according to

$$n = n_0\, e^{-t/\tau} \qquad (4.1.\ 3)$$

where t is time elapsed since there were n_0 nuclei present and τ is the lifetime of the state under investigation. The velocity of the excited nuclei as a function of time may be found by integrating equation (4.1. 2) which then gives :

$$v = v_0 \, e^{-\frac{kt}{m}} \qquad (4.1.4)$$

where v_0 is the initial velocity of the nuclei and m is their mass. The mean value of v when the nuclei decay will be related to the mean observed energy of the de-excitation gamma ray and will be given by

$$\bar{v} = \frac{\int_0^{\infty} v \frac{dn}{dt} \cdot dt}{\int_0^{\infty} \frac{dn}{dt} \cdot dt}$$

$$= v_0 \cdot \frac{a}{a + \tau} \qquad (4.1.5)$$

where a is the characteristic slowing down time of the medium defined by $a = m/k$. Typical values of the parameter a are 2.92×10^{-13} sec and 4.60×10^{-13} sec for ^{15}O ions slowing down in Copper and Aluminium respectively. These values have been calculated for the energy region in which dE/dx is proportional to the velocity. Since the excited nuclei decay with various different velocities the gamma

spectrum will not consist of a single line but will have a shape given by the intensity function I(E) which is defined by :

$$I(E) = I(v) = \frac{1}{n_o}\frac{dn}{dv} = \frac{a}{v_o\tau}\left(\frac{v}{v_o}\right)^{a/\tau - 1}$$

$$= \frac{a}{v_o\tau}\left(\frac{a\,\Delta E}{v_o \cos\theta}\right)^{a/\tau - 1} \qquad (4.1.6)$$

where $\Delta E = E - E_o$ and E is the measured energy of the gamma ray travelling in a direction (θ) with respect to the moving nuclei. Equation (4.1. 1) has been used to relate v and ΔE in its non-relativistic form. The general features of I(E) are shown in Fig. 4.1 where I(E) has been plotted as a function of (v/v_o) for a selection of values of τ/a. The curves are normalised so that they all have equal areas.

More general expressions for the mean velocity of the nucleus which is slowed down may be written down together with more general expressions for the intensity function for the gamma ray (Wa 63). These equations have, in general, no analytical solutions but may be solved by numerical

methods. A reaction process will be considered leading to an excited state with a lifetime τ and a cross-section in the laboratory system $\sigma_l(\theta\phi)$ where θ and ϕ are the spherical coordinates in the laboratory system of the excited nucleus and are shown in Fig. 4.2. The initial velocities of the nuclei are denoted by $v_o(\theta)$ and the velocities after a time t by $v(\theta\ v_o\ t)$. The gamma rays are detected at an angle δ with respect to the coordinate system defining (θ,ϕ). The observation of a gamma ray in the detector essentially measures, in the non-relativistic limit, the quantity $v \cos \varepsilon$ where v is the instantaneous velocity of the decaying nucleus and ε is the angle between the gamma ray and the direction of v. The mean value of the quantity $v \cos \varepsilon$ for the detector at angle δ will be, in the non-relativistic limit :

$$\overline{v \cos \varepsilon} = \frac{\int \sigma_l(\theta\phi)\ v(\theta\ v_o\ t)\ \cos\varepsilon \ d\omega}{\int \sigma_l(\theta\phi)\ d\omega} \qquad (4.1.7)$$

From Fig. 4.2. it can be seen that :

$$\cos \mathcal{E} = \sin \delta \sin \theta - \sin \chi \cos \delta \cos \omega \qquad (4.1.\ 8)$$

and so :

$$\overline{v \cos \mathcal{E}} = \frac{\int \sigma_\ell(\theta,\chi) v(\omega, v_0, t)(\sin\delta \sin\theta \sin\chi + \cos\delta \cos\omega)\sin\theta \, d\omega \, d\chi}{\int \sigma_\ell(\theta,\chi) \sin\theta \, d\omega \, d\chi} \qquad (4.1.\ 9)$$

If $\sigma_\ell(\omega\chi)$ is independent of χ then the integral over χ may be evaluated giving :

$$\overline{v \cos \mathcal{E}} = \cos\delta \frac{\int \sigma_\ell(\omega) v(\omega, t, v_0) \cos\omega \sin\omega \, d\omega}{\int \sigma_\ell(\omega) \sin\omega \, d\omega} \qquad (4.1.\ 10)$$

$$= \bar{v} \cos \delta$$

from which it can be seen that $\overline{v \cos \mathcal{E}}$, which is the quantity which may be determined experimentally, varies in this case according to $\cos \delta$. In the above equations the laboratory cross-section is related to that measured in the centre of mass system by

$$\sigma_\ell \, d\omega_\ell = \sigma_c \, d\omega_c$$

$$\sigma_\ell = \sigma_c \frac{\sin \theta_c}{\sin \theta_\ell} \frac{d\omega_c}{d\theta_\ell} \qquad (4.1.\ 11)$$

and the initial velocity in the centre of mass, the velocity in the laboratory system and the velocity of the centre of mass measured in the laboratory system (v_c v_o V) are related by :

$$\frac{v_o}{\sin \theta_c} = \frac{v_c}{\sin \theta_l} = \frac{V}{\sin(\theta_c - \theta_l)} \qquad (4.1.\ 12)$$

These equations assume that the recoil nuclei from the reaction continue to move in the same direction whilst they are slowed down. It would be expected (Li 63b) that considerable scattering through quite large angles will occur at the end of the nuclei's range since at low velocities the energy loss process is dominated by elastic scattering of the excited nuclei by the nuclei in the stopping medium. In this case the above equations would have to be considerably modified (Bl 66). However, for the experiments reported here these effects will later be seen to be rather unimportant and will not therefore be further discussed. Before leaving equation (4.1. 10) it is noted that $\overline{v \cos \varepsilon}$ is a function of δ v_o and τ and that the quantity also depends upon the dh/dx values of the nuclei in the slowing down medium.

In order to calculate the relationship between $v(\theta\ v_o\ t)$ and $v_o(\theta)$ it is necessary to integrate the equation :

$$\frac{dE}{dx} = m\frac{dv}{dt} = f(v) \qquad (4.1.\ 13)$$

In general this problem must be handled numerically although a particular solution was previously obtained (equation 4.1. 4) for the case $f(v) = k\ v$.

The intensity function of the gamma ray spectrum will be given by

$$I(E) = \frac{1}{n_o}\frac{dn}{dv}$$

$$= \frac{n}{\tau}\ \frac{\int \frac{e^{-t/\tau}\ \sigma_i(\omega\chi)d\omega}{\cos\quad f(v)}}{\int \sigma_i(\omega\phi)\ d\omega} \qquad (4.1.\ 14)$$

where $\cos\varepsilon$ is given by equation (4.1. 8) and the integral on the top line should be evaluated over all values of θ and ϕ which satisfy

$$\cos\varepsilon \geq \frac{c\ \Delta E}{v_o(\theta)} \qquad (4.1.\ 15)$$

since the initial velocity for a solid angle element $d\Omega$ must be greater than $\frac{Q \Delta E}{\cos}$ if it is to give a contribution to I(E) for a particular value of ΔE_o. In equation (4.1. 14) t is a function of v and v_o which in turn depend upon θ. The evaluation of I(E) can only be made if the cross-section for the reaction is known and the integration must be done numerically.

It is seen that in order to calculate the mean value of the observed shift a knowledge of the cross-section is required. This dependence may be to some extent eliminated by either detecting the outgoing light particles from the reaction and observing the de-excitation gamma rays in coincidence with these particles or alternatively if a heavy ion reaction of the sort a(BC)d with B and C the heavy particles is used to produce the excited nuclei. The kinematics of the reaction process often contrains the heavy outgoing nucleus to move in a small forward cone in the laboratory coordinate system. In fact the maximum angle at which the nuclei are produced is given by :

$$\sin \theta_m = \left\{ \frac{m_a m_d}{m_B m_C} \quad \frac{E + Q}{E} \right\}^{\frac{1}{2}} \qquad (4.1. 16)$$

where $E = E_0 \frac{m_a}{(m_a + m_B)}$ and E_0 is the incident beam energy.

In some cases the maximum value of θ_m may be as small as 10 to 20° and so in these cases the lineshapes and centroids of the peak as defined by equations 4.1. 14 and 4.1. 9 will depend less sensitively upon the details of the cross-section. These quantities will still depend upon $v_0(\theta)$ which will have a maximum spread of values given by :

$$\Delta v = 2\sqrt{\frac{m_d \cdot 2(E+Q)}{m_e (m_d+m_e)}} \qquad (4.1.\ 17)$$

In the reactions which were investigated the spread in the initial velocity was typically of the order of about 2%.

The main effect which might be seen for heavy ion experiments have been now outlined. In practice the shape of the spectrum as given by I(E) will be modified due to several factors :

(i) The finite resolution of the gamma ray detector.

(ii) The non-zero width of the energy bins into which the events are sorted.

(iii) The finite acceptance angle of the gamma detector.

(i) If a single gamma of energy E_0 is incident upon a gamma detector then there will be a photopeak in the spectrum which will be described by an intensity function I(E) which will be taken to be

$$I(E) = \frac{1}{4\sigma\sqrt{\pi}} e^{-(E-E_0)/\sigma^2} \qquad (4.1.\ 18)$$

where σ is related to the "width" of the peak. If the gamma ray spectrum is described by the intensity function I(E') then the observed spectrum will be described by :

$$I(E) = \frac{1}{4\sigma\sqrt{\pi}} \int e^{-(E-E')/\sigma^2} I(E')\,\mathcal{E}(E')\,dE' \qquad (4.1.\ 19)$$

where $\mathcal{E}$ is the efficiency of the detector and the integral runs over all values of E' greater than zero.

(ii) If the spectrum is sorted into various energy bins $E_i \rightarrow E_{i+1}$ then the number of counts in each bin would be

$$N_i = \frac{1}{4\sigma\sqrt{\pi}} \int_{E_i}^{E_{i+1}} dE \int e^{-(E-E')/\sigma^2} I(E')\,\mathcal{E}(E')dE' \qquad (4.1.\ 20)$$

It would be expected that these effects would be important when the maximum shifts which might be measured are of the same order of magnitude as the resolution (σ) of the gamma detector and when the bin widths are of about this order of magnitude.

(iii) In order to discuss the effect of the finite size of the gamma detector upon the measured values of $\overline{v \cos \varepsilon}$ it is convenient to recall the similar discussion relating to the angular correlation experiments. There, it was noted that a solid angle element $d\omega$ of length x absorbed gamma rays according to $d\omega(1 - e^{-x\tau})$. In this case these gamma rays will make a contribution to the overall shape of the spectrum and will have a centroid $E_o \frac{v}{c} \cos \varepsilon$. The total contribution to the centroid may therefore be calculated and is :

$$\frac{E_o}{c} \overline{v \cos \varepsilon} = \frac{E_o}{c} \frac{\int W(\theta') (1-e^{-x\tau}) v \cos \varepsilon \, d\omega}{\int W(\theta') (1-e^{-x\tau}) \, d\omega} \qquad (4.1.21)$$

where $W(\theta')$ is the angular distribution of the gamma rays and is included to take into account the different number of gamma rays per unit area striking different parts of the

crystal. The notation is identical to that used in section 3.5. From equation (4.1. 18) it can be seen that, for a reaction for which the cross-section does not depend upon ϕ, $\overline{v \cos \mathcal{E}}$ is proportional to cos δ where δ is the angle between the symmetry axis for the reaction and the (point) gamma detector. Substituting $W(\theta') = \sum a_k P_k(\cos \theta')$ and $\overline{v \cos \mathcal{E}} = \bar{v} \cos \theta'$ into equation (4.1. 21) then gives :

$$\frac{E_o}{c} \overline{v \cos \mathcal{E}} = \frac{\bar{v} E_o}{c} \frac{\sum a_k \int P_k(\cos \theta')(1-e^{-x\tau}) \cos \theta' \, d\omega}{\sum a_k \int P_k(\cos \theta')(1-e^{-x\tau}) \, d\omega}$$

(4.1. 22)

where $\bar{v}$ is defined by equation (4.1. 18). The integrals appearing in the equation can be solved using the methods of section 3.5. The resulting expression is :

$$\frac{E_o}{c} \overline{v \cos \mathcal{E}} = \frac{\bar{v} E_o}{c} \frac{\sum a_k \left[\left(\frac{k+1}{2k+1} \right) \omega_{k+1} \cdot_{k+1} + \frac{k}{(2k+1)} \omega_{k-1} P_{k-1} \right]}{\sum a_k \omega_k \cdot_k}$$

(4.1. 23)

where $P_k \equiv P_k(\cos \alpha)$ and use has been made of the relation

$$(k+1)\, P_{k+1} = (2k+1) \cos\delta\, P_k - k\, P_{k-1} \qquad (4.1.\ 24)$$

Hence, if the angular correlation of the gamma rays is known then the appropriate corrections can be made. In the formula above the a_k coefficients are corrected for the finite size of gamma detector and would be given directly by the theoretical formulae if the details of the decay were known. The formula may be written in terms of the experimentally determined a'_k coefficients giving

$$\frac{E_o}{c}\,\overline{v\cos\mathcal{E}} = \frac{\bar{v}\,E_o}{c}\,\frac{\sum a'_k\left[\left(\frac{k+1}{2k+1}\right)\frac{Q_{k+1}}{Q_k}P_{k+1} + \frac{k}{(k+1)}\,\frac{Q_{k-1}}{Q_k}P_{k-1}\right]}{\sum a'_k\,P_k} \qquad (4.1.\ 25)$$

A particular case of interest is the correction coefficient for an isotropic gamma ray distribution. Since the Q_k's are normalized so that $Q_o = 1$ and $P_{k-1} = 0$ in the sense of the relation given by equation (4.1. 24) the mean value for the centroid is given by

$$\frac{E_o}{c}\,\overline{v\cos\mathcal{E}} = \bar{v}\,\frac{E_o}{c}\cdot Q_1 \cos\delta \qquad (4.1.25)$$

If the acceptance angle of the gamma detector is sufficiently small then the Q_1 coefficients are very nearly equal to unity. A Ge(Li) crystal of radius 1.25 cm with a length 2.5 cm placed 8 cm from the source will have $Q_1 = 0.9952$ (Ha 66) for a 1.53 MeV gamma ray which represents a correction of about 0.5%. If the angular distribution of the gamma rays is not isotropic then the equation (4.1. 25) must be used. For an a_2 coefficient of 0.2 and the same detector as that just described the correction amounts to typically a few percent depending upon the angle between the symmetry axis and the detector.

Historically, the first experiments using the Doppler shift were reported by (De 55). Since that time many experiments of this sort have been performed. The introduction of heavy ion beams (Li 63) and particularly the Lithium drifted Germanium detector (Al 65; Al 65b; Ca 67; Pa 66; Wa 66) have produced major increases in the accuracy and reliability of the method.

4.2 Treatment of the Experimental Data

To compare the experimentally determined spectra with the results of the slowing down calculations it is necessary

to extract the centroids of the peaks appearing in the gamma spectra or, alternatively, to remove the background under the peaks and compare the resulting data to the calculated intensity function I(E). This latter procedure is probably most valuable in cases in which the maximum shifts as determined from the kinematics of the reaction are rather small whilst for heavy ion reactions the extraction of the centroids would seem to be adequate. If the centroid of a given peak is determined to be $\bar{c}$ measured with respect to its unshifted position and the maximum value of $\bar{c}$ allowed by the kinematics of the reaction is c_{max} then the quantity $F(\tau)$ may be defined by :

$$F(\tau) = \left| \frac{\bar{c}}{c_{max}} \right| \qquad (4.2.1)$$

$F(\tau)$ is the ratio of the observed centroid shift of the gamma ray from its unshifted position to the maximum shift allowed and is also equal to $\overline{v \cos \varepsilon} / (v_0 \cos \varepsilon)$ where the appropriate definitions are contained in section 4.1.

In cases in which measurements of the spectra are taken in two slowing down media which lead to substantially different values of $F(\tau)$ it is sometimes convenient to

define a quantity $h(\tau)$:

$$h(\tau) = \left| \frac{F_1(\tau) - F_2(\tau)}{F_1(\tau) + F_2(\tau)} \right|$$

$$= \left| \frac{\overline{(v \cos \varepsilon)_1} - \overline{(v \cos \varepsilon)_2}}{\overline{(v \cos \varepsilon)_1} + \overline{(v \cos \varepsilon)_2}} \right| \qquad (4.2.2)$$

This quantity has an advantage over $F(\tau)$ for analysis of experiments in which v_o, the initial velocity of the ions, has to be estimated (i.e., in heavy ion reactions) since, as a first order approximation, $h(\tau)$ is independent of v_o. For the simple case discussed in section 4.1 dE/dx was taken to vary according to v and the value of $F(\tau)$ was given by :

$$F(\tau) = \frac{a}{(\omega + \tau)}$$

and is independent of the initial velocity of the ion. When the linear linear relationship no longer holds then $F(\tau)$ depends upon v_o, the initial velocity.

For a spectrum with n_i counts in each of c_i channels and with background counts b_i in each channel the centroid of a peak will be given by

$$\bar{c} = \frac{\sum c_i \, (n_i - b_i)}{N - B} \qquad (4.2.3)$$

where N and B are defined by

$$N = \sum n_i \, , \qquad B = \sum b_i$$

The centroid, $\bar{c}$, will have an error given by

$$\sigma (\bar{c})^2 = \frac{\sum (c_i - \bar{c})^2 \, (n_i + b_i)}{N - B} \qquad (4.2.4)$$

Usually the background under the peaks of interest can be estimated in a similar way to that described in Section 3.6. Systematic errors will increase the error over that given by the equation above which just takes into account the statistical errors.

Small corrections can be made to the value of $\bar{c}$ extracted from the data to take into account the variation

in the efficiency of the detector over the observed peak and due to the slight asymmetry usually observed in a peak corresponding to a gamma ray of discrete energy incident upon the detector. For a Lithium drifted Germanium detector, corrections can also be applied for the low energy tail to the photopeaks which appear between the peak and its Compton edge.

4.3 The Calculation of dE/dx values for Heavy Ions

In order to be able to calculate the functions $K(\tau)$ and $F(\tau)$ and the lineshapes, I(E), for a given reaction and subsequent gamma ray decay a knowledge of the energy loss of the excited nuclei in the material into which they recoil is required. The energy loss, in general, has contributions from interaction both with the atomic electrons in the absorber and also due to the scattering of the moving nuclei by the nuclei of the stopping material. The latter effect is rather unimportant for the reactions which will be discussed later on except when the moving ions reach the end of their ranges. This is because the electronic contribution increases with energy (up to a certain maximum which, for nuclei in the ^{16}O region, will typically occur for ion energies of about 15 MeV) whilst the nuclear

contribution will decrease. For ^{16}O ions being slowed down in Nickel the electronic and nuclear contributions to the stopping power become equal when (Pi 67) the velocity of the ions is about 10^8 cm.sec^{-1} whereas the initial velocity of the ions for the reactions which will be discussed later will be roughly about 1.5×10^9 cm.sec^{-1}. The nuclear interaction will also have the effect of scattering the incident particles so that an initially parallel beam will end up with a considerable angular spread.

At high ion energies the rate of loss of a charged particle due to electronic interactions with the medium in which it moves may be written (Be 53; No 63; Ev 55) :

$$-\frac{dE}{dx} = \frac{4\pi e^4 Z_1^2 N Z_2}{m v^2} \left[\ln \left(\frac{2m v^2}{I}\right) - \ln (1-\beta^2) - \beta^2 - \frac{C}{Z_2} \right]$$

(4. 3. 1)

where e and m are the electron charge and mass, Z_1 and Z_2 are the atomic numbers of the incident nuclei and the absorber nuclei, N is the number of atoms per cm^3 in the absorber, v is the velocity of the incident particle ($\beta = \frac{v}{c}$ where c is the velocity of light) and I is the mean ionization potential of the stopping atoms. C is a correction

coefficient which arises from the non-participation of some of the electrons in the inner shells of the stopping nucleus in the slowing down process. This formula was derived using the Born approximation and should only be valid if $\frac{Z_1 e^2}{h v} \ll 1$ although there are reasons to suppose that it might be valid at lower energies than those given by this inequality (Be 53). One of the factors which causes large deviations from Equation 4.3. 1 at low energies is the constant capture and loss of atomic electrons by the moving particles. The mean charge upon the particle is considerably reduced from the value Z_1 which it would have at higher energies and hence the energy loss per unit path length is reduced because of the smaller interaction between the moving nuclei and the electrons in the absorber. Equation 4.3. 1 also shows that the energy loss may be written in the form :

$$-\frac{dE}{dx} = Z_1^2 f(v) \qquad (4.3.\ 2)$$

where f(v) depends upon the velocity of the incident particle and the nature of the absorber. In order to describe the energy loss at velocities at which this equation is not strictly valid attempts have been made to explain the

behaviour of the energy loss in terms of the effective charge of the moving nucleon rather than its actual charge Z_1 (Ne 60; Bo 65; Re 60). It is argued that at low velocities the equation for the energy less may be written :

$$-\frac{dE}{dx} = Z_1^2 \gamma^2 f(v) \qquad (4.3.3)$$

where, $\gamma = \frac{Z_{eff}}{Z_1}$, is the effective charge ratio and f(v) again depends only upon v and the nature of the absorber. It has further been suggested that the effective charge ratio should depend upon the ratio of the velocity of the ion to the velocity of the electron in the orbital into which it is captured (An 41; Pa 56; Mo 63). At high velocities when the effective charge ratio is small compared to unity it would be expected that this latter velocity is just the velocity of the electrons in the lowest k orbital of the moving ion (Mo 60; He 60). At somewhat lower velocities the choice of the Thomas-Fermi velocity would seem to be more appropriate. The effective charge ratio would then be a function of v/v_{TF} which may be written (An 41) :

$$\gamma = \frac{(Z_1)_{effective}}{Z_1} = g\left(\frac{v}{Z_1^{2/3}}\right) \qquad (4.3.4)$$

Accepting for the moment these conjectures as being valid the energy loss of two different ions moving with the same velocities in a given material may be related by :

$$\frac{\left(\frac{dE}{dx}\right)_1}{\left(\frac{dE}{dx}\right)_2} = \frac{r_1^2}{r_2^2}\,\frac{z_1^2}{z_2^2} \qquad (4.3.5)$$

This equation can be extremely useful if particle 2 is chosen to be a proton since proton stopping data in a wide variety of materials and the proton effective charge as a function of velocity are both data which are well known (Wh 58; Al 53; Ev 55). If values of dE/dx are known for a heavy ion in a given material then the equation above may be used to calculate the effective charge, or, alternatively values of dE/dx may be predicted provided that the effective charge of the ion and the proton stopping power in the material at the velocity of interest are known.

In Fig. 4.3 the effective charge has been plotted as a function of $\beta/z_1^{2/3}$. The data of (Be 55; Mo 60;. Mo 60; Po 61; Bo 65) has been plotted which includes a variety of ions from Nitrogen to Chlorine and various absorbers including Aluminium, Nickel Silver and Gold. The effective charge

data for the proton was taken from (Av 55) and the proton energy loss data from (Wh 58). The points all lie on the curve drawn to within the experimental errors which are usually about 5 to 10 per cent. That this is so provides an excellent confirmation of the underlying ideas about the effective charge. It is also of interest to note that if the effective charge is computed from measured charge exchange cross-sections then the points lie quite nicely on the graph.

The curve shown is actually a polynomial fit to the measured points, the coefficients of which are shown in Table 4.1.

The effect upon the energy loss of ions moving through a medium due to the interactions of the ion with the nuclear Coulomb field of the stopping atoms has been investigated by Bohr (Bo 48) who assumed a $1/r$ interaction between the particles and by (Li 63b) who assumed that the interaction was due to a Thomas-Fermi potential. In both of these treatments energy is lost by the incident particle due to collisions with the atoms of the stopping material. This latter treatment allows the introduction of universal curves valid for any ion and any stopping material if the dimensionless variables ρ and ε are introduced which are defined by :

$$\rho = \frac{x\, N\, A_1\, A_2}{(A_1 + A_2)^2} \cdot 4\pi a^2 \qquad (4.3.6)$$

$$\xi = E \frac{a\, A_2}{Z_1\, Z_2\, e^2\, (A_1 + A_2)} \qquad (4.3.7)$$

where $a = a_0\ 0.8853\ (Z_1^{2/3} + Z_2^{2/3})^{-\frac{1}{2}}$ with a_0 the Bohr radius and Z_1 Z_2, A_1 A_2 the charge and mass numbers of the incident and slowing down medium ions. x is the path length of the moving ion and E its energy while N is the number of atoms per cm^3 of the slowing down medium.

The nuclear contribution to the energy loss can then be found from the $\frac{d\xi}{d\rho}$ against $\sqrt{\xi}$ plot (Fig. 2. of (Li 63b)). For values of ξ greater than about 5 the treatments of (Li 63b) and (Bo 48) converge and so the nuclear contribution to the stopping power in this case may be calculated from the formula

$$\frac{d\xi}{d\rho} = \frac{\ln (2.259\, \xi)}{2\xi} \qquad (4.3.8)$$

where the estimate of the "Bohr radius" suggested by (Li 63b) has been inserted.

The nuclear interaction also has the property of

scattering the incident nuclei which, for high energies, will follow Rutherford's Law of scattering whilst for lower energies there will be considerable deviations from this law due to :

a) Departures from the $\frac{1}{r}$ interaction.

b) Quantum mechanical effects which demand that the scattering must be isotropic for sufficiently small velocities for a finite range potential.

However, it is not appropriate to discuss these matters in more detail since it will be seen that the nuclear contribution to the total stopping power will have little effect upon the results which will be quoted and it would therefore appear that the effect of scattering of the nuclei can be safely ignored.

TABLE 4.1

The coefficients of a polynomial fit to the points shown in the effective charge plot. (Fig. 4.3).

Coefficient c_k	k
5.811×10^{-4}	0
-3.545	1
6.370×10^{3}	2
2.857×10^{6}	3
-7.473×10^{8}	4
7.187×10^{10}	5
-3.185×10^{12}	6
5.420×10^{13}	7

The effective charge ratio may be computed from

$$\gamma^2 = \sum c_k x^k \quad \text{where} \quad x = \beta / Z^{2/3}$$

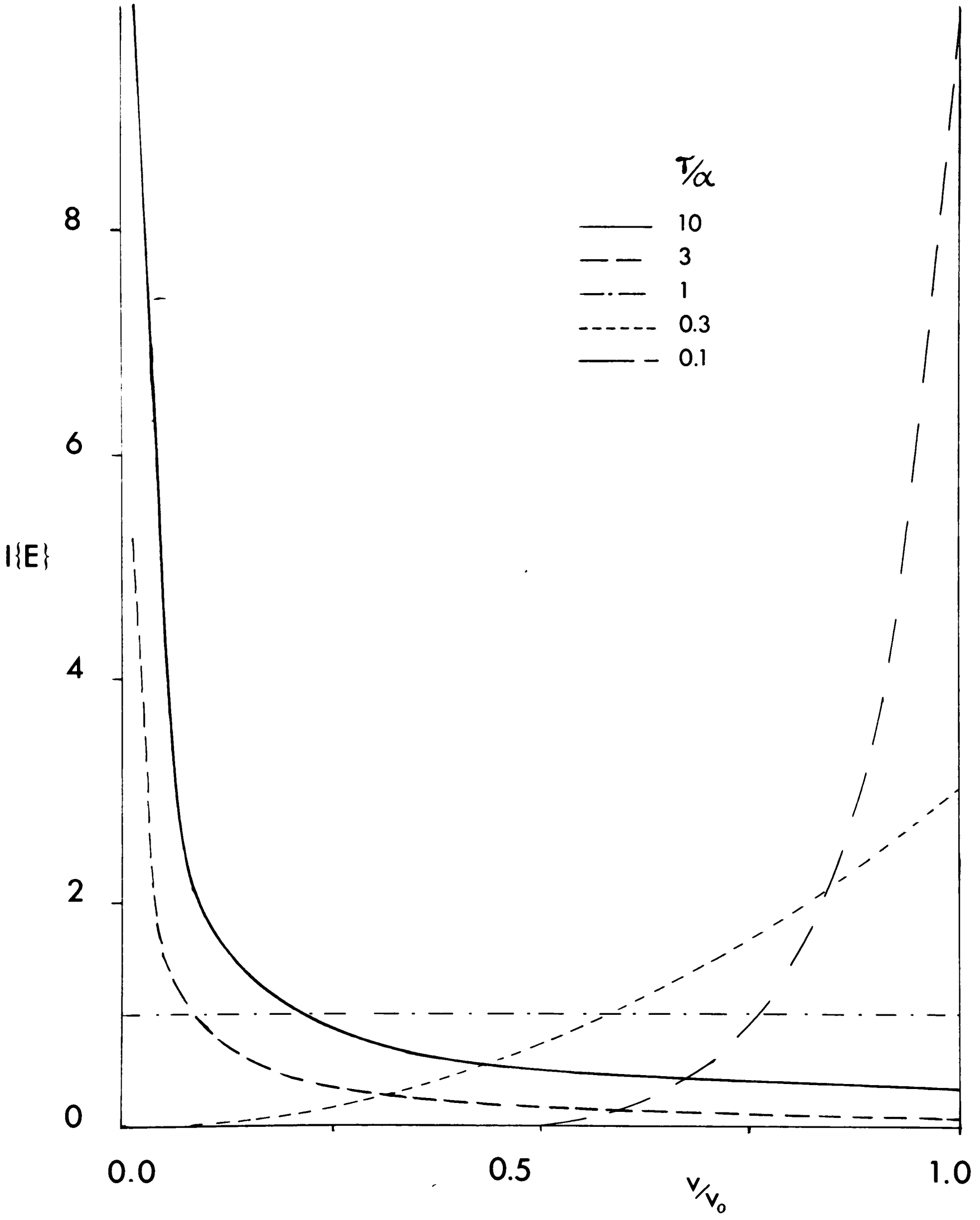


fig. 4.1

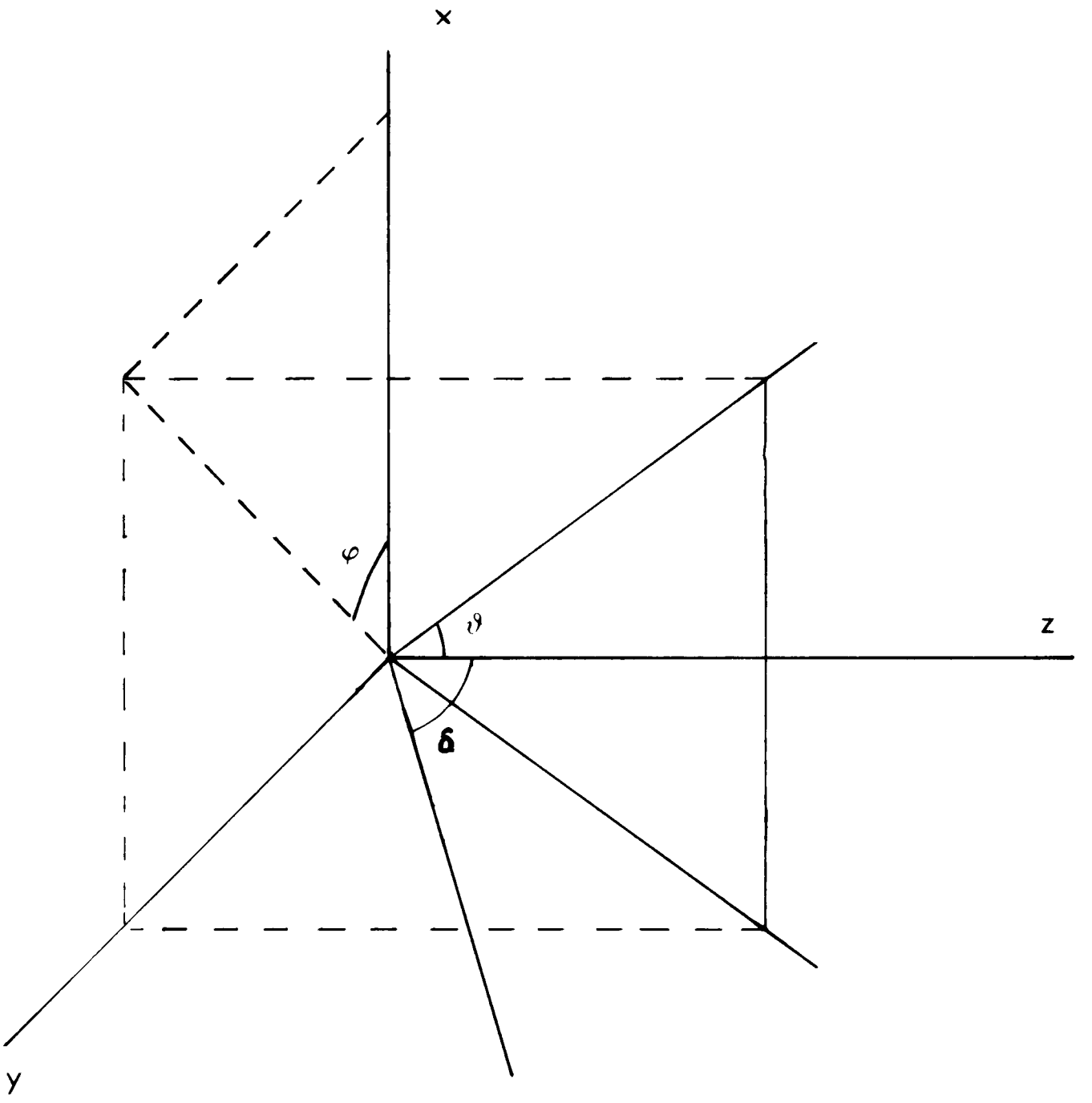


fig. 4.2

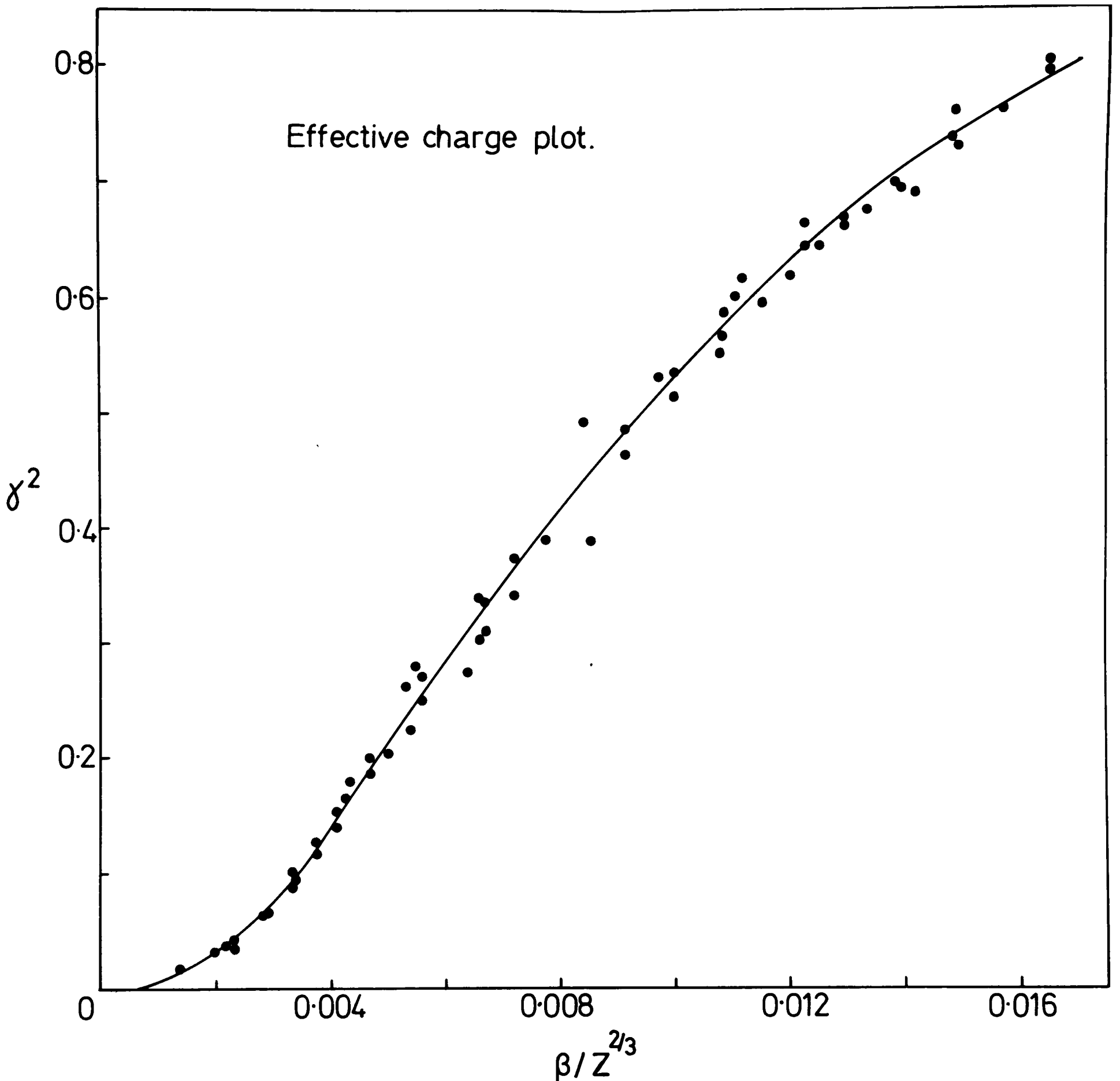

Effective charge plot.
0·8
0·6
0·4
0·2
0
γ^2
0·004
0·008
0·012
0·016
$\beta / Z^{2/3}$

fig. 4.3

C H A P T E R 5

THE ANGULAR CORRELATION RESULTS

5.1 Some Positive Parity States in ^{15}N: Experimental Conditions

The $^{18}O(p,\alpha)^{15}N$ reaction, which has a Q value of 3.980 MeV, was used to populate the ^{15}N states located at excitation energies (Wa 65b) of 7.154, 7.300 and 7.563 MeV. The gamma rays were investigated in coincidence with the relevant alpha particle groups which were observed at angles between 168 and 171° with respect to the incident beam direction. In this case the maximum magnetic substate which may be populated by the detected alpha particles is $|m| = \frac{1}{2}$ and so a simplified form of equation (3.4. 1) is applicable. The angular distribution of the gamma rays may be written as :

$$W(\theta) = \sum_{k_{even}} a_k P_k (\cos\theta) \qquad (5.1.\ 1)$$

where, for a direct transition ($J_1 \rightarrow J_2$), the coefficients a_k are given by equations (3.4. 2-4) :

$$A_k = \rho_k(J_1\ \delta)\ [\ R_k(LLJ_1J_2) + 2\delta_1\ R_k(LL'J_1J_2)$$

$$+ \delta_1^2\ R_k(L'L'J_1J_2)\ ]\ /\ 2\ x\ (1 + \delta_1^2)$$

(5.1. 2)

where L is the lowest multipolarity contributing to the transition, $L' = L + 1$ and :

$$\delta_1 = \frac{\langle J_1 \| T_{L'}^{\langle w' \rangle} \| J_2 \rangle}{\langle J_1 \| T_L^{\langle w \rangle} \| J_2 \rangle} \frac{\hat{L}}{\hat{L}'} \qquad (5.1.\ 3)$$

Higher multipole orders may be taken into account although this is usually not necessary since the ratio of the matrix elements $\langle J_1 \| T_L^{\langle w \rangle} \| J_2 \rangle$: $\langle J_1 \| T_{L+2}^{\langle w \rangle} \| J_2 \rangle$ is usually sufficiently small to be neglected.

For a cascade transition, $(J_1 \rightarrow J_2 \rightarrow J_3)$, in which the second gamma ray only is observed, the appropriate a_k coefficients are given by equation (3.4. 5). If δ_2 is the mixing ratio of the second transition then :

$$a_k = \rho_k(J_1\ \tfrac{1}{2})\ [U_k(LJ_1J_2) + \delta_1^2\ U_k(L'J_1J_2)]$$

$$[R_k(L_1L_1J_2J_3) + 2\delta_2\ R_k(L_1L_1'J_2J_3)$$

$$+ \delta_2^2\ R_k(L_1'L_1'J_2J_3)]\ /\ (1+\delta_1^2)(1+\delta_2^2)\ \times 2$$

(5.1. 4)

where L_1 is the lowest multipolarity of the second transition and $L_1' = L_1 + 1$. These formula are to be χ^2 fitted to the experimental distributions as explained in Section 3.6.

The alpha particles were detected in a 1200 Ω•cm, 50 μM thick, n-type silicon annular surface barrier counter which was totally depleted by the application of a bias of about 40 volts. Alpha particles with energies up to about 8.5 MeV were completely stopped in the counter compared with protons up to an energy of 2.0 MeV. The lowest energy alpha particles of interest had $E_\alpha \approx 2.7$ MeV and were thus detected in a portion of the spectrum free from protons (see Fig. 5.1).

The proton beam was supplied by the Oxford University Tandem Van de Graaff Generator at energies between 8.50

and 9.25 MeV with an analyzed beam current of approximately 0.15 μA. The target consisted of a 150 $\mu gm.cm^{-2}$ layer of $W^{18}O_3$, enriched to about 70 per cent in ^{18}O and evaporated onto a 15 $\mu gm.cm^{-2}$ Carbon backing.

Gamma rays, detected in a 12.7 x 15.2 cm NaI(Tl) crystal with its front face 17.5 cm from the target, were investigated in fast-slow coincidence (with a resolving time of 35 ns) with the relevant alpha groups and stored in the first sub-group of a 2 x 200 channel analyzer. The gamma ray spectra were stabilized through the photomultiplier high voltage supply in the usual way and the particle spectra using a digital stabilizer.

The decay schemes and correlations were extracted from the experimental data as explained in Section 3.6. The spectra taken at the various different angles were normalized to the same total number of alpha particles falling in the analogue window. The effect of the finite size of the gamma detector was corrected for as explained in Section 3.5 using the tables of Rutledge (Ru 59).

5.2. The 7.154 and 7.563 MeV Levels and the $5/2^+$, 5.270 MeV Level.

The ^{15}N levels located at 7.154 and 7.563 MeV were

studied at a beam energy of 9.25 MeV. It can be seen from the partial particle spectrum (Fig. 5.1) that the 7.30 and 7.15 MeV levels were not completely resolved and that the former was excited to the lesser extent. To avoid contamination from the 7.30 MeV level the particle window for the 7.15 MeV state was set at the high energy end of the peak. It will be seen that the 7.30 MeV state decays predominantly to the ground state and so it can be concluded from the summed over angles gamma spectrum (Fig. 5.2) that contamination was avoided. Further, a limit of less than 4 per cent can be placed on the ground state transition of the 7.15 MeV level. An experiment using a Ge(Li) gamma ray detector has shown (Wa 65b) that the two gamma rays appearing in the spectrum correspond to the 7.15 → 5.27 → g.s. cascade. At the time of this experiment a limit of less than 10% had been placed upon the branch to the 5.30 MeV state which later measurements (Al 66 and Chapter 6) reduced to 4 per cent. The angular distribution of the 1.88 MeV gamma ray resulting from the direct transition to the 5.24 MeV level (Fig. 5.3) was χ^2 fitted to various theoretical distributions. The fits which yielded χ^2 values less than the 1 per cent confidence limit have been

listed in columns three and four of Table 5.2. and the fits to the Legendre polynomials of even order have been listed in Table 5.1. The fit shown in Fig. 5.3. corresponds to $J_1 = 5/2$ and $\delta_1 = -0.04$ or -1.8. At the time when this experiment was performed the analysis was done using a different definition of the mixing parameter (x) which appears on the diagrams. The relation between x and δ is $\delta = -x$.

The angular distribution of the cascade 5.27 MeV gamma ray (Fig. 5.4) depends upon the spins of the levels involved and the mixing ratios of the 1.88 and 5.27 MeV gamma rays. For each of the acceptable solutions found for $J_1(7.15)$ and $\delta_1(7.15 \rightarrow 5.27)$ the 5.27 MeV $\rightarrow$ g.s. transition was χ^2 fitted to the theoretical distributions for stepped values of $\delta_2(5.27 \rightarrow 0)$ ranging from $-\infty$ to $+\infty$. In this way certain of the solutions for the first transitions can be excluded and solutions for δ_2 may be found. The results of this procedure are summarised in Table 5.2. The best fits corresponded to a spin for the 7.15 MeV level of $5/2$ and a mixing ratio for the 1.88 MeV gamma ray of -0.04 ± 0.03 in agreement with a previous assignment (Re 66) $\delta = -0.04 \pm 0.05$. The E3/M2 mixing ratio for the

5.27 MeV → g.s. transition was found to have the two possible values $\delta_2 = -0.18 \pm 0.02$ or $+5.7 \pm 0.4$ which agreed with a previous determination (Wa 65) $\delta = -0.15 \pm 0.06$ or 6.1 ± 1.4 but in disagreement with the result of (Pe 66), $\delta = -0.07 \pm 0.02$ or $\delta = 13.7 \pm 0.4$. The errors quoted on the measurements were, for the mixing ratios reported herein, estimated by introducing the standard errors of the Legendre polynomial coefficients into the theoretical distribution formula.

The analysis of the results from the 7.56 MeV level was essentially the same. The gamma ray spectrum again indicated the presence of only two gamma rays with energies of 2.29 and 5.27 MeV resulting from the main decay (Wa 65b; Al 66 and Section 5.9) to the $5/2^+$ member of the 5.3 MeV doublet. A limit of less than 4 per cent can be again placed on the direct transition to the ground state. For the 7.56 MeV to 5.27 MeV transition several values of J_1 and δ_1 give distributions which fit the experimental data, as indicated in Table 5.2. However, only the assignment $J_1 = 7/2$, $\delta_1 = -0.01 \pm 0.03$ survives when the 5.27 MeV → g.s. cascade transition is fitted (Figs. 5.5, 6). This result is in reasonable agreement with the work of

(Fe 66) which yielded J = 7/2, δ = - 0.04 ± 0.01. The E3/M2 mixing ratio for the 5.27 MeV → g.s. transition was found to be δ_2 = - 0.15 ± 0.02 or + 5.6 ± 0.4 which is in agreement with the independent determination from the decay of the 7.15 MeV level. Furthermore, it would seem that the larger value may be excluded from considerations of the average strength of electromagnetic transitions in light nuclei. It will be shown that the observed value of δ_2 = - 0.165 ± 0.015 already requires a considerable enhancement of the E3 component of the transition.

5.3 The 7.300 MeV Level

The 7.30 MeV level was found to be strongly excited compared with the neighbouring 7.15 and 7.56 MeV states at an incident proton energy of 8.50 MeV (Fig. 5.7). A narrow particle window was set at the low energy end of the 7.30 MeV peak to avoid contamination from the $^{18}O(p,t)^{16}O$ ground state group. The gamma ray spectrum in coincidence with this particle group (Fig. 5.8) shows just a ground state transition and a limit of less than 4 per cent can be placed upon the branches to other levels. The angular distribution of the 7.30 MeV gamma ray (Fig. 5.9) was χ^2

fitted to various theoretical distributions. The only acceptable solution was $J = 3/2$ and $\delta = -0.07 \pm 0.02$ or $\delta = 2.1 \pm 0.2$, which are surprisingly large values for an M2/E1 mixture. The best fits for $J = 5/2$ and $7/2$ are shown in Fig. 5.9.

The effect of the finite size of the particle detector upon the angular distributions is relatively important for an initial spin $3/2$ due to the numerical values of the $\rho_k(JM)$ coefficient which enter into the theoretical formula for the a_k coefficients. If it is assumed that the $m = \pm 3/2$ magnetic substate is populated to the extent of 3 per cent (see Section 3.2) due to this effect then the two solutions for the mixing ratio become $\delta = -0.06$ and $\delta = +2.0$. Thus, unless the reaction preferentially populated the $3/2$ substates this effect is smaller than the other, experimental, errors; in particular, the value $\delta = 0$ can be completely excluded.

5.4 Some ^{15}O positive parity states: experimental conditions

The doubly charged ^3He beam of the Harwell Van de Graaff Generator was used to populate the levels under study

in ^{15}O via the $^{16}O(^{3}He,\alpha)^{15}O$ reaction. A beam energy of 9.10 MeV with an analyzed current of about 70 nA was used. The targets consisted of a selfsupporting, 120 $\mu gm.cm^{-2}$, Calcium hydroxide film.

The alpha particles from the reaction were detected by a 300 Ω.cm annular, n-type, surface barrier counter placed 4 cm from the target and disposed at angles between 169 and 174° with respect to the incident beam direction. The counter bias, 30 v, was sufficiently low to ensure that the alpha particles of interest fell in a region of the spectrum free from the protons from the competing $(^{3}He,p)$ reactions. In the geometry used the detected alpha particles correspond to excited ^{15}O nuclei with the $m = \pm \frac{1}{2}$ magnetic substates populated and so the angular correlation formula presented in section 5.1 are directly applicable to this case.

The gamma rays were detected in two 12.7 cm x 15.2 cm NaI(Tl) crystals mounted on opposite sides of the beam line on rotating trolleys with their front faces 17.5 cm from the target. The gains of the gamma ray detectors were stabilized via the photomultiplier high voltage supplies. Fast-slow real and random coincidences were made (the resolving time was 30 ns) between the gamma rays

and the relevant alpha groups. The two gamma spectra were stored in two 512 multichannel analyzers together with their random spectra for which the appropriate corrections have been made. The data reduction process and fitting procedures have been explained in Section 3.5, 6.

5.5 The 6.789 and 6.857 MeV Levels and the $5/2^+$, 5.240 MeV Level

Studies with Lithium drifted Germanium gamma ray detectors have shown that the 6.79 MeV state decays > 97 per cent to the ground state while the 6.86 MeV state decays predominantly to the 5.24 MeV level (Wa 65b and Chapter 6). The analysis of the results will be conducted assuming that both of these decays are 100 per cent pure and that the spins of the 5.24 and 5.19 MeV states are $5/2$ and $\frac{1}{2}$ respectively (Hi 59; Ho 59; Go 66).

In Fig. 5.10 the spectrum is shown for E(^{3}He) = 9.1 MeV from which it is seen that the 6.79 MeV level was unresolved from the 6.86 MeV state. The gamma ray spectrum (Fig. 5.11) coincident with the alpha particle group shows three gamma rays which come from the 6.79 MeV → g.s.

transition and the 6.80 MeV → 5.24 MeV → g.s. cascade. The 1.99 MeV gamma ray is due to the inclusion in the energy window of the particle group leading to the first excited state of ^{11}C produced in the contaminant reaction $^{12}C(^{3}He,\alpha)^{11}C$. This does not disturb the analysis since it was observed that the intensity of this gamma ray was constant throughout the experiment thus not affecting the normalization of each measurement with respect to the number of alpha particles in the energy window. The cross-section for the $^{40}Ca(^{3}He,\alpha)^{39}Ca$ reaction is extremely small compared with that leading to the ^{15}C states; moreover, the ^{39}Ca states formed by the alpha particles falling in the energy window would have been unbound by about 3 MeV and should therefore have decayed almost entirely by particle emission.

The measured correlation of the 6.79 MeV → g.s. decay is shown in Fig. 5.12 and the fit to Legendre polynomials of even order is presented in Table 5.3. The measured points were χ^2 fitted to various values of J and δ, the multipole mixing parameter, with J ranging from $^{3}/_{2}$ to $^{7}/_{2}$ and δ from $-\infty$ to $+\infty$. Of these spin values all except $J = {}^{3}/_{2}$ were excluded for all values of δ in agreement with a previous assignment (Fo 59) and the work of Gallmann et. al. (Ga 66). The best fit occurred ($\chi^2 = 0.38$) for

$\delta = -0.10 \pm 0.02$ or $\delta = +2.2 \pm 0.4$. The effect due to the finite size of the alpha particle detector has been mentioned in Section 5.3. The same considerations apply here and the mixing ratio solutions would be changed by this effect to $\delta = -0.09$ and $+2.1$. The effect is again within the other experimental errors and will be ignored.

The errors quoted on δ have been estimated in the usual way by introducing the errors of the Legendre coefficients into the appropriate angular distribution formula. There has been one other determination of this mixing ratio (Ga 66) which yielded $\delta = +0.08^{+0.02}_{-0.06}$ where the difference in sign is due to the different phase convention used by (Ga 66).

As noted above, the peaks at 5.24 MeV and 1.62 MeV in the summed gamma spectrum are almost entirely due to the decay of the 6.86 MeV level.

The measured angular distributions of these de-excitation gamma rays are shown in Fig. 5.13. The 1.62 MeV transition was χ^2 fitted to the theoretical distributions for spin values between $^3/_2$ and $^9/_2$ and stepped values of the mixing ratio, δ_1, between $-\infty$ and $+\infty$. For each of the acceptable solutions (see Table 5.4) the 5.24 MeV $\rightarrow$ g.s. cascade transition was analyzed for stepped values of

δ_2(5.24 MeV → g.s.). This showed that of the three solutions (J, δ_1) only the combination $J = 5/2$, $\delta_1 = -0.04 \pm 0.03$ was acceptable, the best fit corresponding to δ_2(5.24 MeV → g.s.) = $+0.13 \pm 0.05$ where the errors were again estimated from the Legendre analysis. It was further verified that the cascade distribution was insensitive to variations in δ_1 equal to its error. Gallmann et. al. (Ga 66) assigned the spin of the 0.86 MeV state as most probably 5/2.

5.6 The 5.188 and 5.24 MeV Levels

The distribution of the gamma rays coincident with the alpha groups directly populating the 5.2 MeV doublet is shown in Fig. 5.14. The distribution was fitted to Legendre polynomials of even order. Since the 5.19 MeV level has spin $\frac{1}{2}$, the gamma distribution from this level is isotropic and so affects only the coefficient of the P_0 term of the doublet distribution. Hence the ratio a_2/a_4 is independent of the relative excitation of the two levels. The theoretical values of a_2/a_4 are shown in Fig. 5.15 as a function of δ(5.24 MeV → g.s.). The measured value of this ratio (suitably corrected for the finite size of the

gamma detector) gives a value for δ = + 0.19$^{+0.10}_{-0.06}$, where the errors are estimated from the a_2/a_4 plot. This result is in agreement with the more accurate result from the cascade analysis presented in section 5.5. The other reported values for the mixing ratio of the 6.24 MeV to ground state transition are : δ = 0.035$^{+0.11}_{-0.04}$ δ = 0$^{+0.12}_{-0.05}$, and finally δ = + 0.16$^{+0.11}_{-0.04}$ (Go 66; Ca 66; Go 67).

A weighted average of all five measurements yields δ = 0.12$^{+0.04}_{-0.02}$ while a similar average excluding the two smallest values gives δ = + 0.145$^{+0.04}_{-0.03}$.

5.7 The 2^-, 8.88 MeV Level in ^{16}O : experimental conditions and results

The 8.88 MeV level of ^{16}O was populated via the ^{19}F(p,a)^{16}O reaction using a 7.40 MeV proton beam from the Oxford University Tandem Van de Graaff Generator. The targets were prepared by evaporating a 200 μgm.cm^{-2} layer of BaF_2 onto a 15 μgm.cm^{-2} carbon backing. The particles were detected in a 300 μ.cm annular, n-type, silicon surface barrier counter which was mounted 5 cm from the target and which subtended angles between 170 and 173° to the incident beam direction. The counter was operated at

a voltage which gave a depletion depth which was sufficient to stop the alpha particles of interest but insufficient to stop the protons from the competing $^{19}F(pp')^{19}F$ reaction. Since the ^{19}F ground state has $J = \frac{1}{2}$ both the $m = 0$ and the $m = \pm 1$ magnetic substates of the ^{16}O levels were populated by the detected alpha particles. The relative population of the $m = 0$ magnetic substate is unknown and, therefore, had to be determined from the experiment. The Legendre polynomial coefficients for a direct ($J_1 \rightarrow J_2$) transition may be derived for this case from equations (3.4. 1,2) and are :

$$a_k = \left[p\ \rho_k(J_1\ 0) + \frac{(1-p)}{2}\ \rho_k(J_1\ 1)\right] \frac{\left[R_k(\ldots J_1 J_2) + 2\delta\ R_k(LL'J_1J_2) + \delta^2\ R_k(L'L'J_1J_2)\right]}{(1+\delta^2)}$$

(5.7. 1)

where p is the population of the $m = 0$ magnetic substate and is normalized so that $0 < p < 1$; δ is the mixing ratio for the $J_1 \rightarrow J_2$ transition and L, L' are the lowest possible multipolarities contributing to the transition.

In this experiment the cascade transitions which are

of interest all lead to the ground state which has J = 0 and are therefore of the form $J_1 \rightarrow J_2 \rightarrow 0$. The mixing ratio of the second transition is therefore identically zero and so the appropriate a_k coefficients for the second transition will be (see equations 3.4. 5-7) :

$$a_k = \left[p\, \rho_k(J_1\ 0) + \frac{(1-p)}{2}\, \rho_k(J_1\ 1)\right] \cdot \frac{\left[U_k(LJ_1J_2) + \delta^2\, U_k(L'J_1J_2)\right]}{(1+\delta^2)}\, \rho_k(J_2J_2J_20) \qquad (5.7.\ 2)$$

where the notation is the same as for equation (5.7. 1).

The gamma rays were detected in a 12.7 x 15.2 cm NaI(Tl) crystal mounted with its front face 20 cm from the target. The gamma rays in real and random fast-slow coincidence (the resolving time was approximately 30 ns) with the group feeding the 8.88 MeV level were stored in two 400 channel analyzers. The random coincidences were less than 3 per cent of the real ones in the region of interest and have been taken into account. The summed over angles gamma ray spectrum shown in Fig. 5.16 was de-

composed using for the line shapes for the 2.74 and 6.14 MeV gamma rays the 2.61 MeV gamma ray from a Th radioactive source and the 6.32 MeV gamma ray from the $^{18}O(p\,\alpha)^{15}N$ reaction leading to the state at 6.32 MeV in ^{15}N. The latter lineshape was obtained in coincidence with the relevant alpha particle group. The branching ratios were extracted after applying a correction for the known (Ga 62) relative photopeak efficiencies. The results, which are in agreement with those of other workers (Ai 56; De 57; Ku 59; Br 59), are listed in Table 5.5 together with the results of (Ai 56 and Br 59).

The contribution to the 8.88 MeV peak due to the sum up in the crystal of the 6.14 and 2.74 MeV gamma rays was estimated to be 2 per cent of the observed intensity of the 8.88 MeV gamma ray and was neglected. The effect of the finite size of the gamma ray detector was corrected for using the tables of Rutledge (Ru 59). The effect of the finite size of the alpha particle detector was, in general, neglected. A priori it would be expected that this effect was rather small and its effect would be to modify the values of the B_k coefficients. Since these quantities depend upon p and, in any case, must be determined from the experiment, small changes in the B_k's due to population

of the m = ± 2 magnetic substate could be roughly compensated for by changes in the values of ρ.

In this experiment three independent correlations were performed at the same beam energy. After extracting the experimental angular distributions from the gamma ray spectra the distributions were fitted to the Legendre polynomials of even order and then averaged (see Table 5.6) for the further analysis when it had been noted that the correlations had the same a_k coefficients to well within the experimental errors. By inspection of equations (5.7. 1,2) it can be seen that the correlations of all the transitions, except for the 6.88 MeV → g.s. transition which has $\delta \equiv 0$, depend upon the population parameter and the mixing ratio of either the $2^- \rightarrow 1^-$ (7.12 MeV) or $2^- \rightarrow 3^-$ (6.14 MeV) transition. In the preliminary analysis each experimental distribution was χ^2 fitted to the theoretical one for stepped values of the mixing ratio, δ, where relevant, and the population parameter, ρ, to obtain a complete mapping of χ^2 against these continuous parameters which made apparent the approximate possible solutions for each transition. It was seen that the 8.88 MeV → g.s. distribution was most sensitive to ρ which was then obtained in a more accurate way by minimizing χ^2

with respect to p (Fig. 5.17). The value p = 0.52 was found which was adopted for the further analysis of the other decay modes.

The χ^2 fit to the 8.88 → 6.14 MeV transition yielded the two values for the mixing ratio δ = + 2.9 and δ = + 0.176. Using both of these values the 6.14 MeV → g.s. cascade transition was fitted to the theoretical distributions which excluded the lower value of δ since χ^2 was greater than 20. The experimental distributions together with the theoretical fits for both values of the mixing ratio are shown in Fig. 5.18. The value δ = + 2.9 ± 0.2 is in agreement with the result of a gamma-gamma correlation (Lu 59) which gave δ = 2 ± 1. The error in δ was estimated by introducing the Legendre coefficient errors into the angular distribution formula and allowing for the uncertainty in the population parameter.

The 8.88 MeV → 7.12 MeV → g.s. cascade was analyzed in a similar way. The measured points and the plot of χ^2 against the mixing ratio of the 8.88 → 7.12 MeV transition are shown in Figs. 5.19 and 5.20 respectively. In this case the theoretical value of a_4 for the 7.12 MeV → g.s. transition is zero whilst that for the a_2 coefficient is given by :

$$Q_2 a_2 = -0.36 \left(\frac{1-\delta^2}{1+\delta^2} \right)$$

where Q_2 is the appropriate attenuation coefficient which corrects for the finite size of the gamma ray detector. The mean measured value of a_2 was $+0.39 \pm 0.04$ and so it was not possible to determine a unique value of δ(8.88 → 7.12 MeV) from this equation; the fit improved as $\delta \to \pm \infty$. However, a lower limit of 2.5 can be placed on the mixing ratio corresponding to the 1 per cent confidence limit on the χ^2 plot.

The analysis of the direct 8.88 → 7.12 MeV transition was hampered by the lack of good statistics since the subtraction of the background under the photopeak yielded large errors. This transition was therefore of little assistance although it was possible to conclude that δ is positive if $0 < |\delta| < 16$. If δ is very large then the theoretical distributions for the 8.88 → 7.12 transition become the same for both positive and negative values of δ. It is therefore concluded that for the 8.88 → 7.12 MeV transition, $|\delta| > 2.5$ and $\delta > 0$ if $0 < |\delta| < 16$. This result is compatible with that of (Au 59): $\delta > 5$ or $\delta \approx 0.2$. The lower value is therefore excluded.

The slight discrepancy between the theoretical maximum value and the experimental value for the 7.12 MeV → g.s. transition should have an explanation. The effect of the finite size of the particle detector would be to populate the m = ± 2 magnetic substate. This in turn would make the maximum theoretical value for a_2 somewhat smaller since the term of the B_k coefficient which corresponds to the m = ± 2 substates is opposite in sign to both terms corresponding to the m = 0 and ± 1 substates. This effect is therefore in the wrong direction. The other possible explanation is that the transition is a mixed E2/M1 transition. A priori this effect would be expected to be small since in light nuclei M2 transitions are usually somewhat enhanced whereas the same does not appear to be true for M3 transition strengths. However, the introduction of another variable into the angular distribution formula would mean that it would not be possible, in general, to find unique solutions for both $\delta(E2/M1)$ and $\delta(M3/E2)$ so, in view of the fact that the discrepancy is not too serious (just slightly less than one standard deviation), this matter will not be further pursued.

TABLE 5.1

Coefficients of Legendre Fits to the Experimental Distributions

Level	Transition	a_2	a_4
7.154	7.15 → 5.27	+ 0.46 ± 0.04	- 0.15 ± 0.05
	5.27 → g.s.	+ 0.42 ± 0.03	- 0.02 ± 0.04
7.303	7.30 → g.s.	- 0.31 ± 0.03	- 0.03 ± 0.05
7.563	7.56 → 5.27	- 0.25 ± 0.03	- 0.11 ± 0.05
	5.27 → g.s.	+ 0.61 ± 0.03	- 0.15 ± 0.04

TABLE 5.3

Summary of analysis of experimental results

Level	Direct Transition	J_1	δ_1	δ_2	χ^2 (g.s. transition)
7.154	7.15 → 5.27	$5/2$	- 0.04	- 0.13	0.6
			- 0.04	+ 5.7	0.6
			- 1.8	-	> 15
		$9/2$	- 0.01	-	> 15
7.563	7.56 → 5.27	$3/2$	- 0.21	-	> 8
			± 1.3	-	> 15
		$5/2$	- 0.9	-	> 15
		$7/2$	- 0.01	- 0.15	0.9
			- 0.01	+ 5.6	1.2
7.3[illegible]	7.30 → g.s.	$3/2$	- 0.07		1.9
			+ 2.1		1.9

J_1 is the spin of the level populated by the reaction.
δ_1 and δ_2 are the multipole mixing ratios of the first and second gamma rays of a cascade.

TABLE 5.3

Coefficients of Legendre fits to the Experimental Distributions

Level (MeV)	Transition	a_2	a_4
6.789	6.789 → g.s.	- 0.29 ± 0.02	- 0.03 ± 0.04
6.057	6.057 → 5.240	+ 0.46 ± 0.02	+ 0.03 ± 0.03
	5.240 → g.s.	+ 0.53 ± 0.02	- 0.03 ± 0.03
5.2 doublet	5.2 → g.s.	+ 0.28 ± 0.03	- 0.36 ± 0.05

TABLE 5.4

Summary of the analysis of the 6.857 MeV level

Transition	J(6.86 MeV)	δ_1	δ_2	χ^2
6.857→5.240	3/2	-		> 4.5 all δ_1
	5/2	-0.035		3.5
	7/2	-0.47		1.3
	9/2	-		> 5.0 all δ_1
5.240 → g.s.	5/2	-0.035	+ 0.13	1.8
		-0.035	+ 2.3	1.8
	7/2	-0.47	-	> 15 all δ_2

δ_1 is the mixing ratio of the 6.86 MeV → 5.24 MeV transition and δ_2 refers to the 5.24 MeV cascade transition.

TABLE 5.5

Transition	Branching ratio		
	This work	(Br 59)	(Wi 56)
8.88 → g.s.	7 ± 3%	7%	12%
8.88 → 6.14	77 ± 5%	74%	75%
8.88 → 6.92	< 5%	5%	3%
8.88 → 7.12	16 ± 5%	14%	10%

Branching ratios observed in the decay of the 8.88 MeV (2^-) level of ^{16}O together with the results of (Br 59; Wi 56).

A recent measurement indicates that the branch to the 6.92 MeV state is 4.2%. (Wi).

TABLE 5.6

Transition	a_2	a_4
8.8 → g.s.	+ 0.43 ± .04	- 0.31 ± 0.05
8.8 → 5.14	+ 0.00 ± 0.02	+ 0.0 ± 0.02
6.14 → g.s.	+ 0.1 ± 0.02	+ 0.01 ± 0.02
7.6 → 7.12	- 0.74 ± .1	+ 0.30 ± 0.2
7.12 → g.s.	+ 0.37 ± 0.04	- 0.02 ± 0.04

Coefficients of a fit of the experimental points to the Legendre polynomial series of even order. The values quoted represent an average of the three correlations.

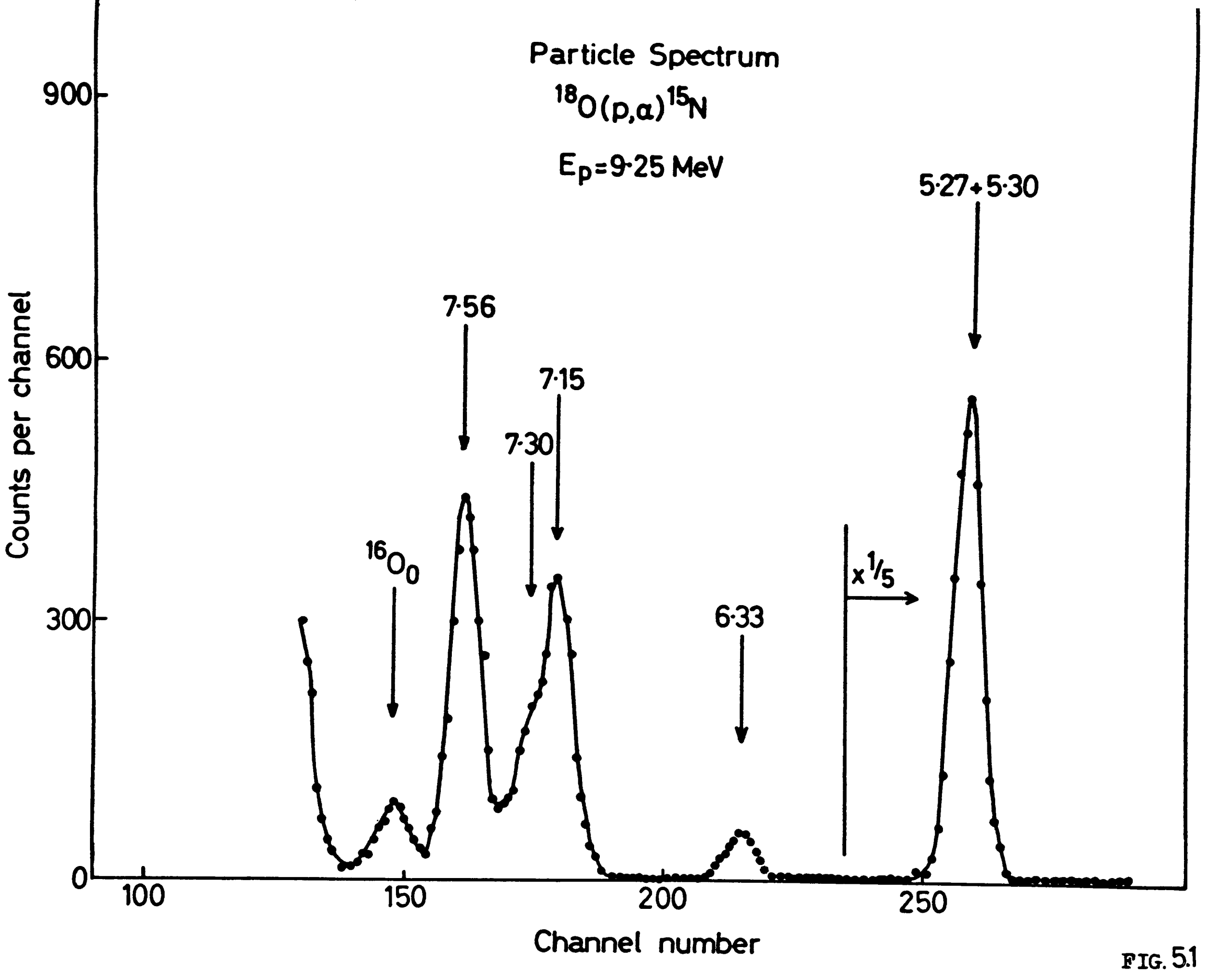

Particle Spectrum
$^{18}O(p,\alpha)^{15}N$
E_p=9·25 MeV
5·27+5·30
7·56
7·15
7·30
$^{16}O_0$
6·33
x 1/5
Counts per channel
900
600
300
0
100
150
200
250
Channel number

FIG. 5.1

^{15}N 7·15 MeV level

Gamma ray spectrum

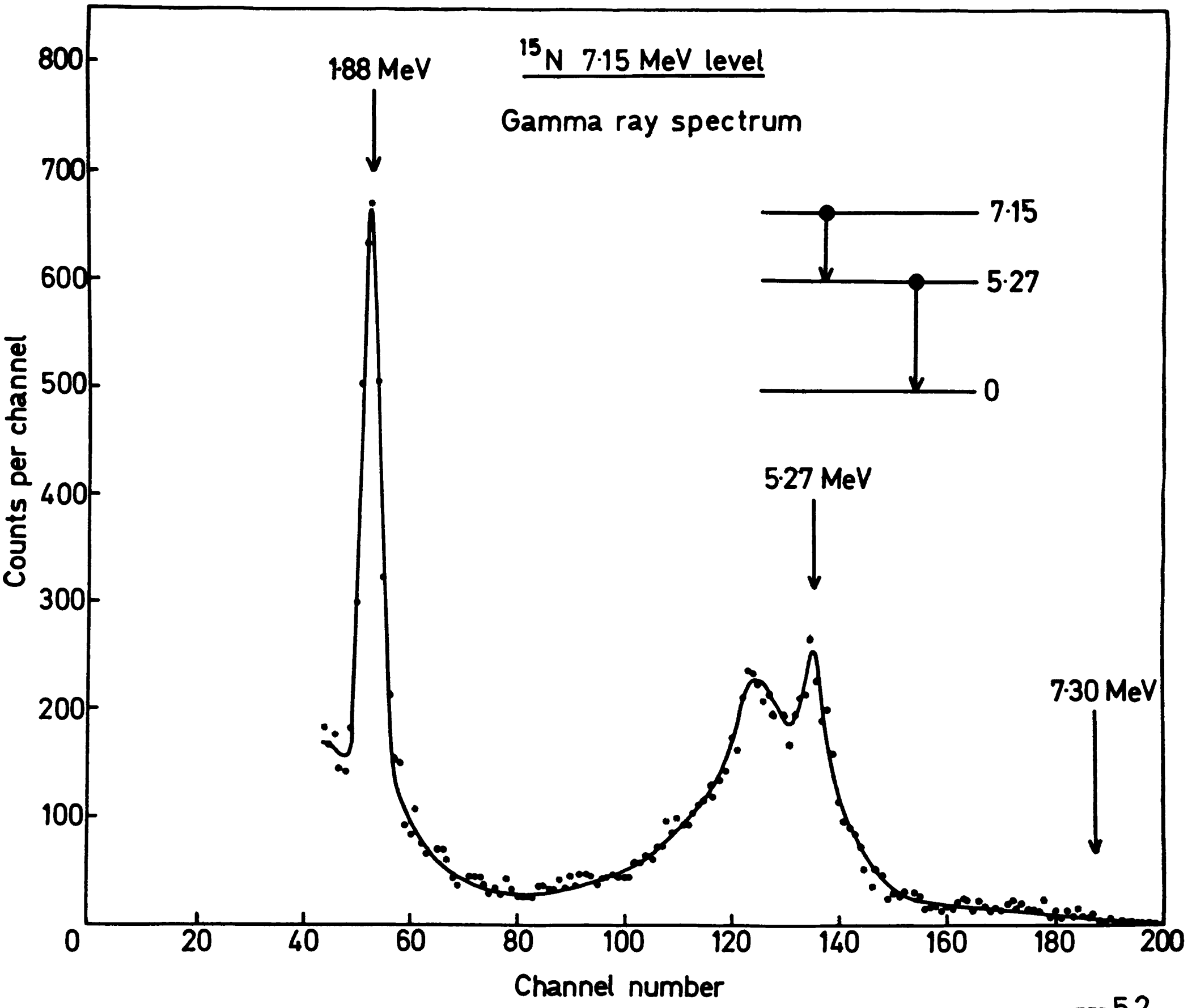


FIG. 5.2

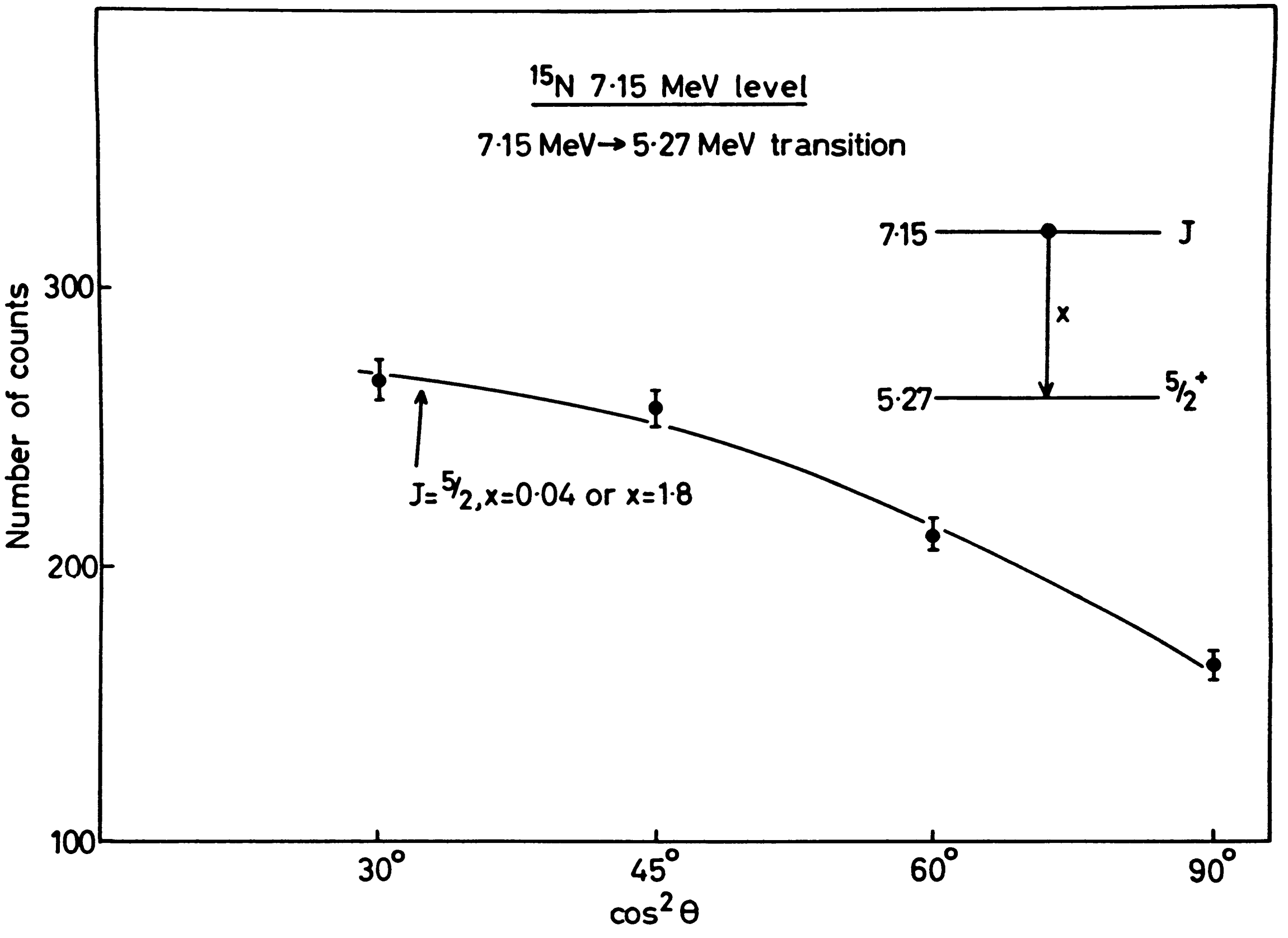

^{15}N 7·15 MeV level
7·15 MeV→ 5·27 MeV transition
7·15
J
x
5·27
5/2+
J=5/2, x=0·04 or x=1·8
Number of counts
300
200
100
30°
45°
60°
90°
cos²θ

FIG. 5.3

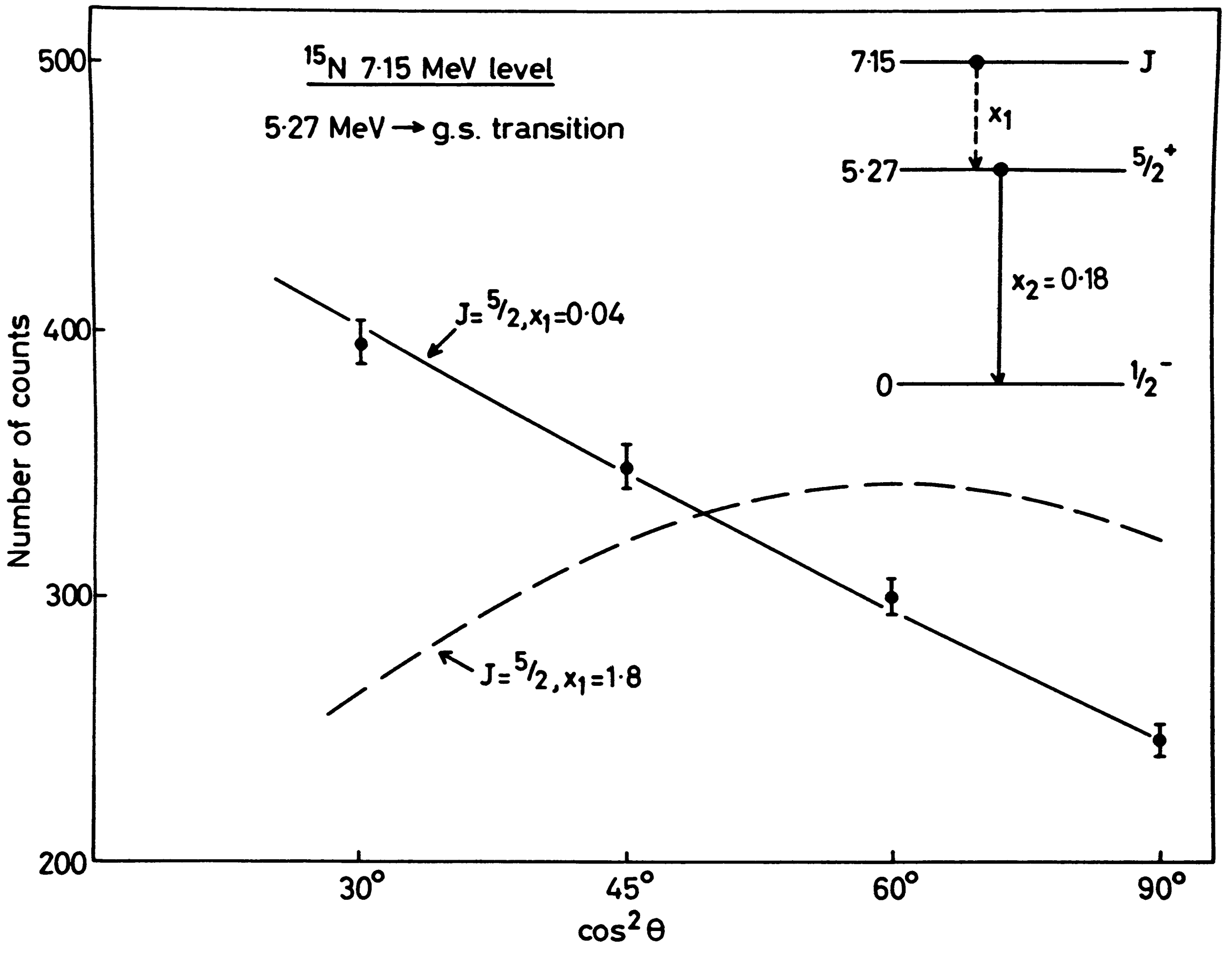

^{15}N 7·15 MeV level
5·27 MeV → g.s. transition
7·15
J
x_1
5·27
$5/2^+$
$x_2 = 0·18$
0
$1/2^-$
$J = 5/2, x_1 = 0·04$
$J = 5/2, x_1 = 1·8$
Number of counts
500
400
300
200
30°
45°
60°
90°
$\cos^2\theta$

FIG. 5.4

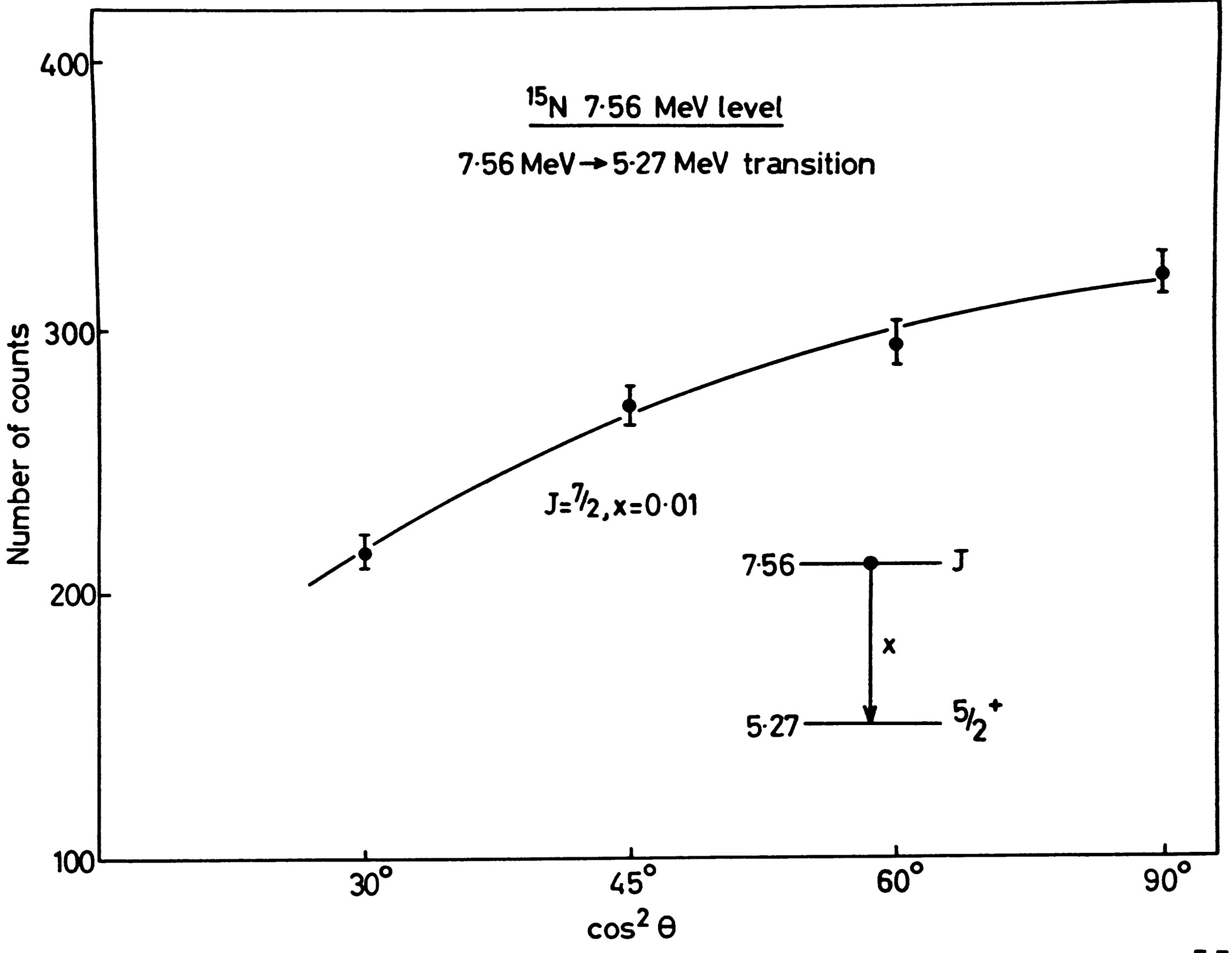

^{15}N 7·56 MeV level
7·56 MeV → 5·27 MeV transition
Number of counts
400
300
200
100
30°
45°
60°
90°
cos² θ
J=7/2, x=0·01
7·56
J
x
5·27
5/2⁺

FIG.5.5

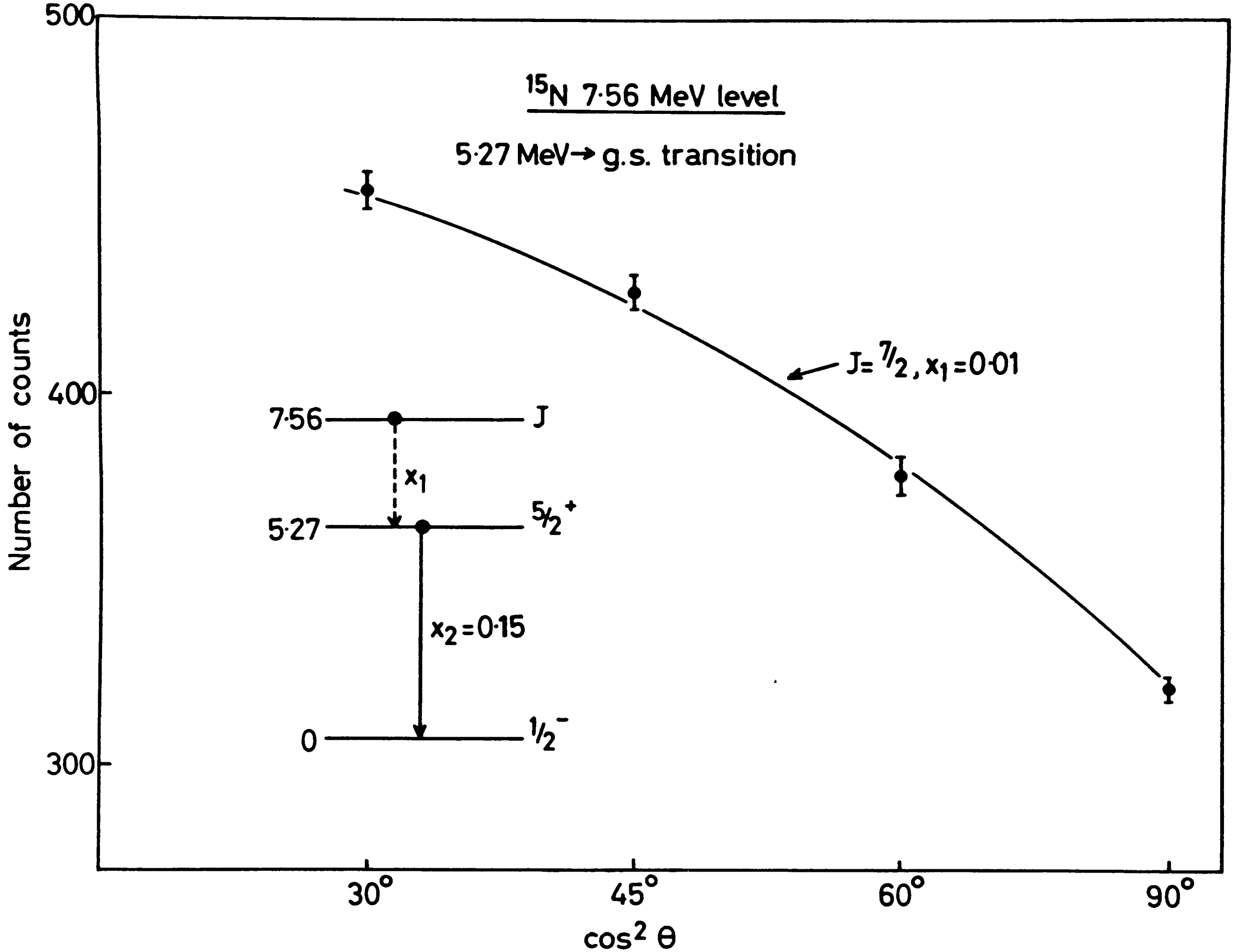

^{15}N 7·56 MeV level
5·27 MeV→ g.s. transition
J= 7/2, x1 =0·01
7·56
J
x1
5·27
5/2+
x2 =0·15
0
1/2−
500
400
300
Number of counts
30°
45°
60°
90°
cos2 θ

FIG.5.6

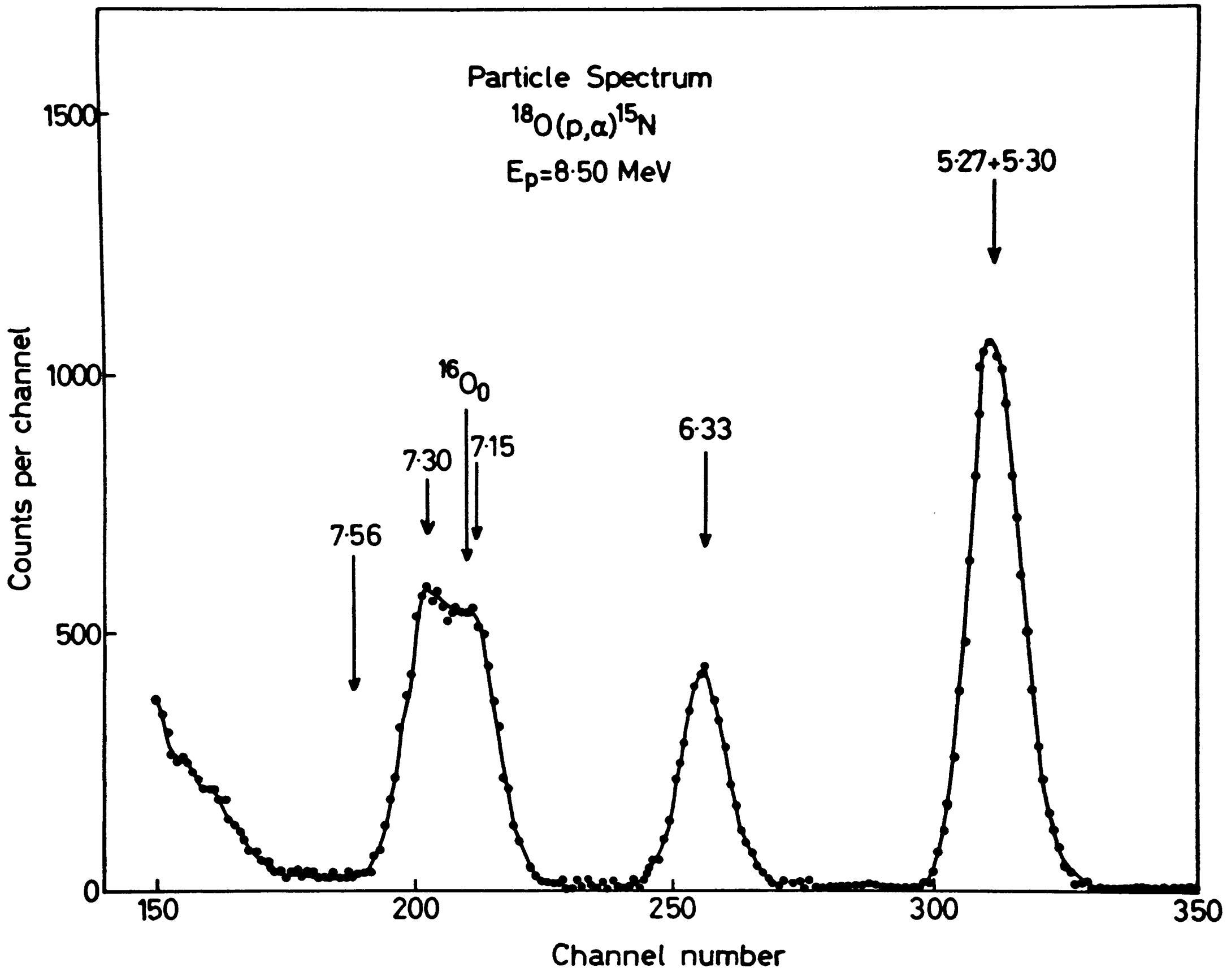

Particle Spectrum
$^{18}O(p,\alpha)^{15}N$
E_p=8·50 MeV
5·27+5·30
$^{16}O_0$
7·30
7·15
6·33
7·56
1500
1000
500
0
150
200
250
300
350
Counts per channel
Channel number

FIG. 5.7

^{15}N 7·30 MeV level

Gamma ray spectrum

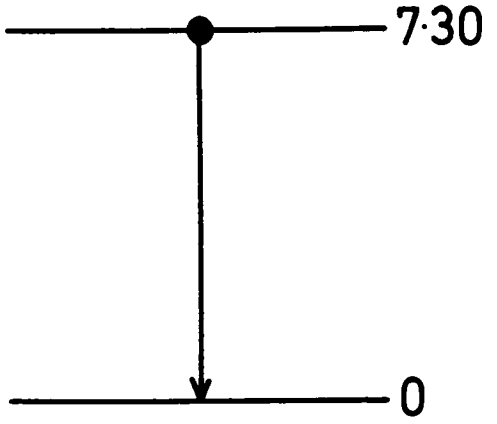


Fig. 5.8

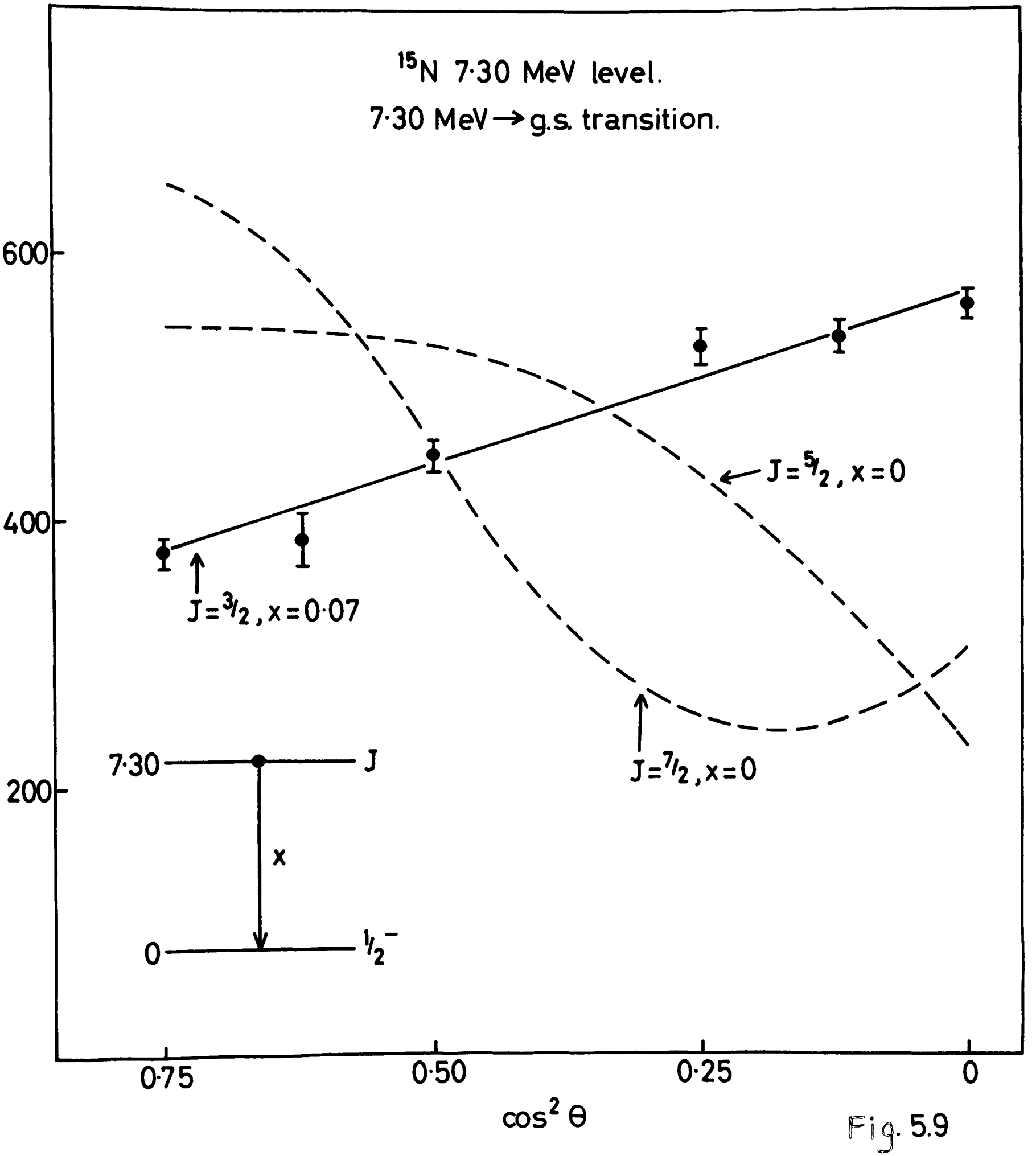

^{15}N 7·30 MeV level.
7·30 MeV → g.s. transition.
600
400
200
J=3/2, x=0·07
J=5/2, x=0
J=7/2, x=0
7·30
J
x
0
1/2⁻
0·75
0·50
0·25
0
cos² θ

Fig. 5.9

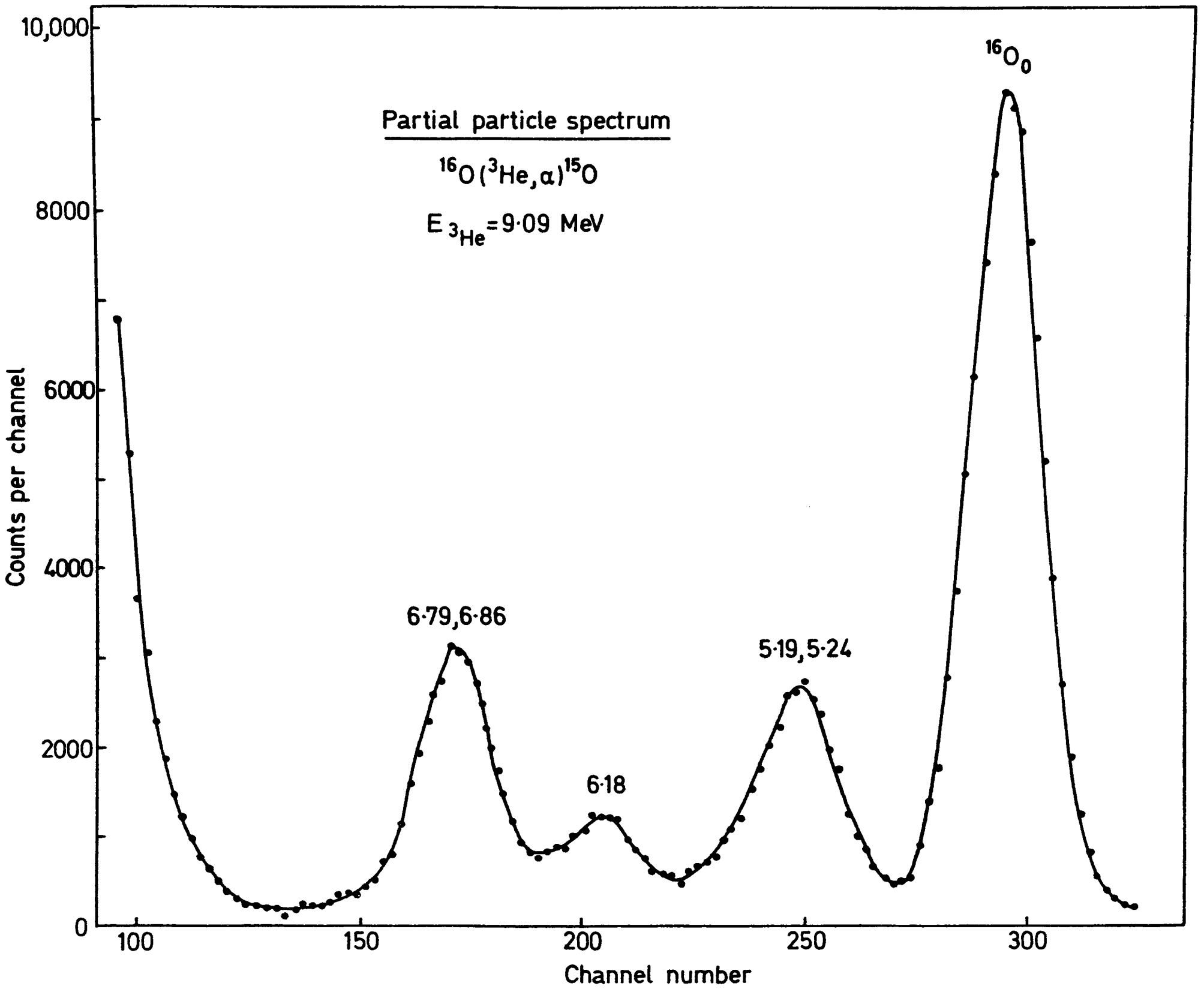

Partial particle spectrum
$^{16}O(^3He,\alpha)^{15}O$
$E_{^3He}$=9·09 MeV
$^{16}O_0$
6·79,6·86
6·18
5·19,5·24
Counts per channel
Channel number
10,000
8000
6000
4000
2000
0
100
150
200
250
300

FIG. 5.10

^{15}O 6·789 and 6·857 MeV levels

Gamma ray spectrum

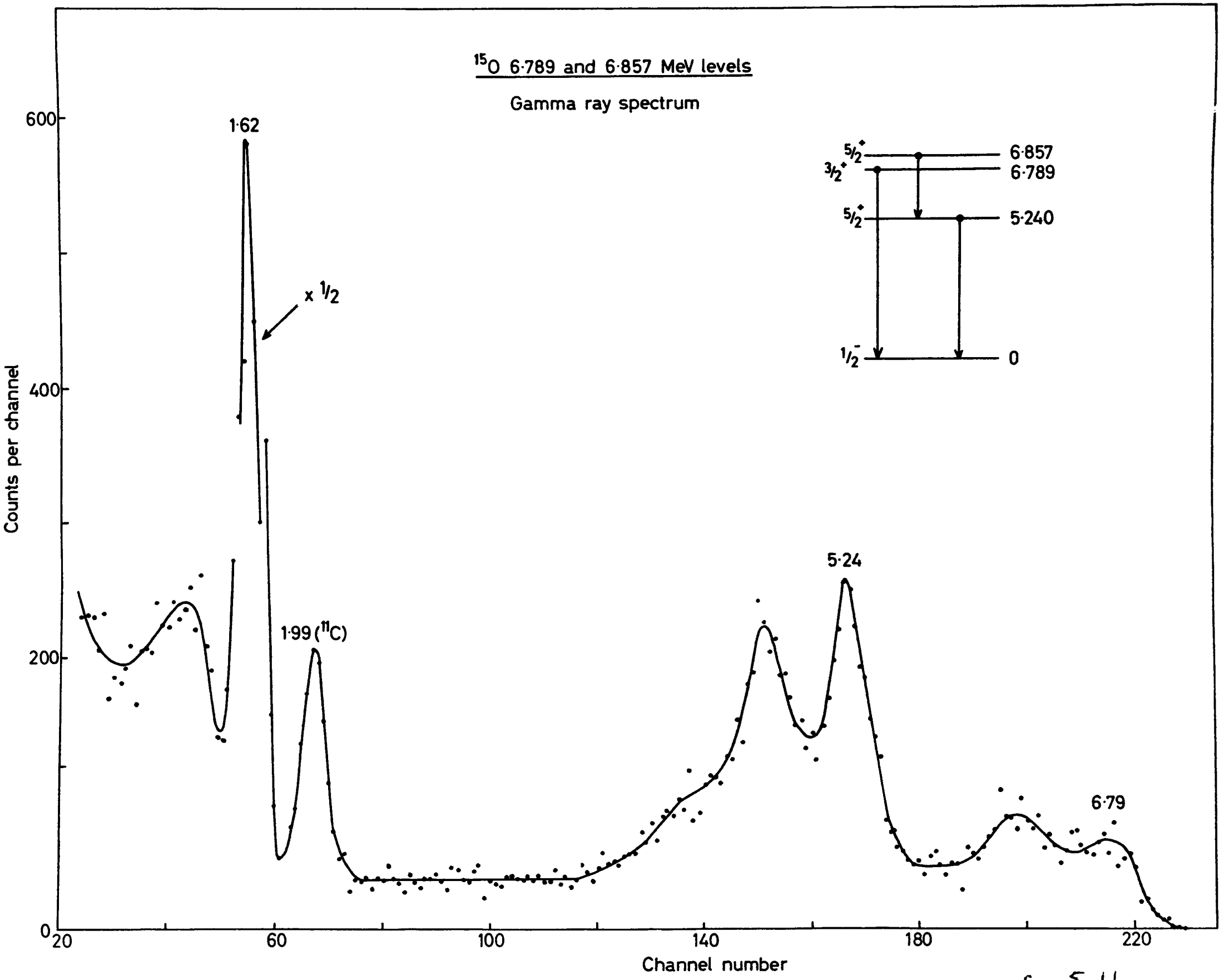


fig. 5.11

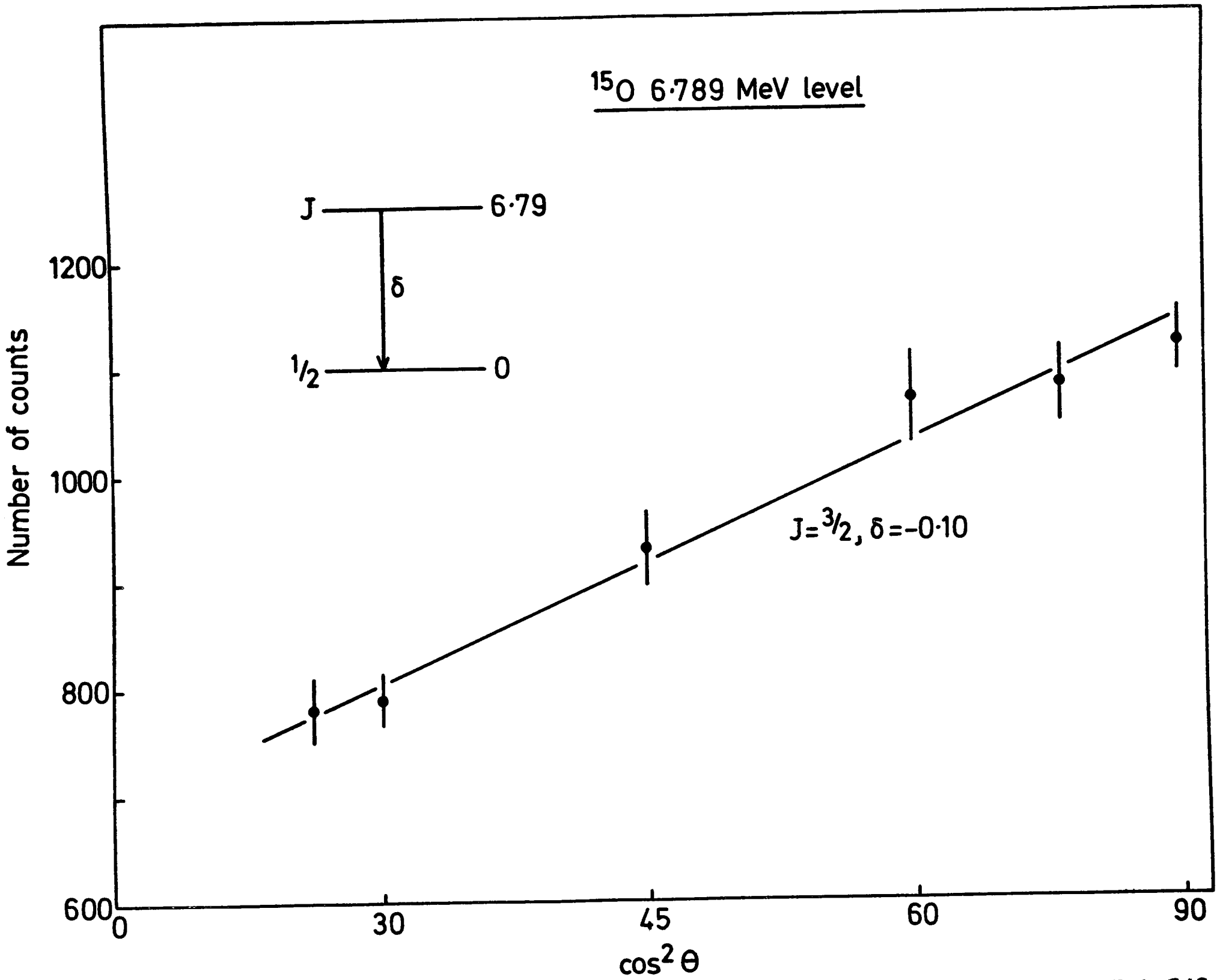

^{15}O 6·789 MeV level
J
6·79
δ
1/2
0
Number of counts
1200
1000
800
600
0
30
45
60
90
cos^2 Θ
J=3/2, δ=-0·10

FIG. 5.12

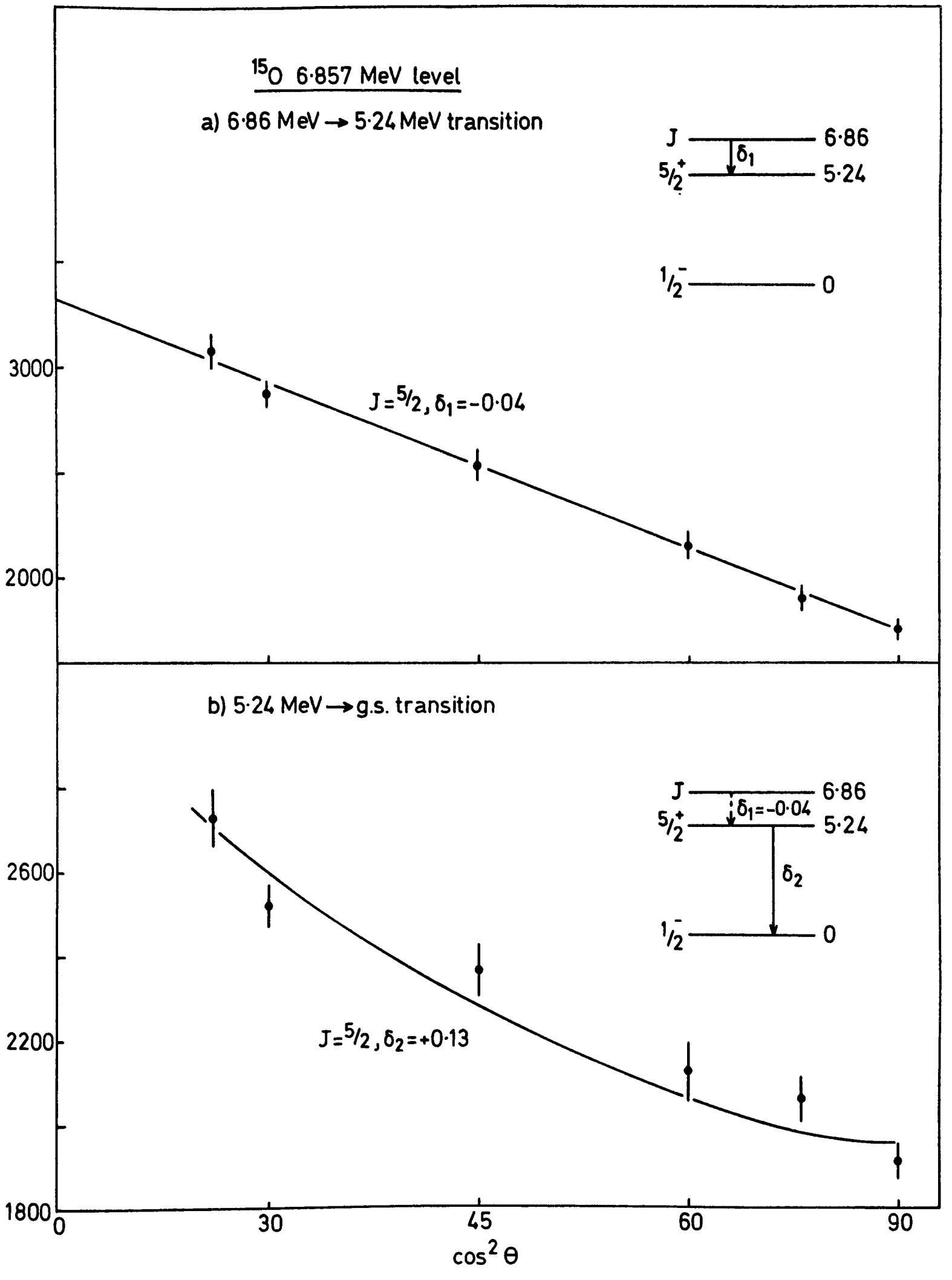

^{15}O 6·857 MeV level
a) 6·86 MeV → 5·24 MeV transition
J
δ_1
$5/2^+$
6·86
5·24
$1/2^-$
0
3000
2000
$J=5/2, \delta_1=-0·04$
b) 5·24 MeV → g.s. transition
J
$\delta_1=-0·04$
$5/2^+$
6·86
5·24
δ_2
$1/2^-$
0
2600
2200
1800
$J=5/2, \delta_2=+0·13$
0
30
45
60
90
$\cos^2\theta$

FIG. 5.13

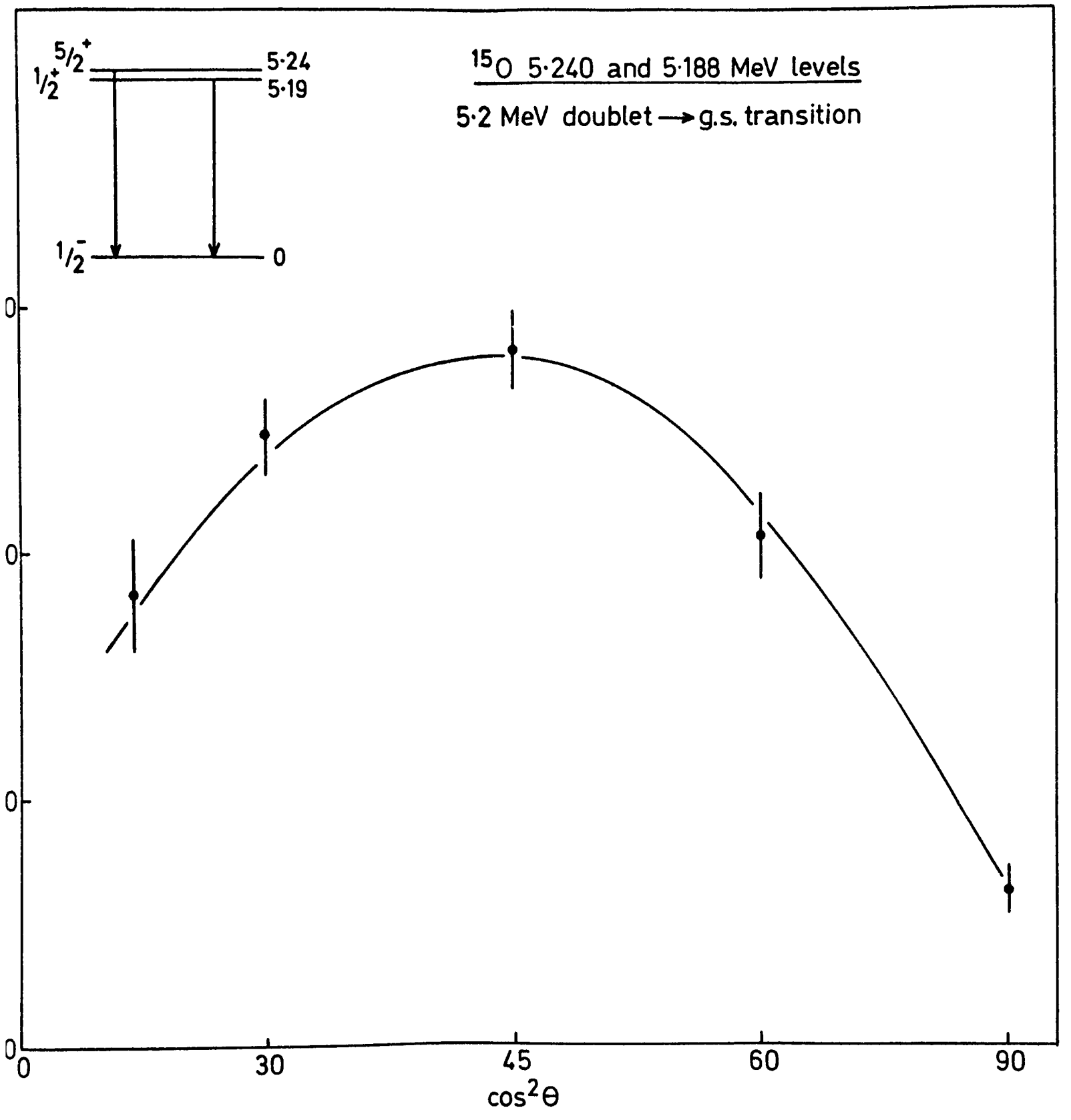

^{15}O 5·240 and 5·188 MeV levels
5·2 MeV doublet → g.s. transition
5/2+
1/2+
5·24
5·19
1/2−
0
0
0
0
0
30
45
60
90
cos²θ

FIG. 5.14

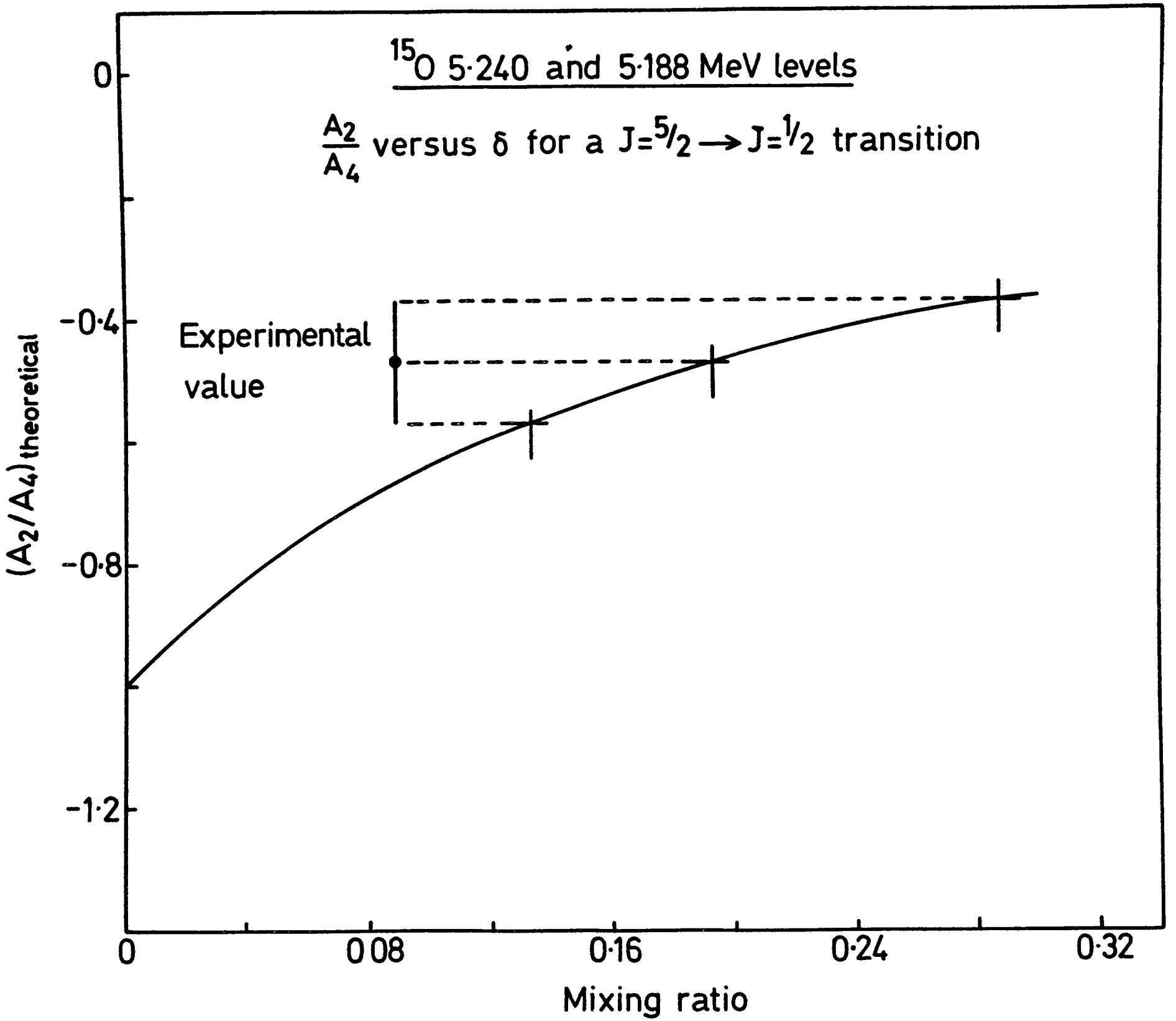

^{15}O 5·240 and 5·188 MeV levels
$\frac{A_2}{A_4}$ versus δ for a J=5/2 → J=1/2 transition
Experimental value
$(A_2/A_4)_{theoretical}$
0
-0·4
-0·8
-1·2
0
0·08
0·16
0·24
0·32
Mixing ratio

FIG. 5.15

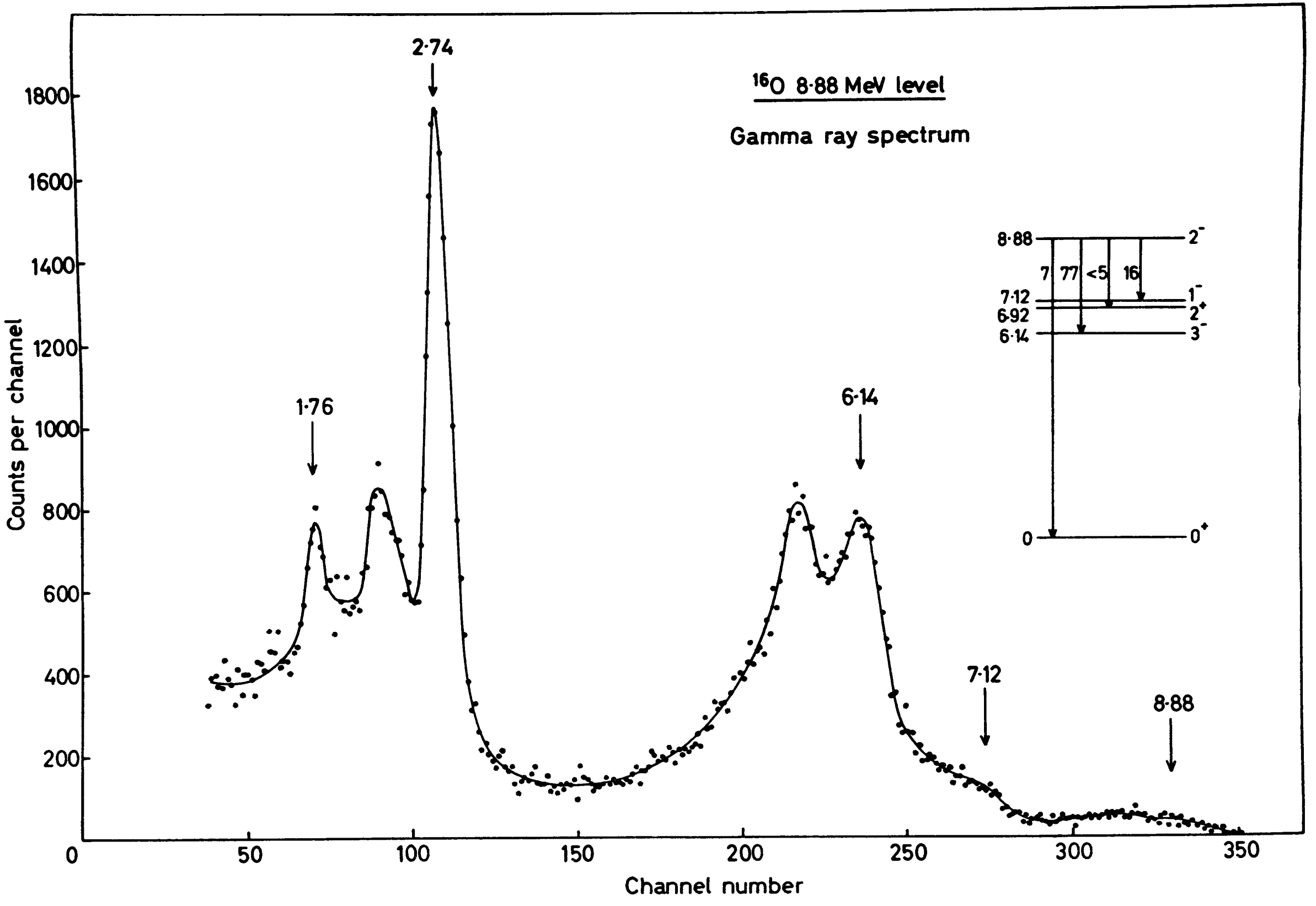

^{16}O 8·88 MeV level
Gamma ray spectrum
8·88
2⁻
7
77
<5
16
7·12
1⁻
6·92
2⁺
6·14
3⁻
0
0⁺
2·74
1·76
6·14
7·12
8·88
Counts per channel
1800
1600
1400
1200
1000
800
600
400
200
0
50
100
150
200
250
300
350
Channel number

Fig. 5.16

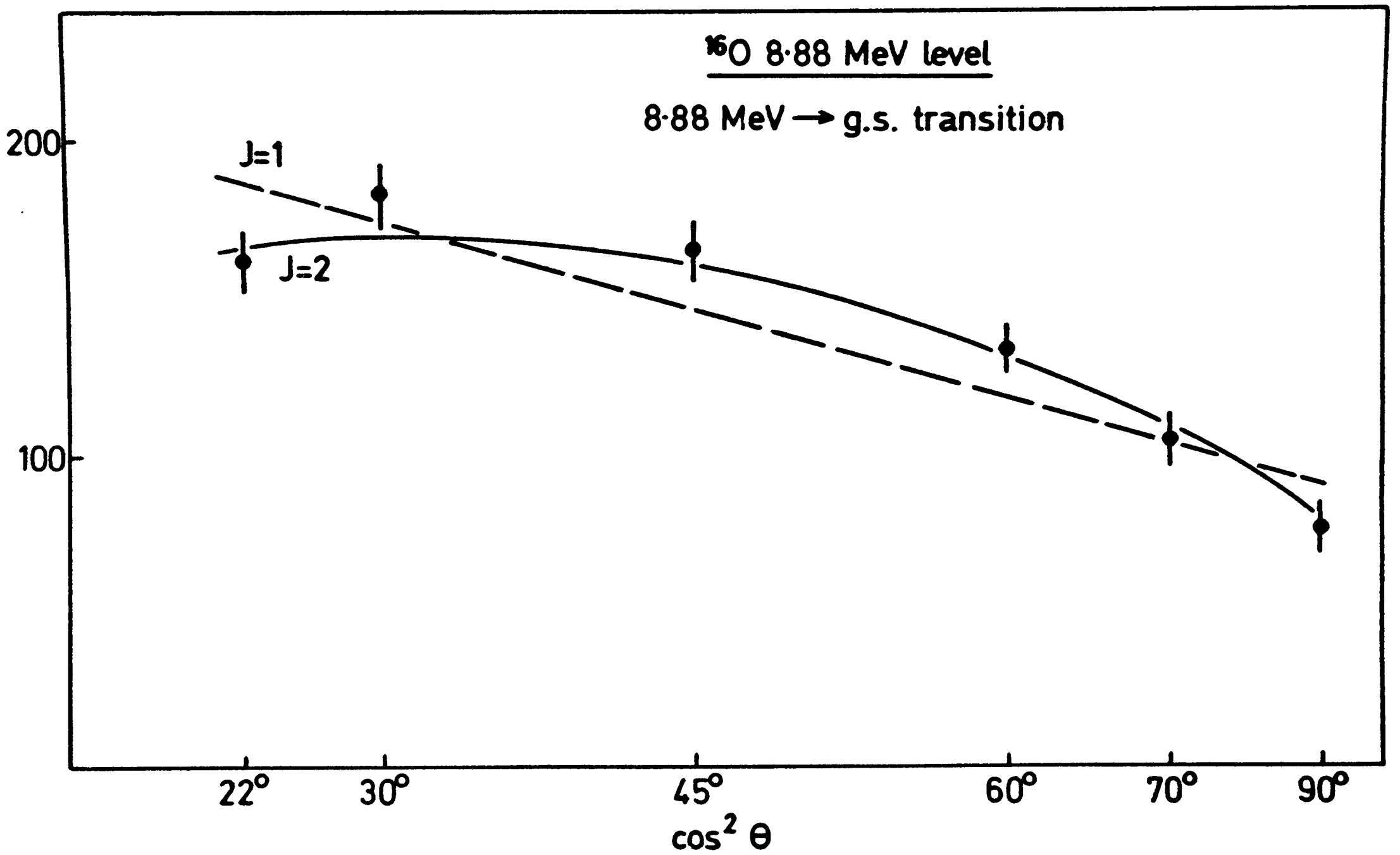

^{16}O 8·88 MeV level
8·88 MeV → g.s. transition
200
100
J=1
J=2
22°
30°
45°
60°
70°
90°
cos² θ

Fig. 5.17

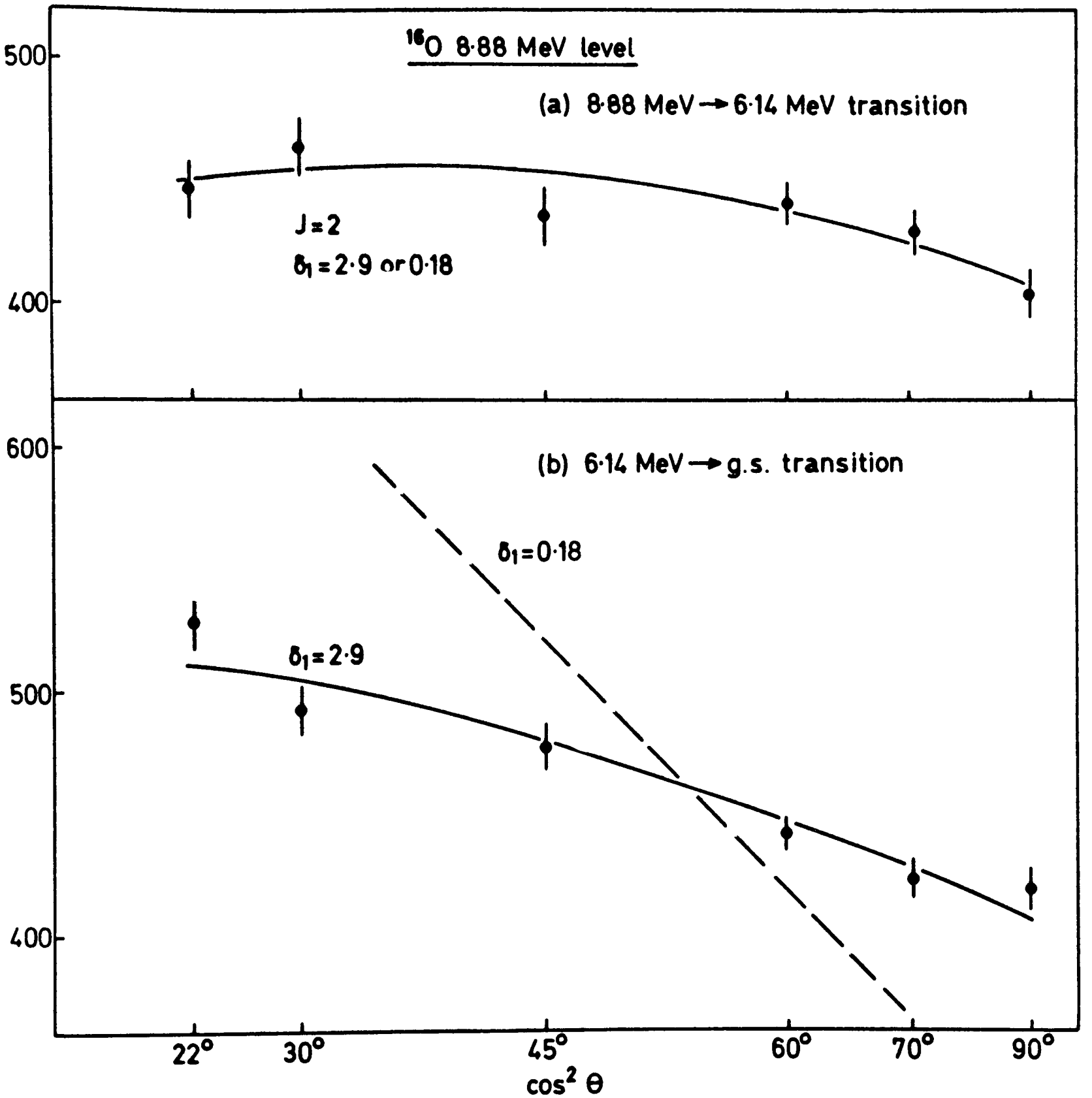

^{16}O 8·88 MeV level
(a) 8·88 MeV → 6·14 MeV transition
J = 2
δ1 = 2·9 or 0·18
500
400
(b) 6·14 MeV → g.s. transition
δ1 = 0·18
δ1 = 2·9
600
500
400
22°
30°
45°
60°
70°
90°
cos² θ

Fig.5.18

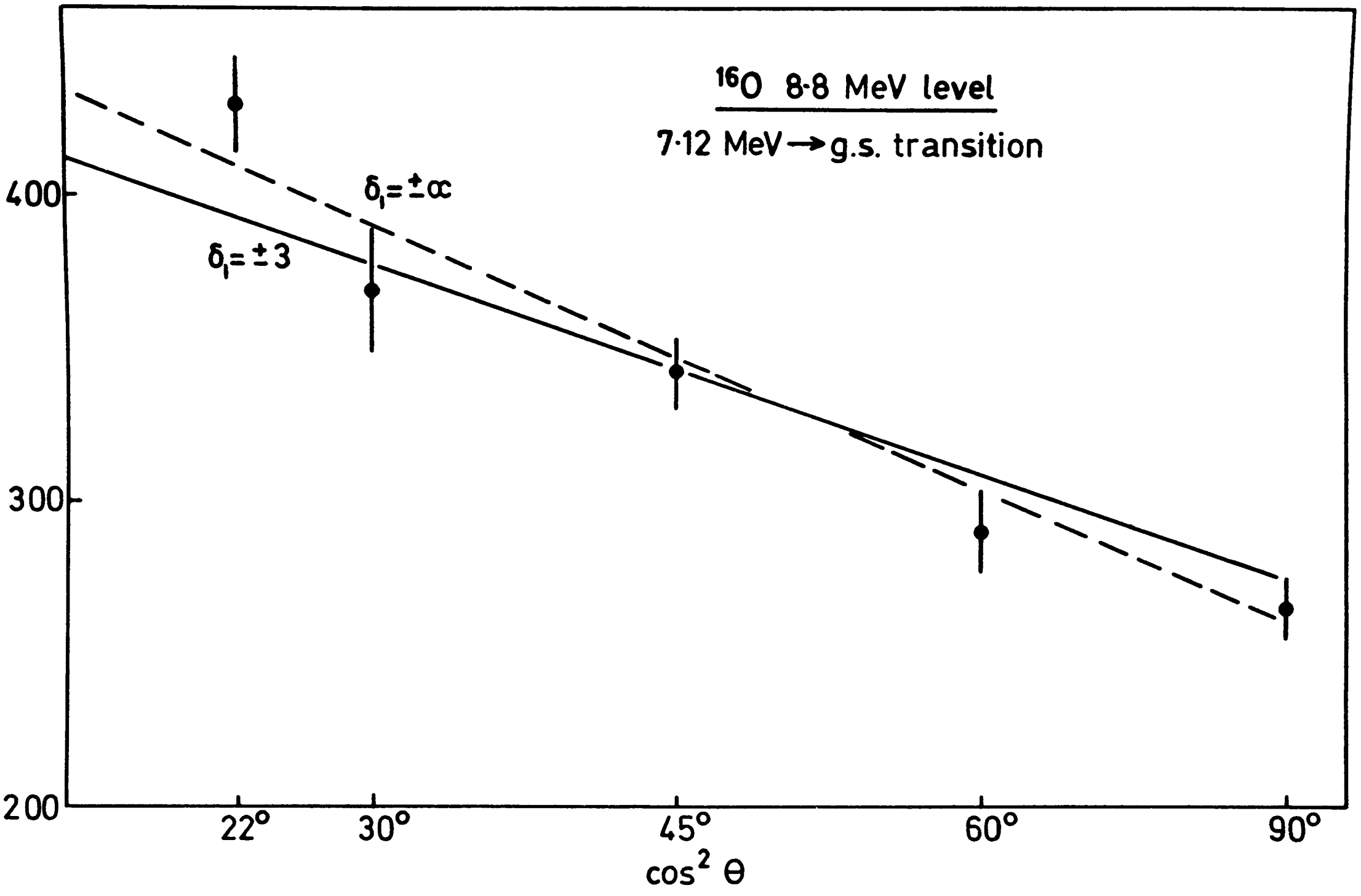

^{16}O 8·8 MeV level
7·12 MeV → g.s. transition
$\delta_1 = \pm\infty$
$\delta_1 = \pm 3$
400
300
200
22°
30°
45°
60°
90°
$\cos^2 \theta$

Fig.5.19

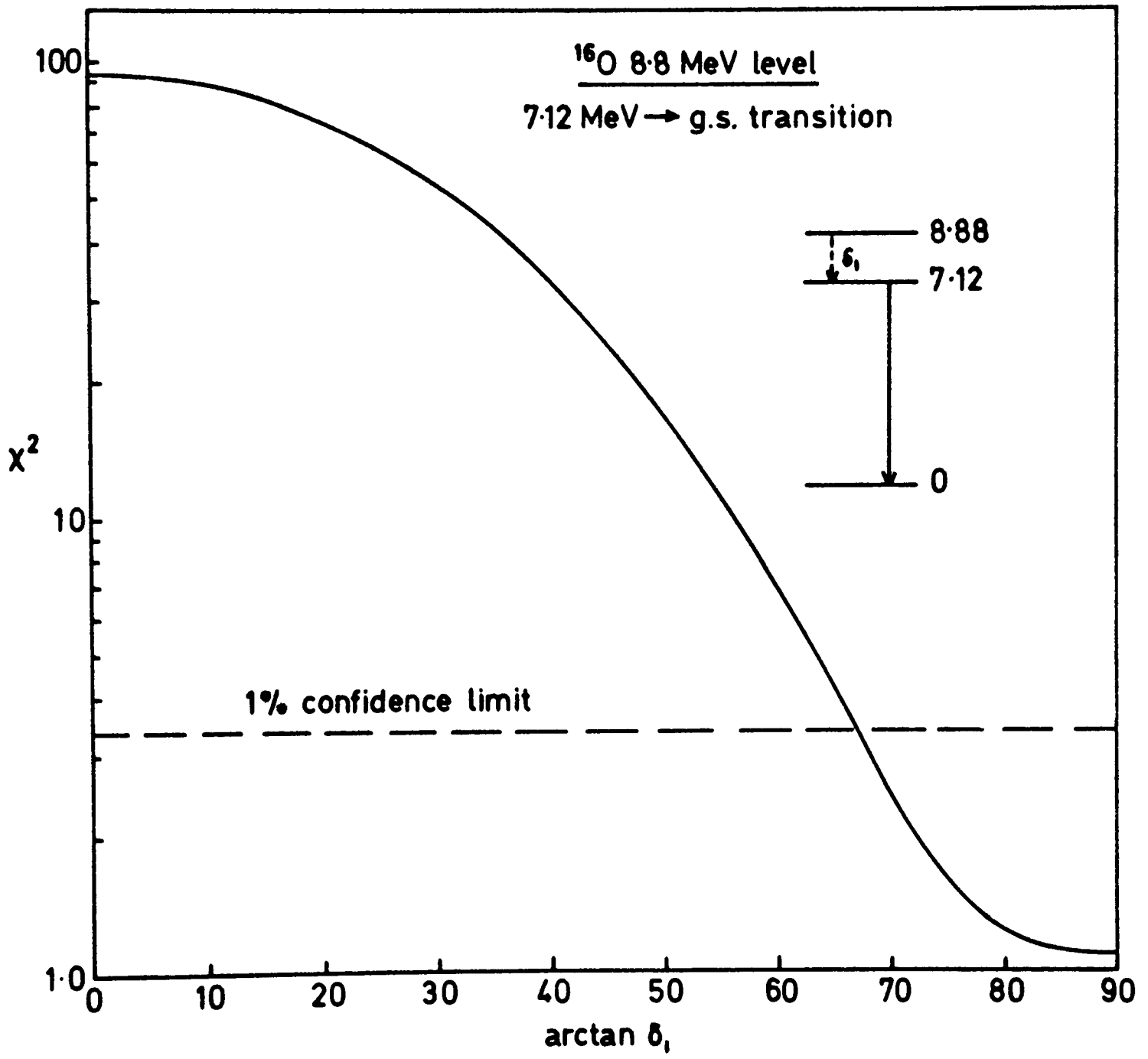

^{16}O 8·8 MeV level
7·12 MeV → g.s. transition
8·88
δ_1
7·12
0
100
10
1·0
χ^2
1% confidence limit
0
10
20
30
40
50
60
70
80
90
arctan δ_1

Fig. 5.20

C H A P T E R 6

LIFETIME MEASUREMENTS IN MASS 15

6.1 Experimental Conditions

A 21.80 MeV beam of 4^+ Nitrogen ions supplied by the Oxford University Tandem Van de Graaff Generator with an analyzed beam current of about 90 na was used to populate levels in ^{15}N and ^{15}O via the d(^{14}N, ^{15}N)p and d(^{14}N, ^{15}O)n reactions. (The Q values for these reactions are 8.610 and 5.066 MeV respectively.) Levels in ^{15}N and ^{15}O up to excitation energies of 11.3 and 7.8 MeV could be populated by the reaction although it would be expected that the levels above 10.81 and 7.28 MeV in ^{15}N and ^{15}O would decay by particle emission since they are unbound with respect to neutron and proton emission respectively. The targets consisted of thin layers of Titanium evaporated onto either Copper or Aluminium backings and impregnated with > 97 per cent purity deuterium; the main impurity being H. The target backings were chosen to be sufficiently thick to completely stop the heavy particles produced in the reactions.

In the first part of the experiment the high energy ground state transitions were investigated. The target layer of Titanium was about 90 $\mu gm.cm^{-2}$ which will impose a limit upon the shortest lifetime which may usefully be investigated from a comparison of the spectra from two targets with different backings. In this case the recoil nuclei produced by the reactions of the ^{14}N with the deuterium in the target will cross the target layer in about 1.3×10^{-14} sec which sets a lower limit upon the lifetimes which can be measured. The targets were mounted in a target chamber the design of which included a liquid Nitrogen cold trap which surrounded the target and virtually eliminated carbon build up on the target. After a week of continuous running the carbon spot on the target was just visible which probably corresponded to a thickness of less than about 30 $\mu gm.cm^{-2}$ thus not seriously affecting the thickness of the layer before the backing material.

The gamma rays were detected in a 30 cm^3 Lithium drifted Germanium detector (RI 66) which was mounted with its front face 9 cm from the target on a rotating trolley. The half acceptance angle of the crystal was 8^{o}. The analogue pulses from the detector were fed via a low noise charge sensitive pre-amplifier and an R-C amplifier to the

1000 channel analogue to digital converters of a PDP7 on line computer. The gains and base lines of the ADC's were adjusted so that gamma rays in the intervals 5.1 to 6.2 MeV, 6.2 to 8.2 MeV and 3.9 to 5.1 MeV were accumulated in separate ADC's which all had dispersions of about 2 keV per channel. The gain of the system was not stabilised but was monitored using a precision pulse generator and, where appropriate, radioactive sources. It was found that if all the connections in the circuit were rigidly made that there were no gain shifts in the system to better than 1 part in 4000 with either time, count rate or upon moving the Germanium detector. The overall resolution of the system was about 12 keV for a 2.61 MeV gamma ray.

Gamma ray spectra were accumulated with the detector at 90° with respect to the incident beam direction to determine the unshifted positions of the peaks. No attempt was made to measure the energies accurately partly because this had been done at the time of the experiment (wa 65b) and partly because the positions of the gamma rays which showed the full Doppler shift would have been extremely sensitive to small deviations of the counter from 90°. Gamma rays were seen in the spectrum corresponding to the ground state decays of the ^{15}N levels located 5.270,

6.323, 7.300 and 8.312 MeV and of the ^{15}O levels at 5.240, 6.180 and 6.789 MeV. A 4.0 to 10.0 MeV gamma ray spectrum showed that the relative population of higher states with ground state decays was rather small. From the known decay schemes of the levels in ^{15}N and ^{15}O (Wa 65b) it can be seen that of these gamma rays all except those from the levels at 5.270 and 5.240 MeV corresponded to direct population of the levels rather than population by gamma decay from higher levels. The 5.270 (^{15}N) and 5.240(^{15}O) MeV levels would have been appreciably populated by the cascade gamma rays from the decay of the 7.154 and 7.563 MeV levels in ^{15}N and the 6.857 and 7.276 MeV levels in ^{15}O.

Spectra were accumulated with the Germanium counter at 0° with respect to the beam direction using both the Aluminium and Copper backed targets. It was noted that none of the peaks from either backing showed any deviation from the maximum shift allowed by the kinematics except for the 5.270 MeV → g.s. and 5.240 MeV → g.s. peaks corresponding to the transitions in ^{15}N and ^{15}O which were seen to be unshifted. A sample of the data is shown in Fig. 6.1 where the double escape 7.300 MeV peak is shown for both target backings. The peaks lie entirely within the limits

allowed by the kinematics - the rather odd shape resulting from the non-isotropy of the reaction process populating the level.

The peak centroids and their errors were extracted after the subtraction of the background. The centroids were calculated with respect to the unshifted position of the peaks and the quantity $F(\tau)$ was found. For all the transitions investigated $F(\tau)$ was found to be entirely consistent with zero allowing a lower limit to be placed upon the lifetimes of the levels. The $\frac{dE}{dx}$ values for the ^{15}O and ^{15}N ions were calculated using the effective charge method and are shown in Figs. 6.4, 5. The lifetime limits for the 6.323, 7.300 and 8.312 MeV levels in ^{15}N and for the 6.180 and 6.789 MeV levels in ^{15}O are listed in Table 6.1. In the calculation of these limits the effect of the finite thickness of the Titanium target layer was taken into account.

In the second part of the experiment the low energy cascade transitions to the states at 5 MeV were investigated. It was not possible to observe these transitions in the raw spectrum as there was a large number of gamma rays present which could not be identified as belonging to either ^{15}N or ^{15}O which obscured the transitions of interest.

It was thought that these gamma rays were probably produced by the reaction of the incident ^{14}N beam with small impurities of light elements, other than Deuterium, which could have been present in the target. The low energy spectrum was essentially unchanged when the backing material was altered. This matter was not pursued but a gamma-gamma coincidence method was used to simplify the spectrum. The 5 MeV gamma rays were detected in one of two 12.7 x 15.2 cm NaI(Tl) crystals which, for the runs taken with the Germanium detector at 0°, were mounted with their front faces about 8 cm from the target and at 90° to the incident beam direction. Fast-slow real and random coincidences were made between the NaI(Tl) crystals and all the gamma rays detected in the Germanium detector. The energy window set in the NaI(Tl) crystals covered the region 4.0 to 5.6 MeV and should have included the photo-peak and escape peaks of a 5.2 MeV gamma ray incident upon the crystal. The logic pulses from the coincidence circuit were used to gate and route one of the ADC's of the on line storage system. The gain and base line of the ADC was set to include the region 1 to 3 MeV. A spectrum was obtained at 90° to the beam line using the copper backed target (Fig. 6.2) which revealed the presence of 5 gamma

rays as indicated in the diagram. Spectra were also accumulated at 0° (Fig. 6.3) using both the Copper and Aluminium backed targets which for this part of the experiment had Titanium layers of 180 $\mu gm.cm^{-2}$. The target thickness had to be increased as compared with the previous part of the experiment in order to obtain a sufficiently high coincident counting rate. The gain of the system was checked before and after each run using a Rd Th radioactive source although the constancy of the gain of the system was further guaranteed by the small widths of the 1.884 and 1.617 MeV peaks.

The four strongest gamma rays in the spectrum taken at 90° (Fig. 6.2) corresponded to the decays of the 7.154 and 7.563 MeV levels to the 5.270 MeV level in ^{15}N and to the decays of the 6.857 and 7.276 MeV levels to the 5.240 MeV level in ^{15}O. The weak gamma ray which appears in the spectrum has an energy of 2.000 ± 7 keV and showed a shift when the detector was moved from 90° to 0° which was consistent with it having come from the 7.300 → 5.299 MeV transition. Insertion of the appropriate efficiency factors (Ja 62; Fr 66; La 67; Al,An) showed that this branch was 2 ± 1 per cent which is in agreement with the 2 per cent branch to one of the 5.3 MeV doublet levels

reported by (wa 65b). In Table 6.2 the decay data for the lower levels in both ^{15}N and ^{15}O is collected and compared with other measurements.

6.2 Extraction of the lifetimes from the Data

The centroids of the gamma ray peaks observed in the coincidence part of the experiment at 0° with respect to the incident beam direction were calculated after the subtraction of the background which was taken to vary linearly under the peaks with the exception of some of the peaks which were superimposed on the Compton background due to higher energy gamma rays. In these latter cases the lineshapes of radioactive sources were used which were obtained at the time of the experiment. The errors on the centroid determinations were found using equation (4.2. 4). A comparison of the centroids due to the different targets showed which lifetimes might be extracted from the data. Neither the 1.884 nor the 1.617 MeV transition showed shifts using the Copper backed target which differed from those from the Aluminium backed target and lifetime limits were therefore placed upon the 7.154 and 6.857 MeV levels in ^{15}N and ^{15}O respectively which are shown in Table 6.1.

In Fig. 6.3 the vertical broken lines indicate the unshifted peak positions as determined from the 90^{o} spectrum and the maximum shifts allowed by the kinematics.

The 2.293 and 2.036 MeV gamma rays both showed considerably different shifts in the spectra corresponding to the two different target backings (Fig. 6.3). Small corrections were then applied to these centroids to take into account the variation of efficiency of the gamma ray detector with energy and to take into account the effect of the small low energy tail associated with a peak due to a monoenergetic gamma ray. The effects due to the angular correlations of the gamma rays were neglected since it has been seen in Section 4.1 that these effects should be small. In this case it would not be expected that there would be large anisotropies of the gamma rays since the magnetic substates of the decaying level may be populated without restriction. For the 2.293 MeV gamma ray it was found that $\bar{c}_{Cu} - \bar{c}_{Al} = 5.02 \pm 0.88$ keV whilst $\frac{1}{2}(\bar{c}_{Cu} + \bar{c}_{Al}) = 112 \pm 1$ keV where the centroids were measured with respect to the unshifted peak positions determined from the 90^{o} spectrum.

This value of $(\bar{c}_{Cu} - \bar{c}_{Al})$ must be corrected for the effect of the finite thickness of the target layer since

an appreciable fraction of the excited nuclei will decay before reaching the target backing. The correction factor is just the ratio of the number of nuclei decaying in the target backing to the total number of excited nuclei produced which may be seen as follows. Suppose that the number of events in each energy bin is divided into n_i^B and n_i^T which are the number of decays in the backing and in the Titanium target layer. The centroid of the peak will be given by :

$$\bar{e} = \frac{\sum (n_i^B + n_i^T)\, e_i}{\sum n_i^B + \sum n_i^T}$$

$$= \frac{\sum n_i^B e_i + \sum n_i^T e_i}{N^B + N^T}$$

If measurements are taken using a second target backing with the same target layer then the difference in the centroids will be :

$$\bar{e}_1 - \bar{e}_2 = \frac{\sum n_{11}^B e_i - \sum n_{21}^B e_i}{N^B + N^T}$$

assuming that the spectra are normalized so that the total number of peak counts is the same in both. The quantity required for further analysis is this quantity multiplied by $\frac{N^B + N^T}{N^B}$ which depends upon the lifetime of the level.

Hence for the 2.293 MeV gamma ray

$$R(\tau) = \frac{5.02}{112 \times 2} \times \frac{N^B + N^T}{N^T}$$

The quantity $R(\tau)$ was calculated by numerically integrating the energy loss curves and calculating the mean values of the velocity for various lifetimes. As has previously been remarked, the quantity $R(\tau)$ depends upon the initial velocity of the ions which in this case varies by about 10 to 15 per cent. The possible variation in $R(\tau)$ due to this cause was seen to be about 2 per cent and can therefore be neglected. It is not possible to decide upon the proper value to use for the initial velocity since the cross-section for the reaction is usually unknown. Using the calculated values of $R(\tau)$ a value $\tau = (6 \pm 2) \times 10^{-14}$ sec was extracted for the lifetime of the 7.563 MeV level. The error was increased over and

above that determined from the statistics to take into account possible errors in the stated target layer thickness and the errors in the $\frac{dE}{dx}$ values used which were of the order of 5 per cent.

In the analysis of the 2.036 MeV gamma ray the quantities $F(\tau)$ were extracted for both backings. The maximum possible shift was estimated from the centre of mass velocity of the excited nuclei. The energy loss curve was integrated and values of $F(\tau)$ were calculated for various lifetimes in the region of interest. It was verified that the inclusion of the contribution from the nuclear interaction change the values of $F(\tau)$ by about 2 per cent and it was therefore concluded that the further effects of the nuclear scattering could be safely neglected. The two values

$$\tau_{Al} = (8 \pm 1.8) \times 10^{-13} \text{ sec}$$

$$\tau_{Cu} = (6 \pm 1.5) \times 10^{-13} \text{ sec}$$

were extracted which may be combined to give $\tau = (7 \pm 1.5) \times 10^{-13}$ sec where the error has been increased to take care of the possible errors in the $\frac{dE}{dx}$ values.

The intensity functions were calculated for both the

2.293 and 2.036 MeV gamma rays assuming that the production cross-section was isotropic in the centre of mass system and that only the electronic contribution to the stopping cross-section was important. This is shown in Fig. 6.6 together with the measured points after the removal of background.

The results obtained in this experiment show some disagreements compared with other measurements (Table 6.1). Lieb (Li 66) has measured τ = 0.115 ± 0.025 ps for the lifetime of the 7.154 MeV state which contrasts with the present limit $\tau < 0.018$ ps. The decay gamma ray from the 7.154 MeV level (E_γ = 1.884 MeV) can clearly be seen to be sharp in the spectra taken using the Aluminium and Copper backed targets (Fig. 6.3) whereas for a lifetime of 0.115 ps it would be expected that the peak would be nearly uniformly spread between the unshifted position and the position of maximum shift. The experiment of Lieb was done using a NaI(Tl) crystal and without the use of a heavy ion beam which made the expected maximum shifts rather small and also difficult to measure because of the poorer resolution of NaI(Tl) crystals compared with Germanium detectors. In the case of the 7.563 MeV level the agreement is nearly reasonable.

Again, in the case of the measurement of Alburger et. al. (Al 66) the agreement is nearly reasonable in the case of the 7.276 MeV state in ^{15}O. In their experiment the gamma ray from the 7.276 MeV was produced in the $^{14}N(d, n)^{15}O$ reaction with the neutrons unobserved. In their analysis it was <u>assumed</u> that the mean centre of mass angle of the ^{15}O ions was $\cos^{-1}(0.33)$: this could be wrong since any average quantity should be properly weighted by the differential cross-section. Alburger et. al. also reported a lifetime for the 6.857 MeV state of "roughly" $\tau = 0.10 \pm 0.06$ which is not inconsistent with the present measurement if their error was estimated "roughly" too.

TABLE 6.1

Nucleus	Level	Main decay mode	Lifetime in psec		
			This work	(L 66)	(Al 66)
^{15}N	6.323	6.323 → g.s.	< 0.045		
	7.154	7.154 → 5.270	< 0.018	0.115 ± 0.025	
	7.300	7.300 → g.s.	< 0.025		
	7.563	7.563 → 5.270	0.06 ± 0.02	0.15 ± 0.05	
	8.312	8.312 → g.s.	< 0.021		
^{15}O	6.180	6.180 → g.s.	< 0.47		
	6.787	6.787 → g.s.	< 0.028		
	6.857	6.857 → 5.240	< 0.18		
	7.276	7.276 → 5.240	0.70 ± 0.15		1.25 ± 0.3

TABLE 6.2

Decays of some levels in ^{15}O and ^{15}N

Nucleus	Level	Transition	Branch (%e)	Gal (%a %b)	(Al 66)	(%e 66)	Adopted
^{15}N	7.154 →	0	≤ 12	≤ 4	≤ 5	≤ 5	≤ 4
		5.270	100	100	100	100	100
		5.299	≤ 4		≤ 10	< 35	≤ 4
	7.300 →	0	100	100	98±1	100	100
		5.270	≤ 1.5	< 4	2±1	≤ 10	≤ 1.5
		5.299	2±1				2±1
	7.563 →	0	≤ 12	< 4	< 3	≤ 3	≤ 3
		5.270	100	100	100	100	100
		5.299	≤ 6		< 5	≤ 20	≤ 4
^{15}O	6.789 →	0	100		100		100
		5.188	≤ 3		≤ 6		≤ 3
		5.240	< 3		≤ 6		≤ 3
	6.857 →	0	≤ 12		≤ 10		≤ 10
		5.188	≤ 4		≤ 15		≤ 4
		5.240	100		0		100
	7.276 →	0	≤ 12		≤ 30		≤ 12
		5.188	≤ 4		≤ 10		≤ 4
		5.240	100		100		100

The first two columns of branching ratio data were taken from the results reported in Chapters 5 and 6.

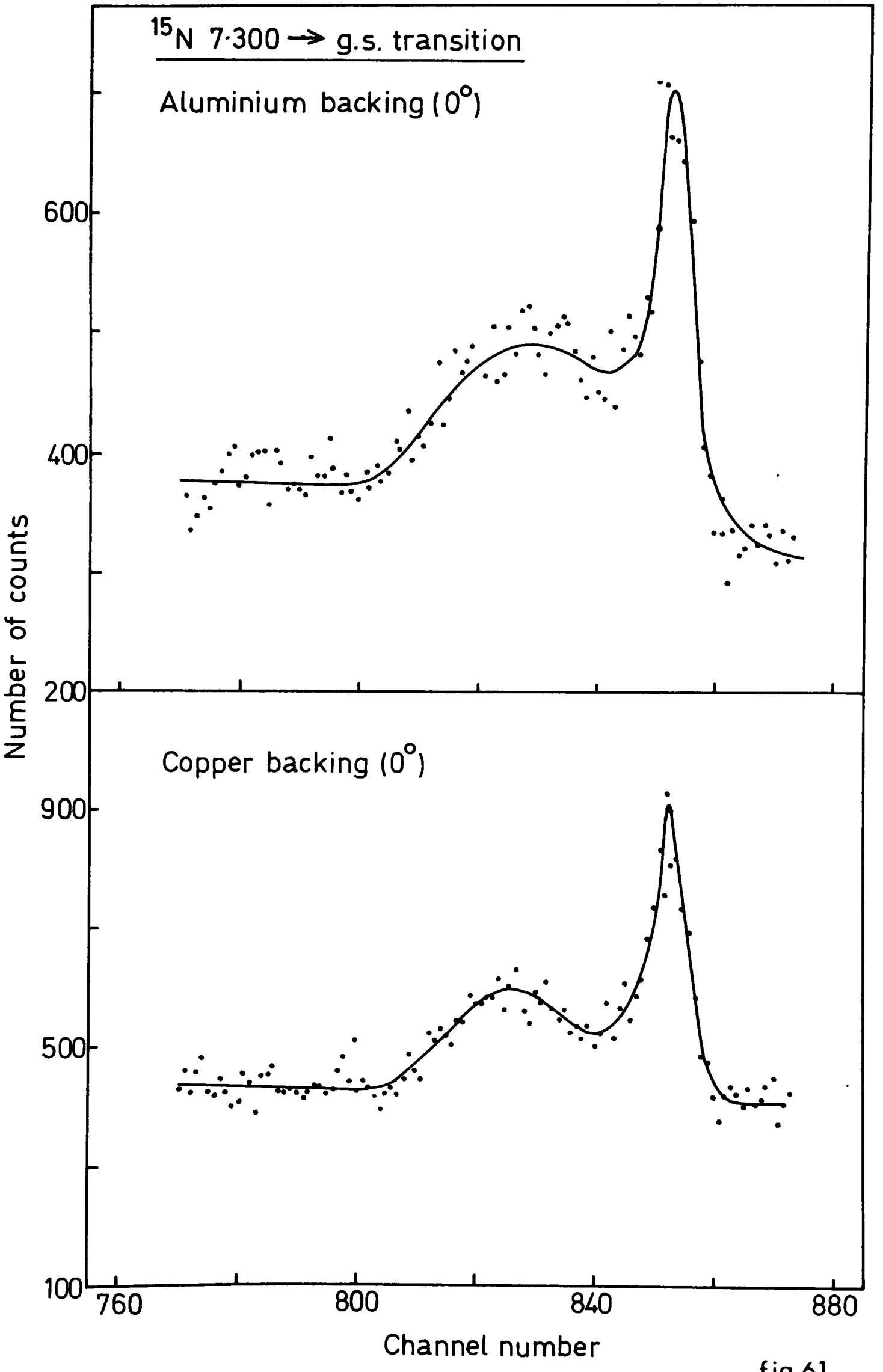

^{15}N 7·300 → g.s. transition
Aluminium backing (0°)
600
400
200
Number of counts
Copper backing (0°)
900
500
100
760
800
840
880
Channel number

fig. 6.1

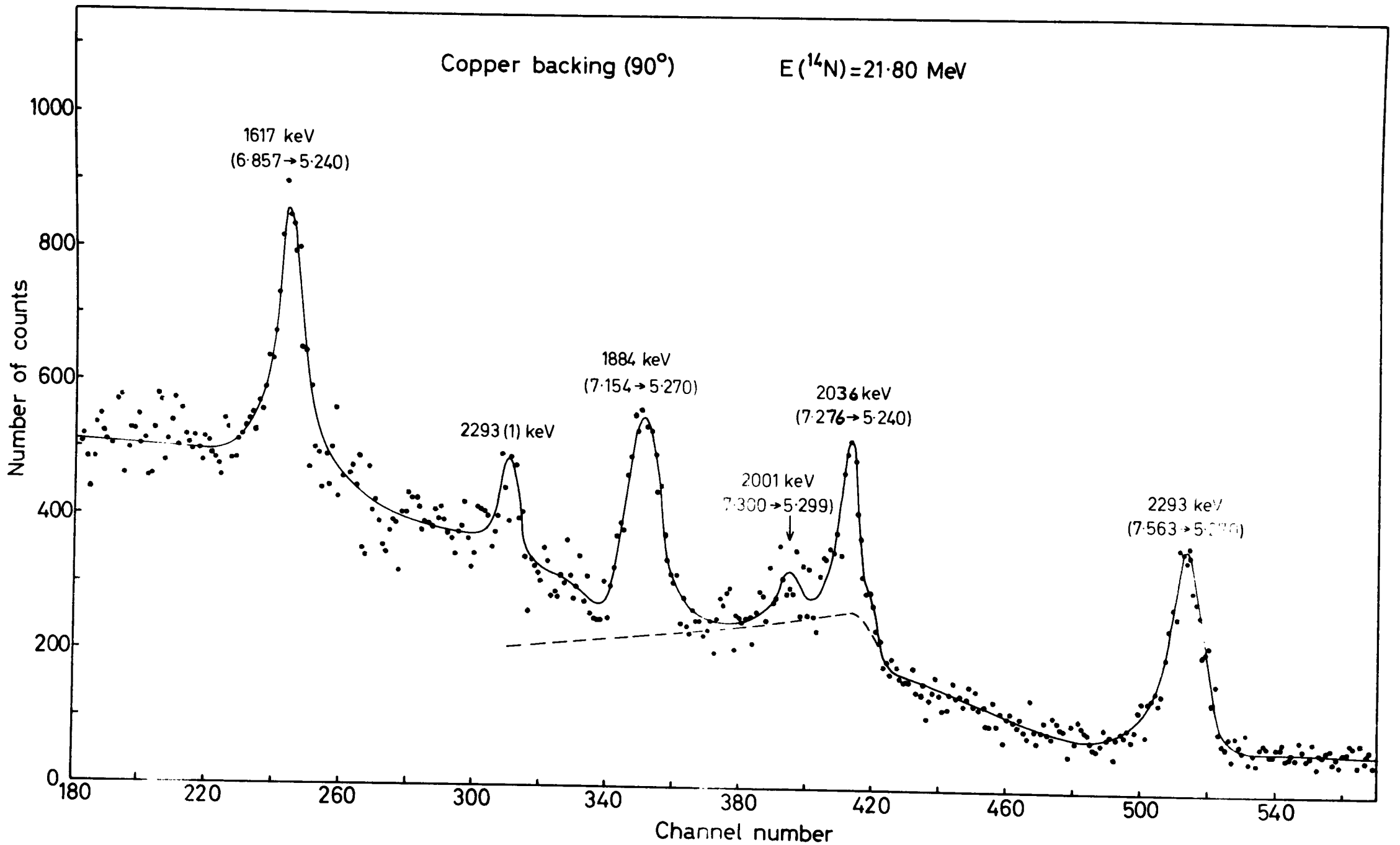

Copper backing (90°)
E(14N)=21·80 MeV
1617 keV
(6·857→5·240)
1884 keV
(7·154→5·270)
2036 keV
(7·276→5·240)
2293 (1) keV
2001 keV
(7·300→5·299)
2293 keV
(7·563→5·270)
Number of counts
Channel number
0
200
400
600
800
1000
180
220
260
300
340
380
420
460
500
540

fig.6.2

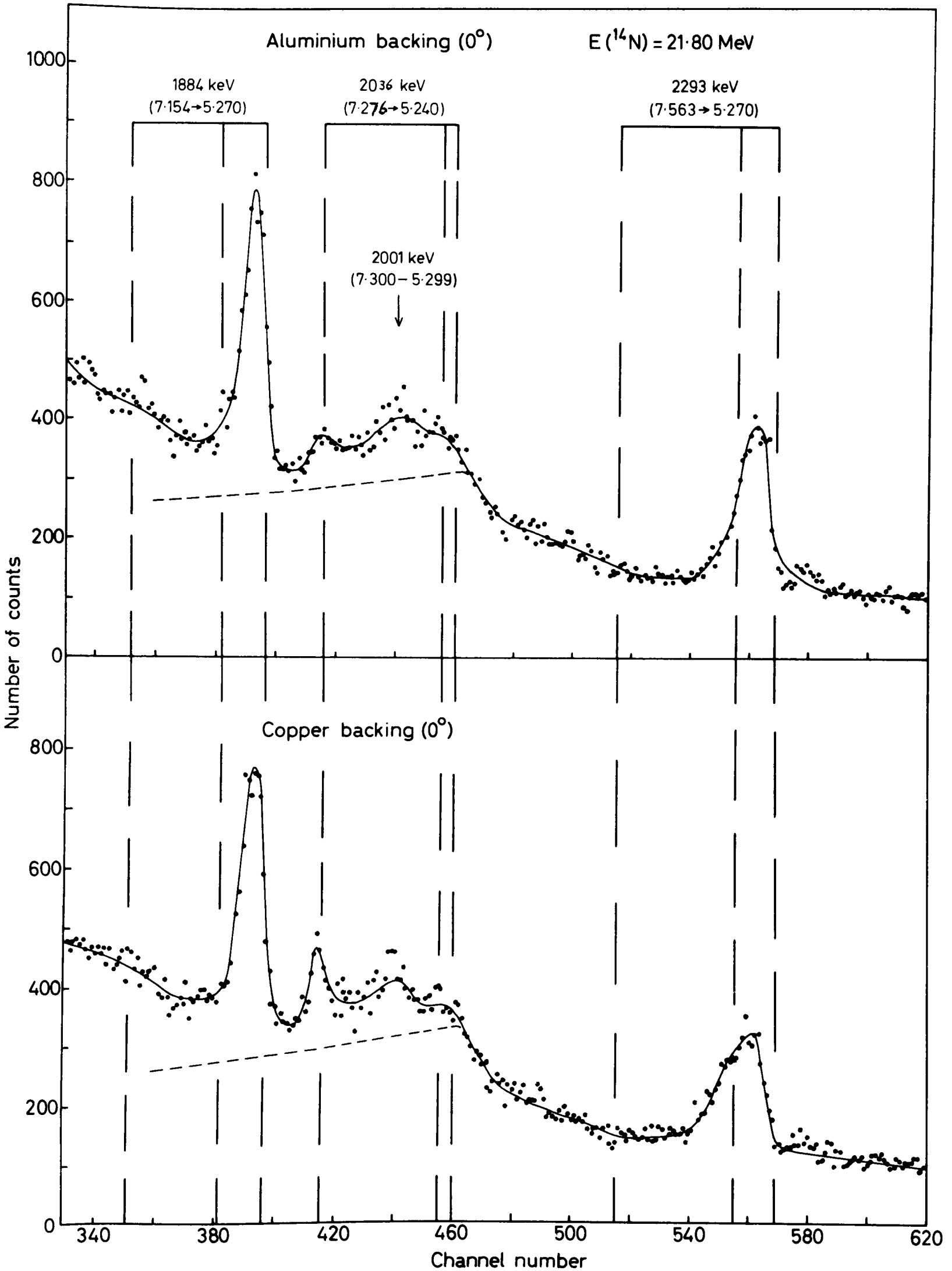

Aluminium backing (0°)
E (14N) = 21·80 MeV
1884 keV
(7·154→5·270)
2036 keV
(7·276→5·240)
2293 keV
(7·563→5·270)
2001 keV
(7·300 – 5·299)
Number of counts
1000
800
600
400
200
0
Copper backing (0°)
800
600
400
200
0
340
380
420
460
500
540
580
620
Channel number

fig.6.3

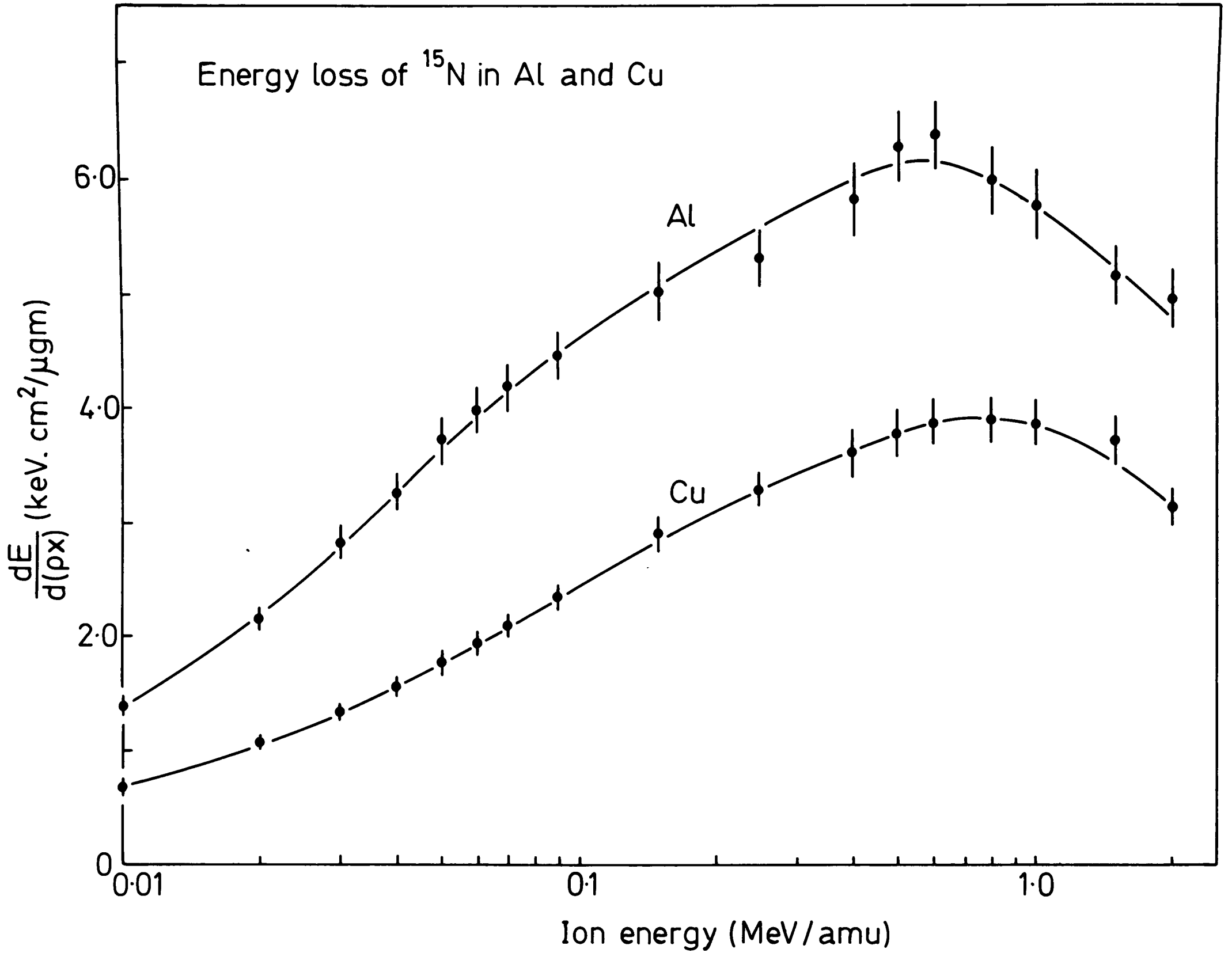

Energy loss of ^{15}N in Al and Cu
Al
Cu
6·0
4·0
2·0
0
$\frac{dE}{d(\rho x)}$ (keV. cm^2/µgm)
0·01
0·1
1·0
Ion energy (MeV/amu)

fig.6.4

Energy loss of ^{15}O in Al and Cu

Al

Cu

$\frac{dE}{d(\rho x)}$ (keV. cm^2/µgm)

8·0
6·0
4·0
2·0
0

0·01
0·1
1·0

Ion energy (MeV/amu)

fig. 6.5

2·036 MeV. ^{15}O

7·276 ⟶ 5·240

$\tau = 0.7 \pm 0.12$ ps

2·293 MeV. ^{15}N

7·563 → 5·270

$\tau = 0.06 \pm 0.02$ ps

Aluminium Backing

Copper Backing

fig. 6.6

C H A P T E R 7

DISCUSSION OF THE RESULTS

7.1 The 2^- State of ^{16}O

In a simple shell model treatment the ground state of ^{16}O is described as a doubly closed shell nucleus. The $1s_{\frac{1}{2}}$, $1p_{3/2}$ and $1p_{\frac{1}{2}}$ neutron and proton shells are completely filled giving a ground state spin of $J = 0$. Excited states of negative parity may be formed by exciting one of the $p_{\frac{1}{2}}$ particles into the (2s,1d) shell in which the $2s_{\frac{1}{2}}$ and $1d_{5/2}$ states are lowest in energy. To a first order approximation the low lying levels would then have the structure $(1p_{\frac{1}{2}})^{-1}(2s_{\frac{1}{2}})$ or $(1p_{\frac{1}{2}})^{-1}(1d_{5/2})$, leading to spin parity values 0^-, 1^-, 2^- and 3^- which appear in the experimental spectrum at about 6 to 12 MeV. (A partial energy level spectrum appears as Fig. 7.1). In fact other negative parity configurations apart from the ones just mentioned should appear in the spectrum at slightly higher energies and should be mixed into the simple configurations by the interparticle residual interaction. Elliott and Flowers (El 57) did a calculation along these lines treating

all possible (p, (sd)) configurations in intermediate coupling. Good agreement was found between the calculated and experimental spectra.

The lowest lying positive parity state is seen in the experimental energy spectrum at 6.06 MeV. It has been suggested (Br 66 and previous references therein) that this state is highly deformed and is formed by lifting either two or four particles to the # 6 Nilsson orbital (Ni 55). A glance at the appropriate part of the Nilsson diagram shows that the energy of this state will decrease with increasing deformation and thus an explanation can be found for the position of the first 0^+ state.

In a series of papers (Br 66) Brown and collaborators have shown that in order to explain the measured electromagnetic properties of the low lying positive parity states it is necessary to mix in these many particle many hole configurations into both the excited states and the ground state. The latter is a new departure since in the shell model in a first order perturbation approach the ground state is always a spherical closed shell.

The mixing in of three particle three hole configurations into the negative parity excited states improves the agreement between their theoretically calculated and the

experimentally determined positions as compared with the one particle one hole model (Gr 65; 61). Some improvement in the agreement between the experimental and theoretical transition rates is achieved. The three particle three hole configurations mix in with the one particle one hole configurations to the extent of about 0.3 in amplitude.

In discussing the observed decay properties of the 2^-, 8.88 MeV state a rather straightforward approach will be adopted: the measured mixing ratios and experimental lifetime (Ai 67) of the state will be compared with the one particle one hole model of Elliott and Flowers (referred to henceforth as EF.). Deviations from this model will then be ascribed to the influence of the three particle three hole configurations. The calculations will be carried out phase consistently throughout (Bo 67).

In EF. the excited states are described as linear combinations of the possible (p,sd) configurations which can lead to a given final spin value.

i.e.,

$$|J\ M\rangle = \sum_{j_a j_b}^{} a^{JM} |J\ M\ (j_a j_b)\rangle$$

where the wavefunctions $|JM\ (j_a j_b)\rangle$ are constructed

as described in Section 3.7. The coefficients $a^{J_T}_{J_a J_b}$ are quoted in BF. for v_c = 40 MeV but their signs must be changed in some cases in order that the results of the calculations will be in accord with the standard phase convention of (Ho 67).

The reduced matrix elements of the T^{M}_{LM} operators may be calculated for the $2^- \rightarrow 1^-$ and $2^- \rightarrow 3^-$ transitions using equation 3.7. 19. The results for the two lowest possible multipolarities which may contribute are :

$$M1(2^- \rightarrow 1^-) = + 0.0143 \times 10^{-7} \text{ meV/G. cm}$$
$$M1(2^- \rightarrow 3^-) = - 0.1765 \times 10^{-7}$$
$$E2(2^- \rightarrow 1^-) = + 0.1821 \times 10^{-7}$$
$$E2(2^- \rightarrow 3^-) = - 0.4250 \times 10^{-7}$$

The radial integrals, where appropriate, were evaluated in a Woods-Saxon potential well. The main features of the experimental data are explained (Tables 7.1 and 7.2) as was noted by BF. who showed that the contributions to the M1 and E2 matrix elements for the $2^- \rightarrow 1^-$ and $2^- \rightarrow 3^-$ transitions should interfere destructively and constructively respectively, thus leading to large multipole mixing ratios. The agreement with the mixing ratio data may even be

improved if use is made of the effective charge formalism: the E2 matrix elements will be increased by a factor of $(1 + 2\beta)$ where the two arises from the extra contributions from both the proton-proton hole and neutron-neutron hole parts of the wavefunction. The calculated mixing ratios then become $\delta(2^- \rightarrow 1^-) = +23$ and $\delta(2^- \rightarrow 3^-) = +4.2$ and the width increases to 20×10^{-4} eV. The value $\beta = 0.64$ which was used for the effective charge parameter is suggested by the measured lifetimes of the $2s_{\frac{1}{2}} \rightarrow 1d_{5/2}$ transitions in ^{17}O.

The E2 matrix element of the 8.88 MeV $\rightarrow$ g.s. transition was calculated and it was found that the $p^{-1}d$ and $p^{-1}s$ configurations interfered destructively to give almost complete cancellation. This point was discussed by EF. who noted that this matrix element was particularly sensitive to variations in their parameters, especially v_c and the relative strength of the spin-orbit interaction for the p and d shells. For a particular set of these parameters they obtained reasonable agreement with experiment for the ratio $\frac{\Gamma(g.s.)}{\Gamma(6.14)}$.

In conclusion, the model of EF. seems to be in fairly good agreement with the experimental decay properties of the 8.88 MeV level although the calculated total width

turns out to be too small. It would be interesting to investigate whether the inclusion in the wavefunctions of three particle three hole configurations as suggested by Brown and collaborators would substantially alter the situation.

7.2 Mass 15 nuclei

Mass 15 nuclei stand one next to the doubly closed ^{16}O shell. It would therefore be expected, in simple shell model terms, that excited levels would appear which correspond to a single hole spectrum. This expectation is fulfilled since the ground states of ^{15}O and ^{15}N have $J^\pi = \frac{1}{2}^-$ which correspond to the $p_{\frac{1}{2}}$ single hole orbit while the $p_{3/2}$ single hole states are found at about 6.3 MeV. These conclusions are supported by the analysis of stripping and pickup reactions (Au 67; Ma 65c; Hi 67). Accurate determinations of the mixing ratios (Lo 66b) of the ground state transitions from these levels have shown that considerable collective admixtures must be present in the wavefunctions of these single hole states. A calculation within the framework of the weak coupling model (Lo 66) has shown that if some amplitude of the state formed by

coupling a $p_{\frac{1}{2}}$ hole to the first excited 2^+ state of the ^{16}O core is mixed into the pure $p_{3/2}$ hole state then, although fair agreement with the experimental value may be reached for the ^{15}N mixing ratio, it is not possible to reach agreement in the ^{15}C case.

This situation has been partially rectified by Brown and Shukla (Br 67; Sh 67) who did calculations using the random phase approximation in which large amplitudes of two particle three hole configurations were mixed into the "single hole" states. In this way better agreement between experiment and theory was achieved (see Table 7.3) although the theoretical mixing ratio for the ^{15}N transition is rather too large. The width calculated for the ^{15}N state was 3.7 eV as compared with the measured value 3.6 eV (Br).

Excited states of positive parity begin to appear in the mass 15 spectrum at about 5 MeV (Fig. 7.2 and Tables 7.7, 8). In a simple shell model these would correspond to the excitation of a $p_{\frac{1}{2}}$ proton or neutron into the $2s_{\frac{1}{2}}$ or $1d_{5/2}$ orbits. Higher energy configurations would be formed by exciting any p nucleon into any of the 2s,1d states. Halbert and French (Ha 57) performed calculations along these lines using a residual interaction between the particles forming the excited states and were able to thus

explain the positions and spins of many of the low lying states.

7.3 The $5/2^+$, 5.2 MeV States

In the latter calculation the $5/2^+$, 5.2 MeV states were described as belonging predominantly to the configuration constructed by coupling a $d_{5/2}$ particle to a $T = 1$, $J = 0$ (p^{-2}) parent state which might be identified as the ^{14}C ground state or the 2.31 MeV state of ^{14}N. This is compatible with the small reduced width observed in the $^{14}N(d,p)^{15}N$ stripping reaction leading to the 5.2 MeV state (Al 59). If the ^{15}N ground state is taken to be a $(p_{\frac{1}{2}})^3$ configuration relative to the closed $(p_{3/2})$ shell then the M3 and M2 matrix elements for the ground state decay may be calculated using standard fractional parentage techniques (Sh 63). The results are $|\delta| = 0.03$ and $\tau = 5 \times 10^{-13}$ sec for the ^{15}N state where the radial integrals were evaluated in a harmonic well and were : $J(1) = 2.66$ fm and $J(3) = 26.3$ fm^3. Experimentally (Al 65; Bi, La), the lifetime of the ^{15}N, 5.2, $5/2^+$ MeV state is known to be $(2.7 \pm 0.3) \times 10^{-12}$ sec. which differs from the calculated value by a factor of 9.

These lowest $5/2^+$ states have also been discussed by BS. (Brown and Shukla, op.cit.) who described them in terms of one particle two hole configurations mixed with three particle four hole configurations. In this way it was hoped that good agreement between the calculated and experimental electromagnetic properties might be found. The results of their calculation are shown in Table 7.5 from which it may be seen that the agreement with experiment is hardly any better than was the case for the crude model mentioned above.

A different approach towards the structure of the $5/2^+$ states has been suggested by Bussiere et. al. (Bu 65; Ha 64; Ha 66b) in the light of(dc') scattering experiments. It was observed that the differential cross-sections for the inelastic scattering of the 3^-, 6.14 MeV state in ^{16}O and the ones for the $5/2^+$, 5.27 MeV and $7/2^+$, 7.56 MeV states in ^{15}N are almost identical. This led to the suggestion that these ^{15}N states can be described as $p_{\frac{1}{2}}$ proton holes coupled to the 3^- state of ^{16}O. This view is supported to some extent by the fact that the centre of gravity of the two ^{15}N levels almost coincides with the 3^- state of ^{16}O. It is also interesting to note that in the extremely simplified description of the 3^- state being a purely

collective state no M2 component would appear in the $5/2^+$ to ground state transition. The large spacing of the $5/2^+$ and $7/2^+$ states indicates a rather strong coupling of the valence hole as has been shown by Ripka (Ri 64) for the mirror states in ^{15}O.

The 3^- state of ^{16}O has been described by Elliott and Flowers (El 57) and, more recently, by Gillet and Vinh-Mau (Gi 64) as one particle one hole excitations in which the $(p_{\frac{1}{2}}^{-1}\, d_{5/2})$ component is dominant. (Gi 64) quote for the wavefunction:

$$|3^-\rangle = 0.934\,|p_{\frac{1}{2}}^{-1}\, d_{5/2}\rangle - 0.284\,|p_{3/2}^{-1}\, d_{5/2}\rangle + 0.216\,|p_{3/2}^{-1}\, d_{3/2}\rangle$$

This wavefunction* does not, of course, include the effect of correlations in the ground state of ^{16}O. In order to calculate the ^{15}N and ^{15}O ground state M2 matrix elements

---

* In comparing the phases of (Gi 64) with those of (El 57) note should be taken of the errata which appeared in Nuc. Phys. 57 (1964) 698.

the mass 15 wavefunctions may be constructed by creating either a proton or neutron hole in the above wavefunction (equation 3.7.20). If the ground states of ^{15}N and ^{15}O are described by a single $p_{\frac{1}{2}}$ hole in the ^{16}O closed shell then the M2 matrix elements for the $5/2^+ \rightarrow$ ground state transitions may be calculated using equation 3.7. 23. The calculated lifetimes are then 0.8 ps and 1.2 ps as compared with the measured values 2.7 ps and 3.2 ps in ^{15}N and ^{15}O respectively. The agreement with experiment is probably reasonable in view of the rather restricted wavefunctions used. If other parent states in ^{16}O are taken into account to some extent (about 0.2 in amplitude), then it is possible to provide the small degree of cancellation in the matrix elements which would be necessary to fit the experimental values.

An attempt to explain the measured E3 matrix element using the simple core model would appear to be doomed to failure since it is known that the observed (Al 65) enhancement of the E3 transition rate for the ^{16}O, $3^- \rightarrow$ ground state decay cannot be explained within the framework of a simple one particle one hole model (Br 61; Br 65; Gi 66). The observed exhancement (14 Weisskopf units) has been explained in terms of ground state correlations which implies

that many configurations contribute constructively to the E3 matrix element. Also, it implies that the wavefunction of the 3^- core will only be slightly modified by the addition of an extra $p_{\frac{1}{2}}$ hole. It is therefore seems justfiable to use the experimentally determined E3 matrix element as extracted from the ^{16}O lifetime measurement to calculate the mixing ratios in mass 15. Using the calculated M2 matrix elements the mixing ratios in ^{15}N is* $|\delta| = 0.10$ ($\delta_{expt} = -0.165$) and in ^{15}O is $|\delta| = 0.14$ ($\delta_{expt} = +0.145$) which represents fair agreement with the measured values. The experimental E3 widths have been listed in Table 7.4 in Weisskopf units.

7.4 The M1 Transition Rates

As mentioned above, the 7.56 and 7.28 MeV $7/2^+$ states in ^{15}N and ^{15}O should have a similar structure to the $5/2^+$, 5.2 MeV states. The decay of the $7/2^+$ to the $5/2^+$ level

---

* The modulus of δ is quoted since the phase relation between the calculated M2 and experimentally determined E3 matrix element is unknown.

---

would therefore be dominated by the spin flip of the valence hole which was coupled onto the 3^- core state. Under this assumption the width of the 7.56 MeV state may be estimated (see Table 7.6) to be 6.90 x 10^{-3} eV as compared with the experimental value of 11.0 x 10^{-3} eV. This agreement is rather surprising considering that this M1 transition is so weak (0.0023 W.U.). In the case of ^{15}O a neutron hole spin flips to give a width of 2.88 x 10^{-2} eV which is different by a factor of about 30 from the measured value. The relative small width is, however roughly explained. From Table 7.6 it can be seen that the 6.86 and 7.15 ($5/2^+$) levels decay by M1 transitions which are unexceptional in their strengths.

7.5 The $3/2^+$, 7.30 and 6.79 MeV States

The mixing ratios for the 7.30 and 6.79 MeV to ground state transitions in ^{15}N and ^{15}O were found to be $\delta = -0.07$ and $\delta = -0.10$ respectively and both lifetimes are faster than 3 x 10^{-14} sec. (cf. Chapters 5 and 6). (It is assumed in both cases that the smaller value of the mixing ratio is correct.) Here, SB. calculate that the lifetime of the 6.79 MeV state in ^{15}O should be 1.5 x 10^{-13} sec which

is at variance with the experimental limit ($\tau < 3 \times 10^{-14}$ sec) and which represents a retardation of 3×10^{4} compared with the Weisskopf estimate. In SB's calculation the E1 matrix elements turn out to be small because of the operation of an SU_3 selection rule which would completely forbid the transition were the level a pure configuration in this classification scheme.

It is interesting to note that the "a priori" estimate of the mixing ratios extracted from an inspection of the s,d → p reduced matrix elements would predict a mixing ratio of roughly 0.002 which, to bring about agreement with the experimental value, would therefore require a retardation of the E1 amplitude of about 50 which in turn represents a retardation factor of 2500 for the squared modulus of the matrix element. Apart from selfconjugate nuclei such retardations are rare in light nuclei (Wi 60).

TABLE 7.1

Transition Strengths for the 2^- State in ^{16}O

Final state		Multipolarity	Width (eV) x 10^4	Calculated Width	Calculated $\beta = 0.64$
g.s.	0^+	M2	2.28	≈ 0	≈ 0
6.14	3^-	M1	2.7	.936	.936
		E2	22.5	3.18	16.5
6.92	2^+	M1 + E2	1.43		
7.12	1^-	M1	5.13	.38	2.0
		E2			

The decay width to the 2^+ state was not calculated since the model of Ref does not provide wavefunctions for this state.

TABLE 7.2

Comparison of theoretical predictions with the experimentally determined quantities

	Experiment	Theoretical
Γ_{Total}	$= 34 \times 10^{-4}$ a)	20×10^{-4}
$\lvert \delta\ (2^- \to 1^-) \rvert$	≥ 5	$+ 23$
$\delta\ (2^- \to 3^-)$	$= 2.9 \pm 0.2$	$+ 4.2$
$\dfrac{\Gamma_{g.s.}}{\Gamma_{6.14}}$	$= 0.09$	$\simeq 0$

a) Ref. 67.

The numbers which appear in the "theoretical" column have been calculated for $\beta = 0.04$.

TABLE 7.3

The $p_{3/2}^{-1} \rightarrow p_{1/2}^{-1}$, 6 MeV transition in mass 15.

Level	Experimental mixing Ratio a)	Theoretical values b)
^{15}N (6.33)	+ 0.13 ± 0.1	+ 0.23
^{15}O (6.18)	- 0.17 ± 0.02	- 0.19

a) Le Gu'b

b) Br 67; Sh 67

The signs quoted in the table are in accordance with the convention used in (Ho 67) and in the present work.

TABLE 7.4

E3 Widths in Weisskopf Units

Nucleus	Transition	E3 Width
16_O	3^-, 6.14 → g.s.	14 [a]
15_O	$5/2^+$, 5.24 → g.s.	6
15_N	$5/2^+$, 5.27 → g.s.	1.5

a) (Al 65)

Table 7.5

Decay of $5/2^+$, 5.2 MeV States in Mass 15

Quantity	Nucleus	Experiment	S.M.
$\tau(5.2, 5/2^+)$	^{15}N	2.7 ± 0.3 ps	.12 ps
$\tau(5.2, 5/2^+)$	^{15}O	3.2 ± 0.3 ps	.25 ps
$\delta(5.2 \rightarrow g.s.)$	^{15}N	− 0.165 ± 0.015	0.029
$\delta(5.2 \rightarrow g.s.)$	^{15}O	+ 0.145 ± 0.04	0.027

Some of the numbers relating to these states in 5B. appear to be in error although it is believed that neither this table nor table 7.3 are affected by this difficulty.

TABLE 7.6

M1 Decay Strengths in Mass 15

Width for E_γ = (eV)	1.62	1.89	2.04	2.29
Transition	(^{15}C)	(^{15}N)	(^{15}O)	(^{15}N)
$p_{\frac{1}{2}} \rightarrow p_{\frac{1}{2}}$ (neutron)	1.45×10^{-2}	2.3×10^{-2}	2.88×10^{-2}	4.1×10^{-2}
$p_{\frac{1}{2}} \rightarrow p_{\frac{1}{2}}$ (proton)	2.44×10^{-3}	3.90×10^{-3}	4.86×10^{-3}	6.9×10^{-3}
$d_{5/2} \rightarrow d_{5/2}$ (neutron)	.058	.091	.110	.163
$d_{5/2} \rightarrow d_{5/2}$ (proton)	.399	.636	.799	1.13
Measured	>0.0365	>0.0365	$.94\times10^{-3}$	1.1×10^{-2}
Level	6.86($5/2^+$)	7.28($7/2^+$)	7.15($5/2^+$)	7.55($7/2^+$)

TABLE 7.7

Summary of decay data for energy levels of ^{15}N

Initial Level	J^π	Final Level	Branch	Mixing ratio	Lifetime or Width
5.270	$5/2^+$	g.s.	100	-0.165±0.015	2.7 ps [a]
5.299	$1/2^+$	g.s.	100		4.3×10^{-14} s [b] $< 2\times10^{-14}$ s [a]
6.323	$3/2^-$	g.s. 5.3 [g]	100 < 1	+0.13±0.02 [c]	3.0 eV [d]
7.154	$5/2^+$	g.s. 5.270 5.299 6.323	< 4 100 < 4 <0.5	-0.04±0.03	< 0.10 ps
7.300	$3/2^+$	g.s. 5.270 5.299 6.323	100 < 1.5 2±1 <0.25	-0.17±0.02	< 0.025 ps
7.563	$7/2^+$	g.s. 5.270 5.299 6.323	< 3 100 < 4 <0.6	-0.04±0.01 [e]	0.16 ps

(continued)

Initial Level	J^{π}	Final Level	Branch	Mixing Ratio	Lifetime or Width
8.312	$\frac{1}{2}^+(\frac{3}{2}^+)$	g.s.	79±1.8		< 0.021
		5.270	< 3		
		5.299	11±2		
		6.323	4.4±1		
		7.154	1.2±0.6		
		7.300	3.3±1.1		
8.570	$3/2^+$	g.s.	33±2	0.16±0.08 f)	
		5.270	65±3	0.03±0.05 e)	
		5.299	< 12		
		6.323	2±1		
		7.154	3.6±0.5		
		7.300	< 0.7		
		7.563	< 3		
9.052	$\frac{1}{2}^+, \frac{3}{2}^+$	g.s.	91.6±0.9		
		5.270 } 5.299 }	4.2±1.2		
		6.323	3.7±0.5		
		7.154	< 1		
		7.300	1.2±0.4		
		7.563	< 1		
		8.312	< 0.5		

(continued)

Initial Level	J^{π}	Final Level	Branch	Mixing Ratio	Lifetime or Width
9.155	$3/2^-$	g.s.	86.5±4.5		
		5.270 5.299	6±2		
		6.323	2.5±0.8		
		7.154	6.1±1.8		
		7.300	< 3		
		7.563	< 1		
		8.312	< 0.5		
9.223	3/2 (+)	g.s.	41.5±2.2		
		5.3 g)	31.2±1.7		
		6.323	24.7±1.5		
		7.154	< 1		
		7.300	2.6±0.7		
		7.563 8.321	< 1		

a) La, Bi; b) Al 65b; c) Lo 66b; d) Br; e) Fe 66;

f) Wa 66b; Fe 66; Wa 65;

g) 5.3 means the 5.270 plus the 5.299 MeV level.

The review is based on that of (Wa 65b). Additional information has been used from this work, the quoted references and from (Ph 67), (Fe 66). In (Wa 65b) lifetime limits ($\tau < 5 \times 10^{-13}$ sec) are presented for many of the bound

levels above 6 MeV. Where mixing ratio and lifetime data has been discussed in the text no reference is quoted.

TABLE 7.8

Summary of decay data for energy levels of ^{15}O

Initial Level	J^π	Final Level	Branch	Mixing Ratio	Lifetime or Width
5.188	$\frac{1}{2}^+$	g.s.	100		$< 3 \times 10^{-13}$ s [a]
5.240	$5/2^+$	g.s.	100	$+0.145^{+0.04}_{-0.03}$	3.2 ps [b]
6.180	$3/2^-$	g.s.	100	-0.17 ± 0.01 [c]	< 0.047 ps
		5.188	< 2.5		
		5.240	< 2.5		
6.789	$3/2^+$	g.s.	100	-0.10 ± 0.02	< 0.028 ps
		5.188	< 3		
		5.240	< 3		
		6.180	< 7		
6.857	$5/2^+$	g.s.	< 10		< 0.010 ps
		5.188	< 4		
		5.240	100	-0.04 ± 0.03	
		6.180	< 0.4		

(continued)

Initial Level	J^π	Final Level	Branch	Mixing Ratio	Lifetime or Width
7.276	$7/2^+$	g.s.	<12		0.70 ps
		5.188	<4		
		5.240	100		
		6.180	<2		
		6.789	-		
7.550	$\frac{1}{2}^+$	g.s.	3.3±0.3		0.02 eV [d]
		5.188	17±1		
		5.240	<4.3		
		6.180	57±1		
		6.789	22.7±1		
		6.857	<5.5		
8.283	$3/2^+$	g.s.	54		0.63 eV
		5.188			
		5.240	43		
		6.180	2		
		6.789			
		6.857	1		
8.749	$\frac{1}{2}^+$	g.s.			0.16 eV
		5.188	67		
		5.240			
		6.180	33		
		6.789			
		6.857			

(continued)

Initial Level	J^{π}	Final Level	Branch	Mixing Ratio	Lifetime or Width
8.915	$3/2^+$	g.s.	21		0.21 eV
		5.188	23		
		5.240			
		6.180	30		
		6.789			
		6.857	26		
8.972	$3/2^-$ $1/2^-$	g.s.	93		0.21 eV
		5.188	6		
		5.240			
		6.180	(0.25)		
		6.789	(0.5)		
		6.857			

a) Al 65b; b) La, Bi; c) 10 66b; d) The total widths for all levels above 7.5 MeV are taken from (Du 51).

The data is taken from the review of (Wa 65b) and, apart from the quoted references, (Ev 65, 66, 67) and (Al 66).

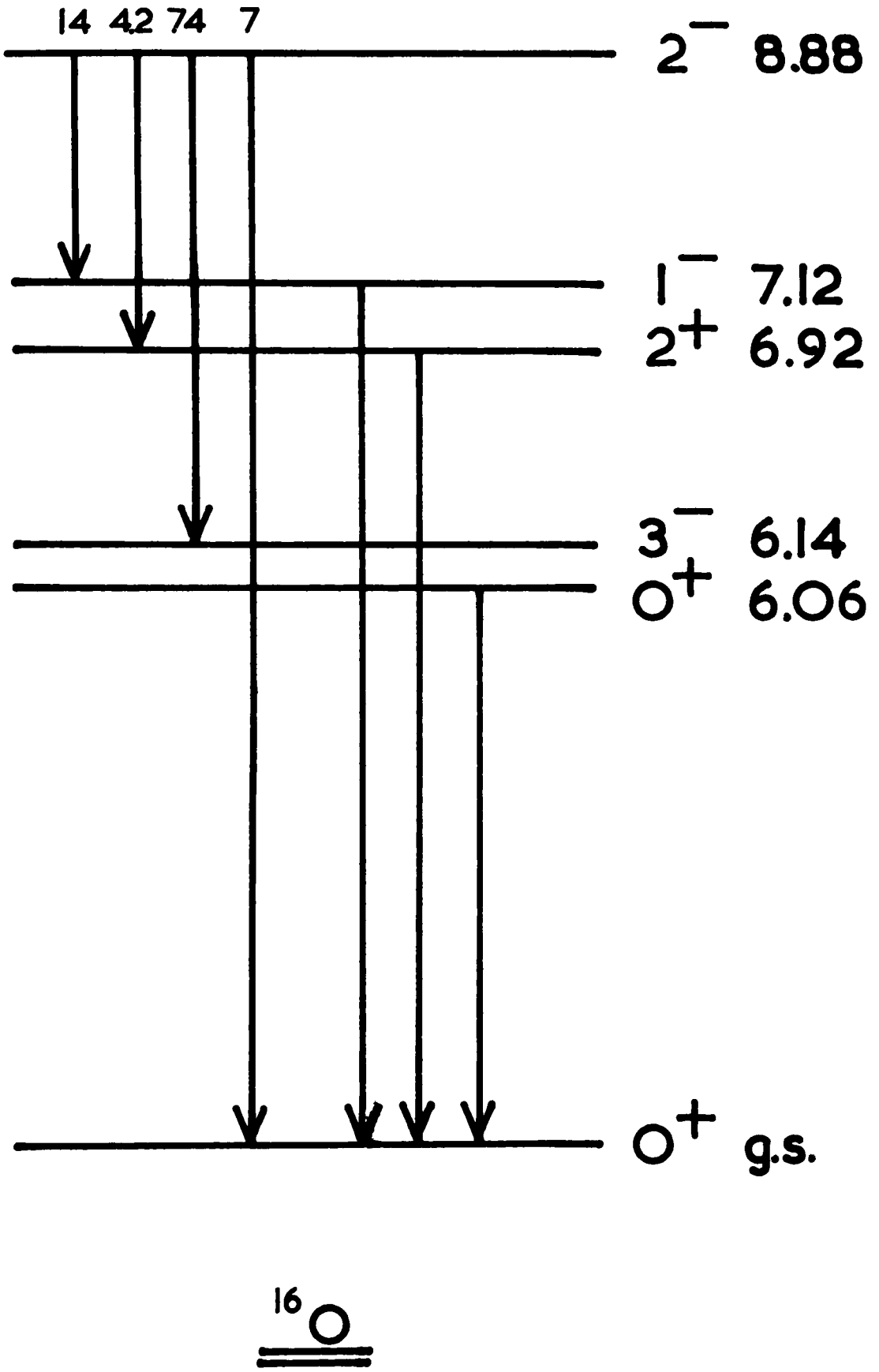


fig. 7.1

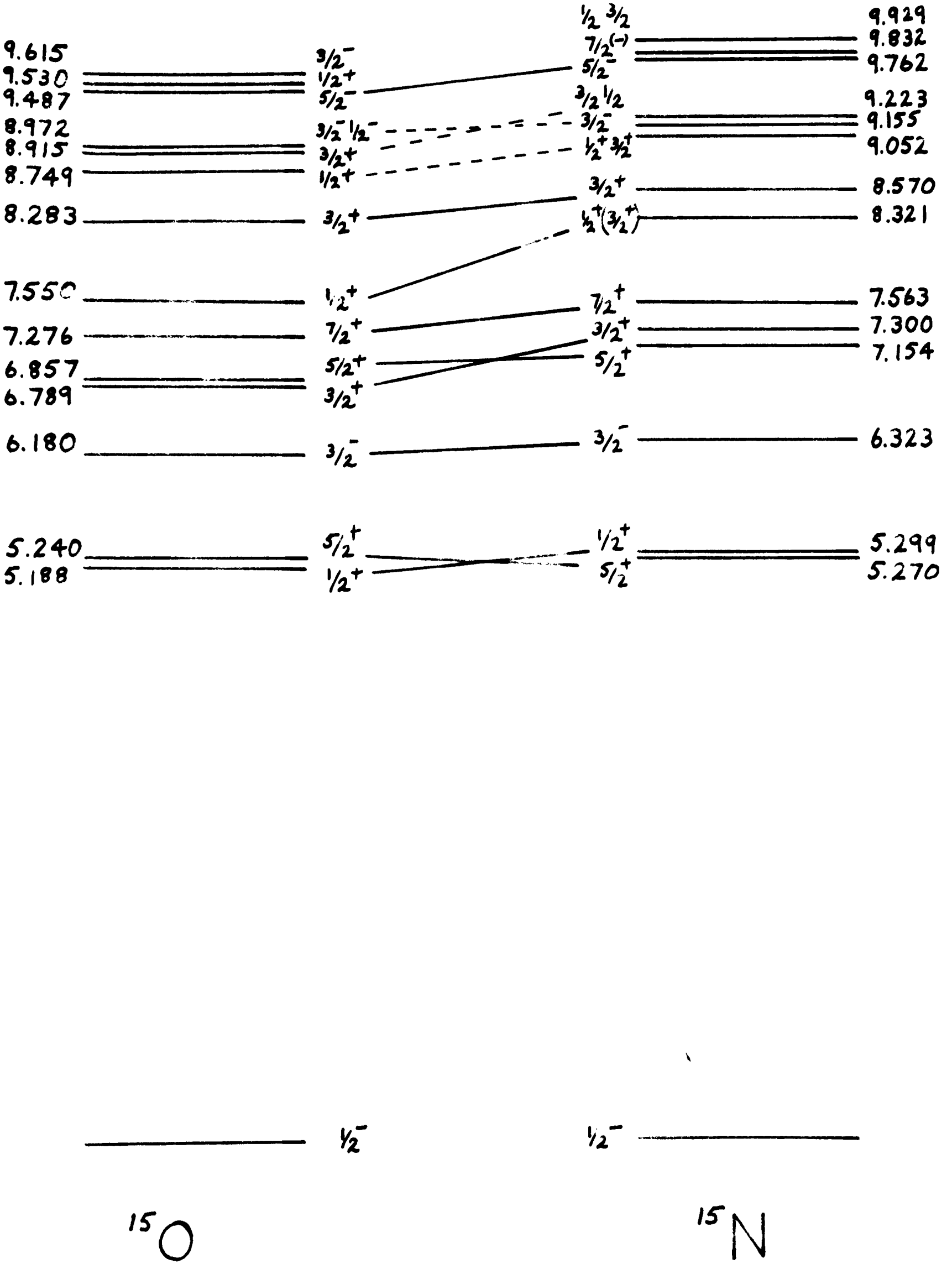

9.615
9.530
9.487
8.972
8.915
8.749
8.283
7.550
7.276
6.857
6.789
6.180
5.240
5.188
3/2⁻
1/2⁺
5/2⁻
3/2⁻ 1/2⁻
3/2⁺
1/2⁺
3/2⁺
1/2⁺
7/2⁺
5/2⁺
3/2⁺
3/2⁻
5/2⁺
1/2⁺
1/2 3/2
7/2(-)
5/2⁻
3/2 1/2
3/2⁻
1/2⁺ 3/2⁺
3/2⁺
1/2⁺(3/2⁺)
7/2⁺
3/2⁺
5/2⁺
3/2⁻
1/2⁺
5/2⁺
9.929
9.832
9.762
9.223
9.155
9.052
8.570
8.321
7.563
7.300
7.154
6.323
5.299
5.270
1/2⁻
1/2⁻
15O
15N

Fig. 7.2

REFERENCES

Aj 59 F. Ajzenberg-Selove and T. Lauritsen, Nuc. Phys. 11 (1959) 1.

Al 53 S.K. Allison and S.D. Warshaw, Revs. Mod. Phys. 25 (1953) 779.

Al 65 T.K. Alexander and K.W. Allen, Can. J. Phys. 43 (1965) 1563.

Al 65b T.K. Alexander, A.E. Litherland and C. Broude, Can. J. Phys. 43 (1965) 2310.

Al 66 D.E. Alburger and E.K. Warburton, Phys. Rev. 152 (1966) 914 .

Al T.K. Alexander, private communication to K.W. Allen.

An K. Anderson, private communication.

Be 53 H.A. Bethe and J. Ashkin, in Experimental Nuclear Physics, Vol. 1, ed. E. Segre (Wiley, New York, 1953).

Be 57 R.D. Bent, T.H. Kruse, L.J. Lidofsky and K.E. Ekland, Bull. Amer. Phys. Soc. (2) 2 (1957) 52.

Bi 53 L.C. Biedenharn and M.E. Rose, Revs. Mod. Phys. 25 (1953) 729.

Bi 60 L.C. Biedenharn, in Nuclear Spectroscopy, Part B, ed. F. Ajzenberg-Selove (Academic Press, New York, 1960).

Bi — F.G. Bizzeti, A.M. Bizzeti-Sona, S. Malbitzer and B. Povh, Nuc. Phys. A164 (1967) 577.

Bl 64 — J.L. Black and E. Valentine, J. Nuc. Instr. Meth. 31 (1964) 325.

Bl 66 — A.E. Blaugrund, Nuc. Phys. 88 (1966) 501.

Bo 48 — N. Bohr, Kgl. Dan.Vid. Sel. Mat. Fys. Medd. 18 No. 8 (1948).

Bo 65 — W. Booth and I.S. Grant, Nuc. Phys. 63 (1965) 481.

Br 47 — E.L. Brady and M. Deutsch, Phys. Rev. 72 (1947) 870.

Br 56 — D.M. Brink and G.R. Satchler, Nuov. Cim. 4 (1956) 549.

Br 59 — D.A. Bromley et. al., Phys. Rev. 114 (1959) 758.

Br 61 — G.E. Brown, J.A. Evans and D.J. Thouless, Nuc. Phys. 24 (1961) 1.

Br 62 — D.M. Brink and G.R. Satchler, Angular Momentum (Oxford University Press, 1962).

Br 65 — G.E. Brown and A.M. Green. Phys. Lett. 15 (1965) 168.

Br 66 — G.E. Brown and A.M. Green. Nuc. Phys. 75 (1966) 401.

Br 67 — G.E. Brown and A.P. Shukla, Preprint (Princeton University, 1967).

Br — P. Brix, private communication to H.J. Rose.

Bu 65 — A. Bussière et. al., Phys. Lett. 16 (1965) 296.

Bu 66 — B. Buck, Nuc. Phys. Computing Report No. 10. (Oxford, 1966).

Ca 67 L.E. Carlson and A.E. Azuma, Phys. Lett. 24B (1967) 462.

Co 35 E.V. Condon and G.H. Shortley, Theory of Atomic Spectra (Cambridge University Press, 1935).

De 55 S. Devons, G. Manning and D. St. P. Bunbury, Proc. Phys. Soc. A68 (1955) 18.

De 57 S. Devons and L.J.B. Goldfarb, in Encyclopedia of Physics 42, ed. S. Flügge (Springer, Berlin, 1957).

Di 58 P.A.M. Dirac, The principles of Quantum Mechanics (Oxford University Press, 1958).

Du 51 D.B. Duncan and J.E. Perry, Phys. Rev. 82 (1951) 809.

El 57 J.P. Elliott and B.H. Flowers, Proc. Roy. Soc. A242 (1957) 57.

Ev 55 R.D. Evans, The Atomic Nucleus (McGraw-Hill Book Co., Inc. 1955).

Ev 65 A.E. Evans, Ph. D. Thesis (University of Maryland, 1965).

Ev 66 A.E. Evans, B. Brown and J.B. Marion, Phys. Rev. 149 (1966) 863.

Ev 67 A.E. Evans, Phys. Rev. 155 (1967) 1047.

Fr 65 M. Frauenfelder and R.M. Steffan, in α.β.γ Ray Spectroscopy, ed. K. Siegbahn (North Holland, Amsterdam, 1966).

Fr 66 J.M. Freeman and J.G. Jenkin, J. Nuc. Instr. Meth. 43 (1966) 269.

Ga 66 A. Gallmann, F. Haas and M.Balaux, Phys. Rev. 151 (1966) 735.

Gi 64 V. Gillet and N. Vinh-Mau, Nuc. Phys. 54 (1964) 321

Go 66 S. Gorodetzky, J.M. Freeman, A. Gallmann and F. Haas, Phys. Rev. 149 (1966) 801.

Go 67 S. Gorodetzky et. al., Phys. Rev. 155 (1967) 1119.

Ha 40 D.R. Hamilton, Phys. Rev. 58 (1940) 122.

Ha 64 B.G. Harvey et. al., Nuc. Phys. 52 (1964) 465.

Ha 66 O. Häusser, J.S. Lopes, M.J. Rose and E.D. Gill, Nuc. Phys. Laboratory Report (Oxford, 1966).

Ha 66b B.G. Harvey et. al., Phys. Rev. 146 (1966) 712.

He 60 H.H. Heckman et. al., Phys. Rev. 117 (1960) 544.

Hi 59 S. Hinds and R. Middleton, Proc. Phys. Soc. 74 (1959) 775.

Hi 67 J.C. Hiebert, L. Newman and R.H. Bassel, Phys. Rev. 154 (1967) 898.

Ja 62 L. Jarczyk et. al., J. Nuc. Instr. Meth. 17 (1962) 310.

Je 66 Sir H. Jeffreys and Lady Jeffreys, Methods of Mathematical Physics. (Cambridge University Press, 1966).

Kn 41 J. Knipp and E. Teller, Phys. Rev. 59 (1941) 659.

Ku 59 J.A. Kuehner et. al., Phys. Rev. 114 (1959) 775.

La 67 B. Lalovic, Nuc. Instr. 47 (1966) 269.

La P.G. Lawson and K.W. Allen, to be published.

Li 61 A.E. Litherland and A.J. Ferguson, Can. J. Phys. 39 (1961) 788.

Li 63 A.E. Litherland, M.J.L. Yates, B.M. Hinds and D. Eccleshall, Nuc. Phys. 44 (1963) 220.

Li 63b J. Lindhard, M. Scharff and H.E. Schiøtt, Kgl. Dan. Vid. Sel. Mat. Fys. Medd., 33 No. 14 (1963).

Li 66 K.P. Lieb, Nuc. Phys. 85 (1966) 461.

Lo 66 J.S. Lopes, D. Phil. Thesis (University of Oxford, 1966).

Lo 66b J.S. Lopes et. al., Nuc. Phys. 76 (1966) 223.

Ma 55 M.G. Mayer and J.H.D. Jensen, Elementary theory of Nuclear Shell Structure, (Wiley, New York, 1955).

Mc 66 W.J. McDonald, J.M. Hobson and R. Malcolm, Nuc. Phys. 75 (1966) 353.

Me 62 A. Messiah, Quantum Mechanics, (North Holland, Amsterdam, 1962).

Mu 61 A.H.P. Muggleton and F.A. Howe, J. Nuc. Instr. Meth. 12 (1961) 192.

Mu 64 A.H.P. Muggleton and C.T. Parsons, J. Nuc. Instr. Meth. 27 (1964) 357.

Mu 67 S. Murbarakmand and D.E.P. Macefield, Nuc. Phys. A98 (1967) 82.

Mu 68 G.L. Murray, D. Phil. Thesis (University of Oxford, 1966).

Ni 55 S.G. Nilsson, Kgl. Dan. Vid. Sel. Mat. Fys. Medd., 29 No. 16 (1955).

No 60 L.C. Northcliffe, Phys. Rev. 120 (1960) 1744.

No 63 L.C. Northcliffe, Ann. Revs. Nuc. Sci., 13 (1963) 67.

Or 63 J.H. Orarod and H.E. Duckworth, Can. J. Phys. 41 (1963) 1424.

Pa 56 A. Papineau, Comptes rend. 242 (1956) 2933.

Pa 62 W.K.H. Panofsky and M. Phillips, Classical Electricity and Magnetism (Addison-Wesley, 1962).

Pa 66 P. Paul, J.B. Thomas and S.S. Hanna, Phys. Rev. 147 (1966) 774.

Pe 66 D. Pelte, B. Povh and W. Scholz, Nuc. Phys. 78 (1966) 241.

Ph 67 G.C. Phillips, F.C. Young and J.B. Marion. Phys. Rev. 159 (1967) 891.

Pi 67 R.E. Pixley and W. Benenson, Nuc. Phys. A91 (1967) 177.

Po 59 B. Povh and D.F. Hebbard, Phys. Rev. 115 (1959) 608.

Po 61 D.I. Porat and K. Ramavataram, Proc. Phys. Soc. 77 (1961) 97; 78 (1961) 1135.

Pr 62 M.A. Preston, Physics of the Nucleus (Addison-Wesley, 1962).

Re 55 H.L. Reynolds, L.D. Wyly and A. Zucker, Phys. Rev. 98 (1955) 474.

Ri 64 G. Ripka, Cong. Int. de Phys. Nuc., Paris, 2 (1964) 390.

Ri 66 J.D. Risley, in Lithium-Drifted Germanium Detectors (I.A.E.A., Vienna, 1966).

Ro 53 M.E. Rose, Phys. Rev. 91 (1953) 610.

Ro 57 M.E. Rose, Elementary theory of Angular Momentum (Wiley, New York, 1957).

Ro 60 P.G. Roll and F.E. Steigert, Nuc. Phys. 17 (1960) 54; 16 (1960) 534.

Ro 66 H.J. Rose and J.S. Lopes, Phys. Lett. 22 (1966) 661.

Ro 67 H.J. Rose and D.M. Brink, Revs. Mod. Phys. 39 (1967) 306.

Ru 59 A.H. Rutledge, Atomic Energy of Canada Ltd., Report CRP-851.

Sh 63 A. de-Shalit and I. Talmi, Nuclear Shell Theory (Academic Press, New York, 1963).

Sh 67 A.P. Shukla, Ph. D. Thesis, Princeton University Technical Report PUC-937-262.

Wa 62 A.H. Wapstra, G.J. Nijgh and R. van Lieshout, Nuclear Spectroscopy Tables (North Holland, Amsterdam, 1962).

Wa 63 E.K. Warburton, D.E. Alburger and D.H. Wilkinson, Phys. Rev. 129 (1963) 2180.

Wa 65 E.K. Warburton et. al., Phys. Rev. 138 (1965) B1004.

Wa 65b E.K. Warburton, J.W. Olness and D.E. Alburger, Phys. Rev. 140 (1965) B1202.

Wa 65c E.K. Warburton, P.D. Parker and P.F. Donovan, Phys. Lett. 19 (1965) 397.

Wa 66 E.K. Warburton et. al., Phys. Rev. 148 (1966) 1072.

Wa 66b E.K. Warburton and J.W. Olness, Phys. Rev. 147 (1966) 698.

We 57 C.E. Weatherburn, Mathematical Statistics (Cambridge University Press, 1957).

Wh 58 W. Whaling, in Encyclopedia of Physics 34, ed. S. Flügge (Springer, Berlin, 1958.

Wi 56 D.H. Wilkinson, B.J. Toppel and J.E. Alburger, Phys. Rev. 101 (1956) 673.

Wi 60 D.H. Wilkinson, in Nuclear Spectroscopy, Part B, ed. F. Ajzenberg-Selove (Academic, New York, 1960).

Wi 62 A.V. Wijngaarden and H.E. Duckworth, Can. J. Phys. 40 (1962) 1749.

Wi D.H. Wilkinson, private communication.